UNIVERSIDAD DE JAÉN

ÁREA DE MECÁNICA DE FLUIDOS.
DEPARTAMENTO DE INGENIERÍA
MECÁNICA Y MINERA

TESIS DOCTORAL

•

FLUID DYNAMICS OF SMOKE FROM ENCLOSURE FIRES

•

PRESENTADA POR:
GABRIELE VIGNE

DIRIGIDA POR:
CÁNDIDO GUTIÉRREZ MONTES, ALEXIS CANTIZANO GONZÁLEZ

JAÉN, 4 de junio de 2020

To my Family, Pamela, Diamante
and Gherardo Maria

Resumen

Esta tesis revisa los modelos actualmente disponibles para evaluar el humo producido por incendios en recintos cerrados, desde las correlaciones más básicas de entrada de aire en el penacho hasta los modelos más avanzados de Mecánica de Fluidos Computacional (CFD). Con el fin de revisar estos modelos, se realizaron varios experimentos a escala real, con diferentes tamaños de incendio, combustibles, dimensiones y condiciones ambientales, en dos instalaciones diferentes: el Murcia Fire Atrium en Murcia, España, y la ITB Chamber en Varsovia, Polonia. Los datos obtenidos por estos experimentos se utilizaron para comprender y profundizar diferentes aspectos de los métodos actuales de modelización numérica del humo.

En primer lugar, se investigaron las correlaciones tradicionales del penacho de humo. Se compararon las cuatro correlaciones de entrada de aire al penacho más utilizadas con los datos experimentales obtenidos a escala real. Estas cuatro correlaciones son el modelo de Thomas, el modelo de Zukoski, el modelo de McCaffrey y el modelo de Heskestad. Específicamente, se investigó su adecuación para predecir la producción de humo y la evolución de la capa de humo en grandes volúmenes. En segundo lugar, se investigó la visibilidad a través del humo. Después de determinar la tasa de hollín como el factor más influyente para la visibilidad del humo en análisis CFD, se analizaron una serie de combustibles con varios valores de tasa de hollín en un centro de ensayos de incendios comparándolos con datos numéricos. Estos datos numéricos se obtuvieron utilizando dos paquetes de CFD diferentes, ANSYS Fluent y Fire Dynamics Simulator (FDS). El objetivo principal fue identificar claramente cómo la tasa de producción de hollín de un combustible influye en la visibilidad a través del humo producido. Finalmente, se validó la herramienta computacional FDS mediante una comparación experimental y numérica de un experimento a escala real con cuatro incendios iniciados en diferentes momentos, donde además se consideraron las condiciones transitorias de ventilación de humo. Se registraron mediciones de temperatura en el campo cercano (penacho de incendio) y campo lejano (cerca de las paredes) y también se evaluó la altura de

la capa de humo. Las simulaciones se llevaron a cabo utilizando la versión 6 de FDS.

En el primer estudio, es decir, el relativo a los modelos de entrada da aire hacia el penacho, se observó que, para el estado estacionario, la correlación de McCaffrey proporcionó resultados más cercanos a los experimentos. Sin embargo, para la evolución transitoria de la capa de humo, la correlación de Zukoski dio los resultados más cercanos a los experimentos. Por otro lado, el popular método de Thomas, ampliamente utilizado en Europa y Australia para el diseño de sistemas de control de humos en atrios, subestima la producción de humo y la entrada de aire al penacho, resultando en alturas de capa de humo más altas y dando lugar a estimaciones que no son conservadoras (con errores entre 36.5% y 101%).

En cuanto a la investigación sobre la visibilidad y la tasa de hollín, el análisis numérico mostró una tendencia hiperbólica de la visibilidad al cambiar la tasa de producción de hollín con consecuencias claras en el Tiempo de Evacuación Seguro Disponible (ASET en sus siglas inglesas). Por debajo de un punto límite que existe en un valor de tasa de producción de hollín de alrededor de 0.10 g/g, un pequeño cambio en el parámetro provoca un cambio sustancial en los resultados (en la visibilidad y en el ASET). Sin embargo, por encima de este valor, un aumento de la tasa de hollín apenas influye en los resultados. Una evaluación cualitativa de los resultados mostró que deben utilizarse valores conservadores de la tasa hollín (es decir, valores superiores a 0.10 g/g) en Análisis de Ingeniería si no se dispone de datos detallados y precisos del combustible.

Respecto a la validación de FDS, la comparación entre el experimento y la simulación mostró discrepancias medias inferiores al 20% y al 10% para las temperaturas en el campo cercano y lejano, respectivamente. Si bien cerca de la región de la llama el análisis numérico no coincide con los resultados experimentales de manera satisfactoria, lejos de la región de la llama existe un buen acuerdo entre los resultados numéricos y las medidas experimentales. Esto confirma que FDS es una herramienta robusta para determinar la propagación del humo y sus características razonablemente lejos de la región del incendio.

Los resultados presentados en esta tesis muestran que la producción de humo y su evolución temporal (capa de humo) pueden predecirse con cierto grado de precisión utilizando métodos simples. Sin embargo, el uso de estos modelos para predecir la producción de humo de un incendio determinado sólo se debe utilizar como una primera aproximación y no una herramienta de diseño, ya que entre los modelos disponibles existe un nivel considerable de incertidumbre. Esta tesis también ha puesto de relieve la importancia de definir correctamente las propiedades al modelar numéricamente el incendio, ya que pequeñas diferencias en los datos de entrada pueden generar un impacto importante en los resultados. Específicamente, se ha encontrado que la definición adecuada de la tasa de hollín es profundamente importante, ya que tiene un gran impacto en la determinación de la visibilidad a través del humo y, en consecuencia, del Tiempo de Evacuación Seguro Disponible (ASET en sus siglas inglesas). Por último, los modelos CFD han demostrado tener un rendimiento satisfactorio en la reproducción del fenómeno de incendios y humos, pero se han demostrado también extremadamente sensibles a las variables de entrada.

Abstract

This thesis reviews the current models available to represent smoke produced by fire in enclosures, from the basic plume entrainment correlations to the most advanced CFD models. In order to review such models, several large-scale tests, with different fire sizes, fuels, physical dimensions and ambient conditions were performed in two different large-scale facilities: the Murcia Fire Atrium in Murcia, Spain, and the ITB chamber in Warsaw, Poland. The data obtained from those tests were used to understand different aspects of the current methods of numerically modelling the smoke.

First, the traditional smoke plume correlations were investigated. The results obtained from the four most used plume entrainment correlations were compared with the full-scale experimental data. These four models are namely the Thomas model, the Zukoski model, the McCaffrey model and the Heskestad model. Specifically, their adequacy to predict smoke production and the smoke layer evolution in large atria were investigated. Second, the visibility through smoke was investigated. After determining soot yield as the most influential factor for the visibility in smoke in CFD, fuels with various values of soot yield were analyzed in a fire chamber and then compared to numerical data. These numerical data were obtained using two different CFD packages, ANSYS Fluent and Fire Dynamics Simulator (FDS). The main objective was to identify clearly how the soot yield of a fuel influences the visibility through the smoke produced. Finally, the computational tool FDS was validated by means of an experimental and numerical comparison of a new full-scale atrium fire test with four fires ignited at different times.

As for the visibility and soot yield investigation, the numerical analysis showed a hyperbolic trend of the visibility when changing the soot yield with clear consequences on the Available Safe Egress Time (ASET). Below a cut-off point that exists at a soot yield value of around 0.10 g/g, a small change in the parameter causes a substantial shift in the results (on the visibility and on the ASET). However, above this cut-off value, an increase in soot yield barely influences the results. A qualitative assessment of the results showed that conservative values

of the soot yield (i.e. values above 0.10 g/g) should be used in engineering analyses if detailed and precise material data are not available.

With regards to the FDS validation, the comparison between the empirical experiment and the simulation showed average discrepancies lower than 20% and 10% for the near and far field temperatures, respectively. Whilst close to the flame region the numerical analysis does not match satisfactorily the experimental results, away from the flame region the results are extremely good. This confirms that FDS is a robust tool in determining the smoke spread and its features reasonably away from the fire region.

The results presented in this thesis show that the smoke production and its temporal evolution in terms of smoke filling (smoke layer) may be predicted with some degree of accuracy using simple methods; however, the use of such models to predict the smoke production of a given fire shall be only a first approximation and not a design tool, since among the available models there is a considerable level of uncertainty. This thesis has also highlighted the importance of properly defining the properties when numerically modelling the fire, since small differences in the input data, can generate a major impact on the output. Specifically, it has been found that the proper definition of soot yield is profoundly important, since it has a great impact in determining the visibility through smoke and consequently ASET in an evacuation analysis. Finally, CFD models have shown to perform quite well in reproducing the fire and smoke phenomenon, but they have also shown to significantly depend on the input parameters.

Declaration

This thesis and the work described within have been completed solely by Gabriele Vigne under the supervision of Dr. Cándido Gutiérrez Montes and Dr. Alexis Cantizano González. I would like to thank Prof. Guillermo Rein for his insights and invaluable contribution. Where others have contributed or other sources are quoted, full references are given. This work has not been submitted for any other degree or professional qualification.

Gabriele Vigne

2020

Acknowledgements

I commenced this work while working in the Fire Safety Engineering Industry. One of the main goals of this work was to help professionals to better predict smoke produced by fire in enclosures. I always believed in this work and I am glad that I was finally be able to define some new paths to follow, together with some clear answers.

I have an incredible list of people to thank and I am sure I am missing many of them, please accept my sincere apologize if you are one of them.

First of all, thanks to my first supervisor, Cándido Gutierrez-Montes, for his continuous encouragement, for his set of red ink pens and for believing in me and in this work. I will never forget the first time we met in Santander talking about the Murcia Fire Atrium.

Thanks to Alexis Cantizano, my second supervisor, who highly contributed to get this finalized. Thanks for your gentle support and supervision.

Thanks to Guillermo Rein for his "shadow supervision", for his unlimited positiveness and for his true help.

Thanks to Carlos Martínez Bazán for his Tutorship and help along the whole adventure.

Thanks to Jimmy Jönsson for his continuous support, both technically and personally, and for his true friendship.

Thanks to Jamie Stern-Gottfried for inspiring me into this adventure and to "teach me what I knew" at the time I started with this.

Thanks to Wojciech Węgrzyński for his invaluable help in making this happens.

Thanks to Robert Jönsson, Patrick Van Hees, Daniel Nilsson and Philip Rubini for the great experience I had attending the course “Simulation of Fires in Enclosures” at Lund University many years ago.

Thanks to Björn Karlsson, for being inspirational to me.

Thanks to by brother, Gianluca, who unconsciously or deliberately defined my career in Fire Safety Engineering.

Thanks to Pablo Ayala to involve me in his work and contribute to part of this work.

Thanks to JVVA for giving me the time and resources to complete this. Thanks to Olaf Albano, Valentin, Carola. Thanks to Javier for your priceless help in getting this finalized. Thanks also to Krzysztof and Mateusz.

Thanks to George Faller for believing in me when I started as a young engineer in Arup. Thanks also to Arup for inspiring me. Thanks to Felipe, Javier, Ben, Charles, Philip. Thanks to Barbara Lane and Arup Fire UK. Thanks to Mohammad Tabarra for the great experience in the Tunnel Ventilation group at Arup in London.

Thanks to Orlando Abreu Menendez. Thanks to the whole GIDAI’s team.

Thanks to Kostas, Rocco and the Larch. The Larch.

Thanks to Fernando Vigara, for his passion and dedication to the Fire Safety Engineering society, and for his friendship.

Thanks to Brian Meacham and Chris Jelenewicz, for their support. You were both in Hong Kong back in 2011 in the SFPE Conference when I presented the first insight of what I had in mind. Thanks to Juan Echeverria who was there too, and we have been friends since then.

Thanks to Santos Bendicho and César Pérez for making the Murcia Fire Atrium experiments possible.

Thanks to my father Michele for his continuous example to follow. I would have never imagined following your steps into this field. And I must admit that I am so proud of it.

Thanks to my mother Wilma, for just everything.

Thanks to all my extended family, Miriam, Beatrice, Gianmarco and to my family in law Aurelio, Nadia, Nicola, Marika and Vita.

And finally, but the most important, thanks to my Family, Pamela, Diamante and Gherardo Maria. I am so happy and proud of you. Thanks for giving me a light every day of my life.

Contents

List of Figures

List of Tables

Scholarly Output

Journal Papers

- G. Vigne, C. Gutierrez-Montes, A. Cantizano, W. Węgrzyński, G. Rein, - Review and Validation of the Current Smoke Plume Entrainment Models for Large-Volume Buildings December – 2018 Fire Technology [DOI: 10.1007/s10694-018-0801-4].
- G. Vigne, W. Węgrzyński, A. Cantizano, P. Ayala, G. Rein, C. Gutierrez-Montes - Experimental and Computational Study of Building – 2020 Sent to Scientific Journal and under review.
- W. Węgrzyński, G. Vigne - Experimental and numerical evaluation of the influence of the soot yield on the visibility in smoke in CFD analysis – 2017 Fire Safety Journal [DOI: 10.1016/j.firesaf.2017.03.053].
- P. Ayala, A. Cantizano, G. Rein, G. Vigne, C. Gutierrez-Montes - Fire Experiments and Simulations in a Full-Scale Atrium Under Transient and Axymmetric Venting Conditions – 2015 Fire Technology [DOI: 10.1007/s10694-015-0487-9].

Conference and Magazine Papers

- The design of smoke management systems in complex buildings through the FSE – G.Vigne – SafetyEXPO 2019, Bergamo, Italy, September 19, 2019.
- Fire Safety Engineering in Large and Complex Industrial Buildings - Challenges for Everyone - G.Vigne, J.Jönsson, W.Wegrzynski - 3rd SFPE Europe Conference on Fire Safety Engineering, Malaga, May 21-23, 2019.
- Advanced Simulations for Building Design – Best Practice and Future Developments – G.Vigne, J.Jönsson - Fire and Evacuation Modelling Technical Conference 2016 - Malaga, November 16-18, 2016.
- Experimental and Numerical Analysis of the Influence of the Soot Yield when Conducting CFD Analysis for the Estimation of the Available Safe Evacuation Time – G.Vigne, JVVA Fire and Risk, Spain, W.Węgrzyński, ITB, Poland – Interflam 2016, 4-6th July 2016, Fire Science & Engineering

Conference, Royal Holloway College, University of London, UK [ISBN 978-0-9933933-2-7].

- Novel Full-Scale Atrium Experiments and Numerical Validation Under Steady and Transient Venting Conditions – P.Ayala, A.Cantizano, G.Rein, G.Vigne, C. Gutiérrez-Montes– Interflam 2016, 4-6th July 2016, Fire Science & Engineering Conference, Royal Holloway College, University of London, UK [ISBN 978-0-9933933-2-7].
- Influence of Variability of Soot Yield Parameter in assessing the safe conditions in Advanced Modelling Analysis. Results of Physical and Numerical Modelling Comparison - 11th SFPE Conference on Performance-Based Codes and Fire Safety Design Methods, Warsaw - G.Vigne, W. Wegrzynski, May 25, 2016 [ISBN 978-83-938077-5-8].
- The complexity of smoke control design, theory and practice - G.Vigne, SFPE Europe Magazine, Q1 2015, Issue n.1.
- Modelización de Humos / Smoke Modeling, G.Vigne - 7º congreso internacional de ingeniería de seguridad contra incendios , Madrid 20,21,22 of February 2013, Madrid (Spain).
- Full Scale Fire Tests in Atria And The Use of FSE Methods To Predict The Smoke Layer Interface, G.Vigne - Eurofire 2013, Basel (Switzerland) 9th and 10th of October 2013.
- Uncertainty of Smoke Filling Calculations in a Large Atrium through Comparison to Experimental Results, G.Vigne, C. Gutiérrez-Montes, G.Rein - 9th International Conference on Performance-Based Codes and Fire Safety Design to be held 20-22 June 2012 at the Excelsior, Hong Kong [ISBN 978-1-6227691-8-6].
- Conceptos básicos sobre control de humo en grandes recintos , G.Vigne, C.Gutiérrez-Montes, G.Rein - Spanish magazine Prevención de Incendios, Numero 52, 2011 [ISSN 1575-8915].

Preface

This thesis is written in manuscript format. Although the chapters are not manuscripts on their own, they are loosely based on the following papers:

- G. Vigne, C. Gutierrez-Montes, A. Cantizano, W. Węgrzyński ,G. Rein, - Review and Validation of the Current Smoke Plume Entrainment Models for Large-Volume Buildings December – 2018 Fire Technology [DOI: 10.1007/s10694-018-0801-4]
- G. Vigne, W. Węgrzyński, A. Cantizano, P. Ayala, G. Rein, C. Gutierrez-Montes - Experimental and Computational Study of Smoke Dynamics from Multiple Fire Sources Inside a Large-Volume Building – 2020 Sent to Scientific Journal and unders review.
- W. Węgrzyński, G. Vigne - Experimental and numerical evaluation of the influence of the soot yield on the visibility in smoke in CFD analysis – 2017 Fire Safety Journal [DOI: 10.1016/j.firesaf.2017.03.053].
- P. Ayala, A. Cantizano, G. Rein, G. Vigne, C. Gutierrez-Montes - Fire Experiments and Simulations in a Full-Scale Atrium Under Transient and Asymmetric Venting Conditions – 2015 Fire Technology [DOI: 10.1007/s10694-015-0487-9]

The thesis layout is described below:

Chapter 1 includes a general introduction to the research.

Chapter 2 is devoted to the description of the experimental analyses undertaken in the Murcia Fire Atrium and in the ITB Chamber in Warsaw.

Chapter 3 addresses the review and validation of the current smoke plume entrainment models for large-volume buildings.

Chapter 4 presents a numerical analysis of the influence of the fuel soot yield value on the visibility in smoke.

Chapter 5 presents the results from the simulations of a full-scale atrium multiple fire under transient and asymmetric venting conditions.

Chapter 6 is devoted to the overall conclusions of the investigation and presents proposals for related future research.

1 Introduction

Smoke produced by fire has been studied for decades, but the knowledge we have of smoke as part of the complex fire phenomenon still presents major uncertainties. It is very important to understand the properties of smoke, as well as its formation and behavior, because nowadays smoke represents one of the biggest risks present in the built environment [1]. The risk presented by fire in modern constructions is well known, however, the risk it poses on life safety is mostly due to the smoke it produces [2]. This is why, when designing a building, it is of utter importance to deal with the smoke produced by a potential fire, understanding how the smoke can spread through the building, its effects on the evacuation process, and how it can affect the firefighters when they approach the building to fight the fire and rescue the occupants.

The danger posed by smoke can be understood by explaining its characteristics; how it forms, its composition and what the reason for its toxicity is (see section 1.1). Fire statistics from many countries around the world show that most fire deaths are due to the inhalation of smoke and toxic gases (see section 1.2). For this reason, the correct design of a smoke management system in a building is crucially important. This is a very challenging task, so, in order to facilitate the design, several models have been developed since the 1970s. Some of them consist of equations with only a few parameters and others consist of computational tools capable of generating complex simulations of fire and smoke dynamics. These models have frequently been tested and validated with small-scale experiments and in room-sized compartments. However, very rarely have these models been validated for large-volume spaces. In spite of that, they are nonetheless being used to design smoke management systems for atria and other types of large-volume spaces by fire safety engineers all over the world. Fires and smoke movement in large-volume enclosures present challenges which are very distinct from those for which the mentioned models have been validated (see section 1.3), constituting a source of great uncertainty on the real performance of such designs.

1.1 Smoke properties

NFPA 92B [3] gives the following definition for smoke: "The airborne solid and liquid particulates and gases evolved when a material undergoes pyrolysis or combustion, together with the quantity of air that is entrained or otherwise mixed into the mass". According to this definition, the great majority of smoke consists of air. However, the airborne particulates are responsible for the toxicity of smoke and for the reduction in visibility caused by smoke. This combination of toxicity and obscuration presents the greatest threat to the occupants of a building involved in a fire [4].

Most of the solid particulates contained within smoke are formed as a result of incomplete combustion in localized areas of the gas phase, where the oxygen concentration is not high enough for the reactants (fuel) to undergo complete combustion [1,4,5]. While the products of complete combustion are the stable gases, water vapor and carbon dioxide, the particles that result from incomplete combustion are still combustible [4]. For this reason, smoke is combustible.

1.1.1 Soot production

Under conditions of complete combustion, fuel will be converted into stable gaseous products, carbon dioxide and water, but this is rarely, if ever, achieved in diffusion flames [4]. In a typical fire, mixing of the fuel vapors and air within the flame involves buoyancy-induced turbulent flows in which substantial temperature and concentration gradients exist. In regions of low oxygen concentration such as the fuel-rich core of a large hydrocarbon pool fire, a proportion of the volatiles may undergo a series of pyrolysis reactions which lead to the formation of unsaturated molecular species. Under these conditions, these species can undergo quasi-polymerization reactions to produce aromatic species, the simplest of which is benzene (C_6H_6). Benzene is the precursor of polycyclic hydrocarbons, which in turn grow to produce minute particles of soot within the flame [6–8].

Although the mechanism of soot formation is extremely complex, some of the chemical species involved in the process, which commonly represent intermediate steps in the formation of soot, are shown in Figure 1. All these steps are reversible, and any of the intermediate species may undergo oxidation, although, once formed, the aromatic ‘nucleus’ (a hexagonal ring of six carbon atoms) is remarkably stable at high temperatures and has a degree of resistance to oxidation. Furthermore, it is the presence of soot particles within the flame that gives the diffusion flame its characteristic yellow color and provides the principal mechanism for radiative heat loss.

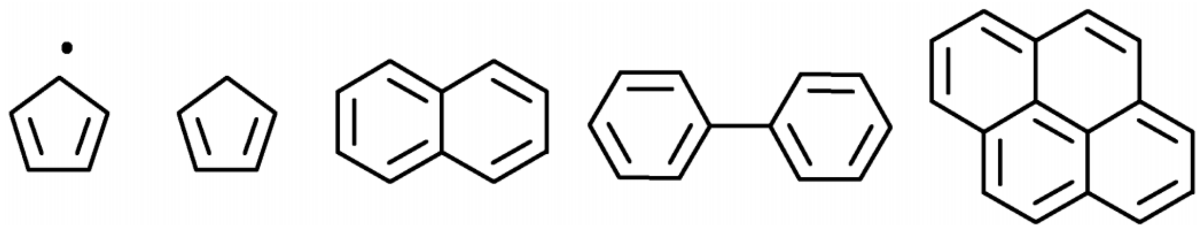

(a) (b) (c) (d) (e)

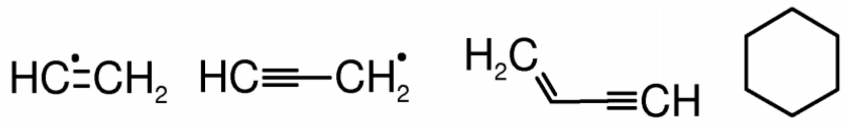

(f) (g) (h) (i)

Figure 1 – Chemical species commonly involved in the formation of soot [9]**.**

(a) Cyclopentadienyl (CPDyl), c-C_5H_5. (b) Cyclopentadiene (CPD), c-C_5H_6. (c) Naphthalene, $C_{10}H_8$. (d) Biphenyl, $C_{12}H_{10}$ (a biaryl). (e) Pyrene, $C_{16}H_{10}$. (f) Vinyl, C_2H_3. (g) Propargyl, C_3H_3. (h) Vinylacetylene, C_4H_4. (i) Cyclohexane, C6H12. A radical is represented by a dot on the structure.

These minute particles (10-100 nm diameter) may oxidize within the flame and be destroyed [10]. However, if the temperature and oxygen concentration are not high enough, they will tend to grow in size and agglomerate to give substantially larger particles which will escape from the flame as ‘smoke’.

Smoke particles are complex agglomerations of minute soot particles which have come together to form chains and clusters, growing to an overall size in excess of 1 µm. When their size becomes of the same order as the wavelength of light (0.3-0.7 µm), they cause obscuration and reduced visibility by a combination of absorption and light scatter [4].

1.1.2 Toxicity

Poor visibility will make it difficult for the occupants to find and navigate through the escape routes, thus increasing the length of time that they are exposed to the combustion products, many of which are harmful to humans. The toxic combustion products of a fire may be subdivided into two groups, asphyxiants (which deprive the body of oxygen) and irritants (which inhibit breathing by stimulating pain receptors in the respiratory tract and can also cause severe eye irritation). The most important asphyxiants are carbon monoxide (CO) and hydrogen cyanide (HCN). Unlike other asphyxiants known to be present, these have been measured in smoke at concentrations sufficient to cause significant acute toxic effects. The toxicity of these products is due to their capacity of reducing the rate at which oxygen is metabolized in the body. Typical irritants that may be encountered are acrolein (CH_2=CH-CHO) and hydrogen chloride (HCl) [4].

1.2 Statistics

The most common cause of death in fires is by inhalation of smoke. In Spain, between the years 2010 and 2017, 48.3% of people who died in fires died overcome by smoke, compared to 37.8% that died due to burns, and only 5.3% that died for other causes (for 8.5% of the deaths, the cause was not identified) [11]. Table 1 shows a summary of yearly statistics of causes of deaths in fires in Spain during this period.

Table 1 – Yearly statistics of causes of deaths in fires in Spain from 2009 to 2017 [11]**.**

Year	Cause of death (%)			
	Overcome by smoke	**Burns**	**Other**	**Unspecified**
2010	38.0	38.6	7.8	15.6
2011	32.4	43.9	2.9	20.8
2012	45.3	50.6	3.5	0.6
2013	44.0	50.0	3.0	3.0
2014	59.3	25.3	3.7	11.7
2015	62.9	21.0	3.5	12.6
2016	63.4	31.4	2.9	2.3
2017	45.3	40.6	12.2	1.9
Total	48.4	37.8	5.3	8.5

Similarly, statistics collected in the USA suggest that more than 50% of all fatalities can be attributed to the inhalation of '(particulate) smoke and toxic gas' [12].

Table 2 presents statistics from the UK. It shows the percentage of deaths for each different cause in every financial year since 2009/2010. The UK statistics have an additional cause category titled “Overcome by smoke and burns”; this accounts for deaths to which it is suspected that both smoke and fire burns contributed.

As it can be seen in Table 2, in the UK, 35.5% of fire deaths were caused by smoke inhalation and 17.6% by smoke inhalation and fire burns, while 25.8% were caused by just fire burns.

Table 2 – Yearly statistics of causes of deaths in fires in UK from 2009 to 2018 [13]

Year	Causes of death (%)				
	Overcome by smoke	**Burns**	**Overcome by smoke and burns**	**Other**	**Unspecified**
2009/10	37.4	27.6	15.3	5.6	14.1
2010/11	36.4	24.5	17.6	7.8	13.7
2011/12	34.3	28.2	16.2	9.2	12.1
2012/13	32.5	32.9	21.4	6.6	6.6
2013/14	41.3	20.3	19.2	6.9	12.3
2014/15	35.0	28.5	17.9	6.1	12.5
2015/16	35.6	20.5	20.1	5.0	18.8
2016/17	38.4	26.2	16.4	4.9	14.1
2017/18	29.6	24.0	15.0	3.9	27.5
Total	35.5	25.8	17.6	6.2	14.9

This collection of fire statistics highlights the importance of smoke management to ensure life safety in fire scenarios since smoke is responsible for most deaths in fire events.

1.3 Smoke management in large-volume enclosures

Smoke management in large-volume enclosures poses separate and distinct challenges from well-compartmented spaces[14]. For the purpose of this thesis, a large-volume space is defined as an uncompartmented space, generally two or more stories in height, within which smoke from a fire either in the space or in a communicating space can move and accumulate without restriction [1]. Without physical barriers, smoke propagation is unimpeded, spreading easily throughout the entire space. In addition, the tall ceiling heights in many large-volume spaces create additional challenges in terms of substantial quantities of smoke production and delayed detection times[15].

When a fire takes place in large-volume enclosures the smoke can travel along vertical distances, affecting multiple floors simultaneously and threatening life safety of occupants far away from the fire origin [1]. Thus, detection, control and extinction of fires in large volumes differ significantly from those in small enclosures.

The distinctive features of large-volume spaces, such as large volume and height, can also be considered as a positive feature. First, due to the increased volume of the smoke reservoir, the time necessary to fill the compartment with smoke is prolonged, and the smoke layer is diluted. Dilution reduces the level of hazard posed by the smoke. Second, due to the available height of the space, less resources might be required to maintain the smoke layer at a tenable height. Finally, due to the typical occupancy of such spaces, the fire threat is limited, although this may not be the case in atria, hotel lobbies and similar spaces, in which large temporary gathering of combustible materials can occur (commercial stands, festive decorations, gathering of luggage, etc.). In large-volume spaces such as warehouses, airports, stations, etc., there is an increasing need of maintaining very large compartments without physical barriers, often due to operational requirements[15].

The design of a smoke management system in large-volume enclosures is of utter importance for life safety, property protection, fire brigade access and business continuity. Despite its importance and the increasing use of CFD models, the design is often performed using basic formulae. Those basic formulae, presented in national codes and design guides, are currently used to design the number of smoke reservoirs, the smoke exhausting system, the makeup air, etc., because it is frequently assumed that the rationale behind the quantification of the prescriptive requirements embedded in building codes is based on previous "good practices" and partial empirical evidence [1]. However, the use of these basic formulae in atria or large-scale construction projects should be carefully examined, as it has not been demonstrated that such specifications in existing codes are supported by systematic research with experimental justifications [16]. Thus, simple correlations should be used only as a first order approximation, helping to the final design in terms of preliminary values and reducing the cost of a more detailed approach. In fact, fire engineers in a building design process should start with an initial assessment using simple methods and gradually continue with the use of more complex methods [17].

Admittedly, the use of performance-based fire engineering design approaches is now a common practice in many jurisdictions. Nevertheless, in some countries, authorities having jurisdiction tend to prefer simplified approaches rather than more complex design methods that use advanced fluid dynamics models. This is because local codes legally authorize those simplified methods and many regulatory authorities do not possess the level of competence needed to assess non-prescriptive design approaches. This results in the refusal to approve engineered designs. Unfortunately, this is leading designers to move away from more specific methods like performance-based designs and towards prescribed criteria [18].

1.4 Problem statement

Smoke produced by fire is responsible for the majority of fire deaths in buildings. Hence, smoke control is vital to ensure fire safety in many buildings. However, it is very difficult to predict the amount of smoke that will be produced and the rate at which specific fires will produce smoke. Research that provides knowledge about the characteristics and development of smoke is very beneficial for the fire safety community.

Due to the complex nature of fire dynamics and smoke formation, scientists and engineers have been developing models of smoke production so that these could be used by fire safety professionals aiming to design smoke management systems. These models are often tested with small-scale tests, and they are rarely tested using full-scale experiments. Nevertheless, more often than not, the behavior of a fire in a large compartment cannot be predicted from the behavior of a fire in small-scale experiments.

In addition, each model has its range of applicability; however, these are not always well defined, and some professionals use them in situations for which they have not been validated. Producing full-scale experimental data and using them to validate and define ranges of applicability, is necessary to determine the appropriateness of the models being used by the fire safety community.

1.5 Aim and objectives

This doctoral thesis aims to study in depth the characteristics of the fluid and thermal fields of smoke produced by fires in confined spaces. Having a deeper knowledge of these characteristics will make it possible to optimize the numerical modeling of the fire phenomenon in these types of constructions. In order to achieve this aim, the following series of objectives was set:

- Produce a set of brand new full-scale tests in order to better understand smoke produced by fire, its properties and its development through time.
- Generate a complete and robust set of experimental data.
- Validate commonly used plume correlations with new experimental data.
- Assess the suitability and applicability of the plume correlations for large-volume spaces such as atria. As a result, it will be determined which correlation is the most suitable and which is the least suitable for use in large-volume spaces.
- Determine the most influential parameter of smoke in the determination of visibility through smoke.
- Determine how critical the soot yield is for the development of visibility through smoke and for the determination of the ASET in a building.
- Use new experimental data to validate CFD software.

1.6 Summary of the chapters

Under the aforementioned conditions, the next chapters address the issues highlighted in order to give response or shed some light on the questions raised.

Section 2 provides a detailed description of the fire experiments undertaken for this thesis. First, the facilities that were used for the experiments are described in detail, starting with a description of the Murcia Fire Atrium in Spain. Then the three series of experiments carried out in the Murcia Fire Atrium are described, considering the measurements' procedure in each test, as well as the purpose of each series. Section 2 also includes the description of the ITB research center in Poland, i.e. the characteristics of the center and the experimental setup, and it concludes with a description of the different fire tests that were conducted in these facilities, as well as of the parameters that were measured during these experiments.

Section 3 considers the suitability and applicability of four plume entrainment correlations, included in most of the fire safety codes and regulations, to properly predict the fire induced conditions within large volumes. This is achieved by comparing the experimental data obtained from the three series of experiments performed in Murcia to the results given by the plume entrainment correlations.

Section 4 explores the effect that different values of soot yield have on the visibility through the smoke. The results from the large-scale experiments carried out in the ITB installations in Warsaw are analyzed and discussed. First, the importance of visibility in smoke for fire safety design and evaluation is revised. Subsequently, the impact of the soot yield value on the visibility is characterized. Additionally, section 4 includes a comparison between the experimental results and simulations performed with CFD tools, where the two most commonly used CFD codes for fire safety engineering are validated and the experimental results are reinforced.

Section 5 consists of the validation of a CFD modelling tool, Fire Dynamics Simulator (FDS), the most commonly used in the fire community, under transient, complex conditions. Thus, simulations of multiple fires in a full-scale atrium under transient and asymmetric venting conditions are included and compared with the experimental results given by the third series of experiments carried out in the Murcia Fire Atrium.

Finally, section 6 is devoted to the conclusions of the present thesis, where a compilation of the overall findings is presented. Section 6 also incorporates several suggestions of topics on which future research projects could be based, and that would build on the findings of this thesis project.

2 Experimental set-ups and analysis

The generation of a robust comprehensive set of experimental data of full-scale fire tests constitutes one of the most important contributions of the present thesis. This is achieved through complementation of the experiments conducted by Gutiérrez-Montes et al. [19] in 2008 and then by Ayala et al. [20] (including the author) in 2013 on full-scale atrium fires and through the generation of a new series of experimental data on fire soot yield and visibility.

Thus, large-scale experiments were performed in the Murcia Fire Atrium, in Murcia, Spain, and in the Building Research Institute (ITB), in Warsaw, Poland, with the aim of better understanding the fluid dynamic characterization of smoke produced by fires in enclosures. In the Murcia Fire Atrium, large-scale experiments with heptane pool fires were performed with HRR varying from 1.43 MW up to 5.30 MW, including a peculiar 4 pools fire. On the other hand, in the ITB facility, different fuels were used with much smaller fires – ranging from 130 kW to 160 kW.

2.1 Fire Atrium of the Centro Tecnológico del Metal (CTM) [15]

As it has been previously commented, in addition to the generation of new full-scale experimental data, one of the purposes of the experiments carried out in Murcia was the study of the suitability and applicability of the traditional plume models to predict and describe the evolution of the layer of smoke that develops under the ceiling when there is a fire in a compartment. To this aim, results from full-scale experiments were compared with the predictions from the different empirical formulae derived by Thomas [21], Zukoski [22], Heskestad [23] and McCaffrey [24]. This study is included in section 3.2. Moreover, another purpose of the experiments carried out in Murcia was to compare the results with predictions obtained from CFD tools, in order to validate the latter. Therefore, several large-scale fire experiments, with HRR varying from 1.43 MW up to 5.30 MW under different exhaust flow rates and make-up air supply configurations were performed. The following subsection describes in detail the experimental setup, as well as the dimensions and characteristics of the Murcia Fire Atrium.

2.1.1 Experimental Setup

The experimental facility that has been used to perform the large-volume enclosure fire experiments is the Fire Atrium of the Centro Tecnológico del Metal (CTM), in Murcia, Spain. Figure 2 illustrates the geometry of the facility and includes a photograph. The unique characteristics of the Fire Atrium make it an ideal facility for this kind of research [15,19,25,26].

(a) **(b)**

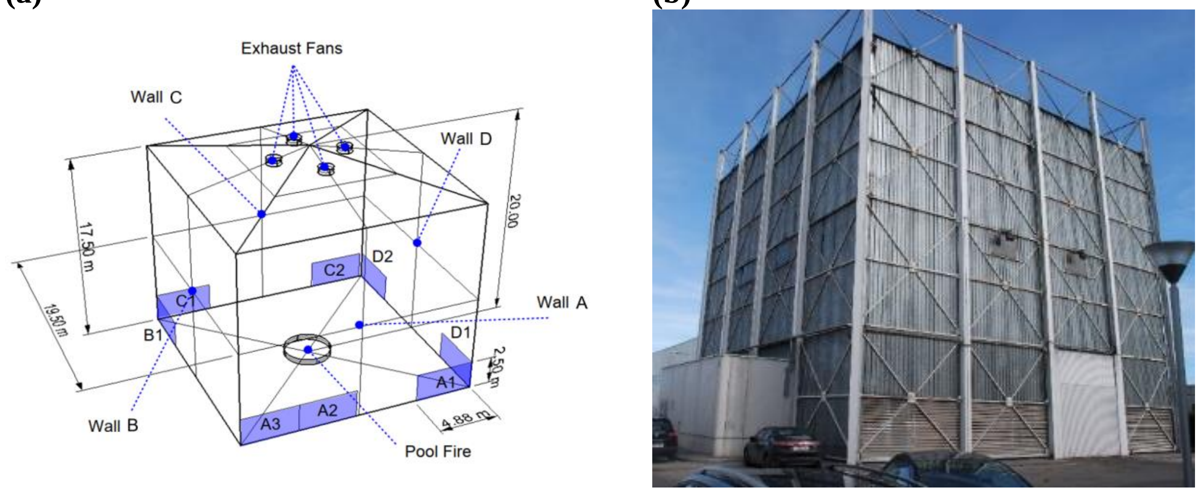

Figure 2 – Geometrical sketch (a) and Photo (b) of the Fire Atrium of the Centro Tecnológico del Metal, Murcia, Spain.

Both the walls and the roof are made of steel sheets with a thickness of 6 mm. The floor is made of concrete. The atrium is provided with inlet air on each side and four exhaust fans installed on the roof - see Figure 4a. The make-up air flows through eight identical grilled vents arranged at the lower parts of the walls whose dimensions are 4.88 x 2.5 m². Those vents can be partially or fully opened, or completely closed[15]. The open area of each vent can be controlled by covering part of their section with 1 mm thick steel sheets - see Figure 5.

(a) **(b)**

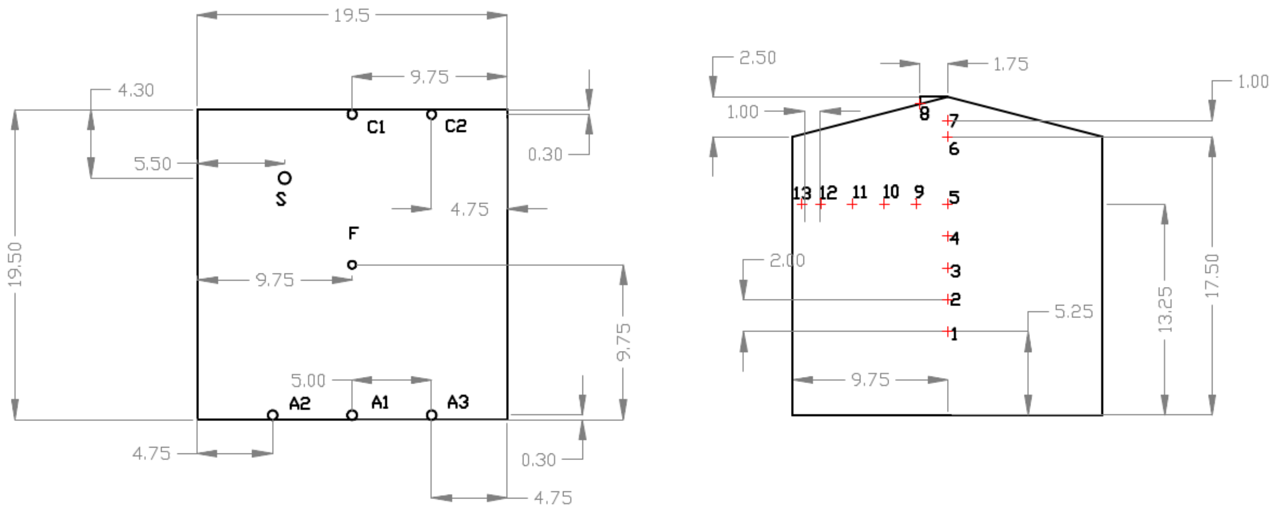

(c) **(d)**

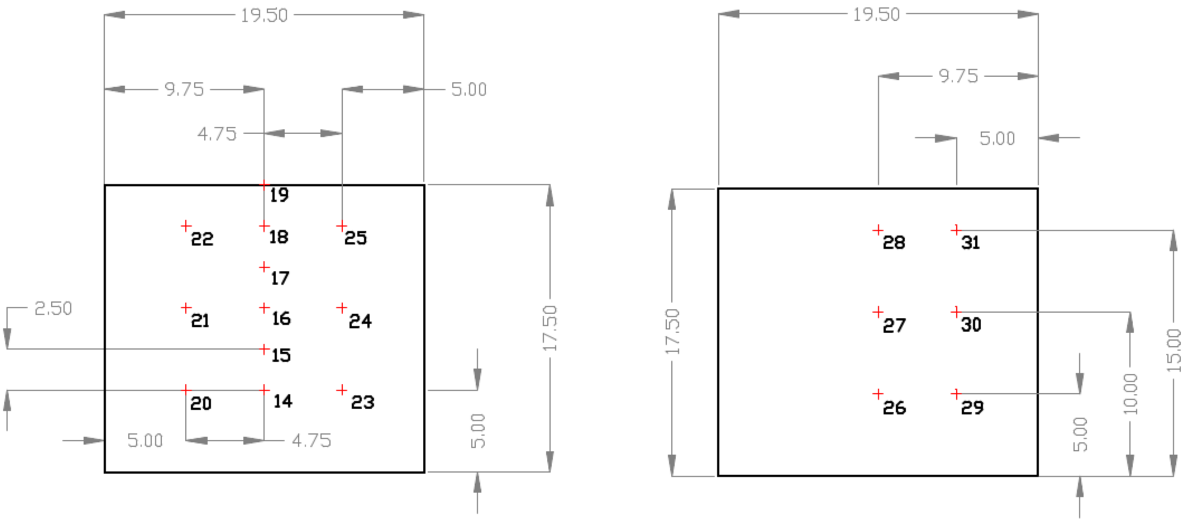

Figure 3 – Thermocouple layout in the Fire Atrium. (a) Top view showing the thermocouple tree locations; thermocouple locations at (b) central section, (c) section at 30 cm away from wall A, and (d) section at 30 cm away from wall C [25]**. In (a), thermocouple locations are represented as near wall A (A1, A2), near wall C (C1, C2), vertical line over central fire (F), and smoke layer tree (S). Single thermocouples are numbered in figures (b) to (d).**

(a) **(b)**

Figure 4 – Fans installed on the roof (a) and one of the pools used for the tests (b).

(a) (b)

Figure 5 – Make up air vents, during the set up (a) setup of vent A and (b) setup of vent B.

The fire experiments were carried out in four different periods. In all of them heptane was used as burning fuel, contained in circular steel pans of different diameters. In all experiments, a layer of 2 cm of water was added to the pan before the heptane was poured to insulate the metal from the burning pool heat, thus providing a more stable steady burning regime. At the end of each experiment the volume of water was measured again to confirm that no water had been lost. Each pool size showed a different burning time proportional to the initial volume of fuel in the pan. A full description of the experiments can be found in [15,19,25,26]. The atrium was equipped with temperature, pressure and velocity sensors, in order to study the thermal and flow fields induced by the fire. Initially, up to 61 sensors were installed. Measurements of walls and roof metal temperature, and air temperature at several locations (i.e. next to walls A and C, at a central section, through the exhaust fans and through the inlet vents) were recorded. Differential and absolute pressure sensors at the exhaust fans have been also installed to check from the fan performance curves the mass and volume flow rate evacuated[15]. Along the years, some sensors have been included or removed, although the configuration has been preserved. Figure 3 shows the thermocouple layout used in the last series of experiments.

2.1.2 First series of experiments (#MX)

Several experiments were performed by C. Gutiérrez Montes et al. [26]. Three of them have been studied (herein referred to as experiments #M1-3), having all the same pan diameters of 0.92 m (therefore having similar HRRs), filled with n-heptane and with the same extract rate and similar overall ambient conditions. The smoke layer interface was extrapolated from the vertical temperature profiles using the N-percent method [15][27]. In large-volume spaces with a relatively small fire, temperature rise of smoke is relatively low. Therefore, the smoke layer interface was determined at the position where the temperature rise started to be larger than 30% of the highest temperature rise along the vertical direction. A summary of the experimental data utilized in this analysis can be found in Table 3.[15]

Table 3 – Summary of laboratory and ambient conditions during the set of fire experiments #MX.

Parameter	#M1	#M2	#M3
Pool diameter (m)	0.92	0.92	0.92
Pool area (m^2)	0.665	0.665	0.665
Fuel volume (l)	44	52	52
Burning time (s)	837	883	1094
Extract rate (m^3/s)	15.2	15.2	15.2
Temperature (°C)	16.7	28.9	27.5
Pressure (mbar)	1018	1008	1007
Calculated average HRR (MW)	1.58	1.77	1.43
Open vents	A1,A3,C1,C2	A1,A3,C1,C2	A1,A3,C1,C2
Free Area of Open Vents (m^2)	48.8 (4x12.2)	48.8 (4x12.2)	48.8 (4x12.2)
HRRPUA (kW/m^2)	2377	2661	2150

The main objective of the experiments was to get a set of new brand full-scale tests in order to better understand smoke produced by fire.

2.1.3 Second series of experiments (#GX)

Several experiments were performed later in the same facility, out of which three were chosen as relevant to this study based on the size of fire and ventilation conditions (referred further as experiments #G1-3). In these experiments the source of fire were pans filled with n-heptane with two different dimensions – 0.92 m and 1.17 m. The atrium was equipped with a total of 59 thermocouples distributed at different positions to measure the smoke temperature in the fire plume as well as close to the walls. Additionally, three load cells were installed under the pool fire to measure the mass loss rate and determine the HRR of the fire. A summary of the experimental data utilized in this analysis can be found in Table 4.[15]

Table 4 – Summary of laboratory and ambient conditions during the set of fire experiments in #GX.

Parameter	#G1	#G2	#G3
Pool diameter (m)	1.17	0.92	1.17
Fuel volume (l)	36.5	28.8	36.5
Burning time (s)	647	708	671
Extract rate (m^3/s)	18.3	18.3	18.3
Temperature (°C)	18	20.1	18
Pressure (mbar)	1016	1016	1016
Calculated average HRR (MW)	2.30	1.70	2.30
Open vents	A1,A3,C1,C2	A1,C1	A1,A3,C1,C5
Free Area of Open Vents (m^2)	48.8 (4x12.2)	48.8 (4x12.2)	48.8 (4x12.2)
HRRPUA (kW/m^2)	2199	2559	2199

While during each experiment from the first series of experiments just three measurements of the smoke layer height were taken (i.e. the time at which the layer height was 5 m, 10 m, and 15 m), several more measurements were taken during this second series of experiments. This allowed the use of the least squares method to determine the smoke layer boundary. Consequently, having more frequent measurements of the smoke layer height provided a more detailed analysis of the smoke layer evolution. [15]

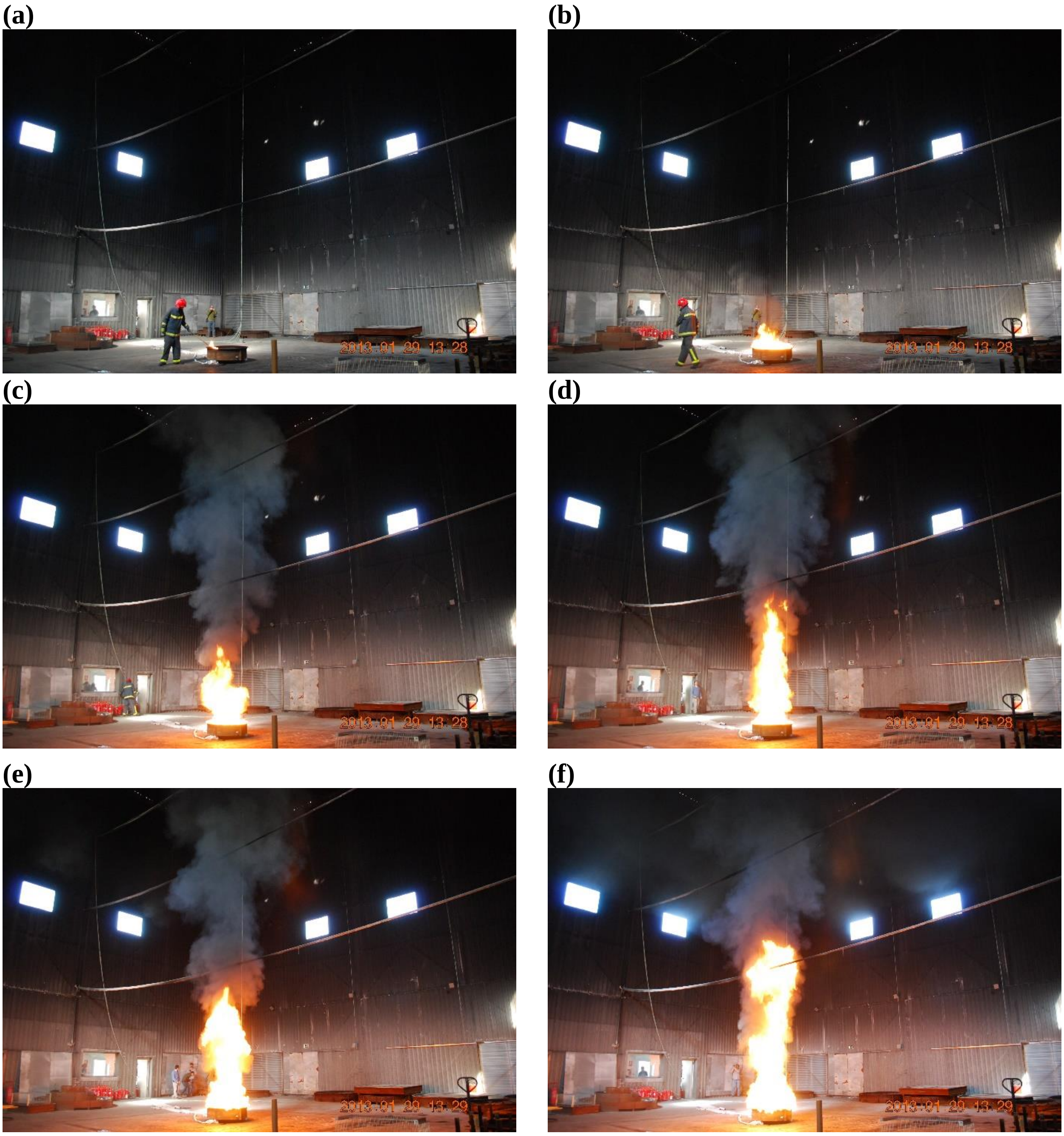

Figure 6 – Evolution of the fire in one of the #GX tests in the first 60s from the ignition.

2.1.4 The experiment with four sources of fire (#4FX)

Among the experiments performed in the last testing campaign in the Fire Atrium, the 4 Fires experiment was carried out (further referred to as #4FX). As previously mentioned, experimental data exist of single fires in large compartments, but little information exists about experiments performed with different fires, igniting at different times, with different plumes contributing to the same smoke layer. Four (4) pans with a diameter of 0.92 m were filled with n-heptane. Pan 1 ignited at the reference time of 0 s, pan 2 at 116 s, pan 3 at 236 s and pan 4 at 296 s. Figure 7 shows the position of the pans and the sequence of ignition (pan 1 the first to be ignited and pan 4 the latest). The experimental conditions are included in Table 5.

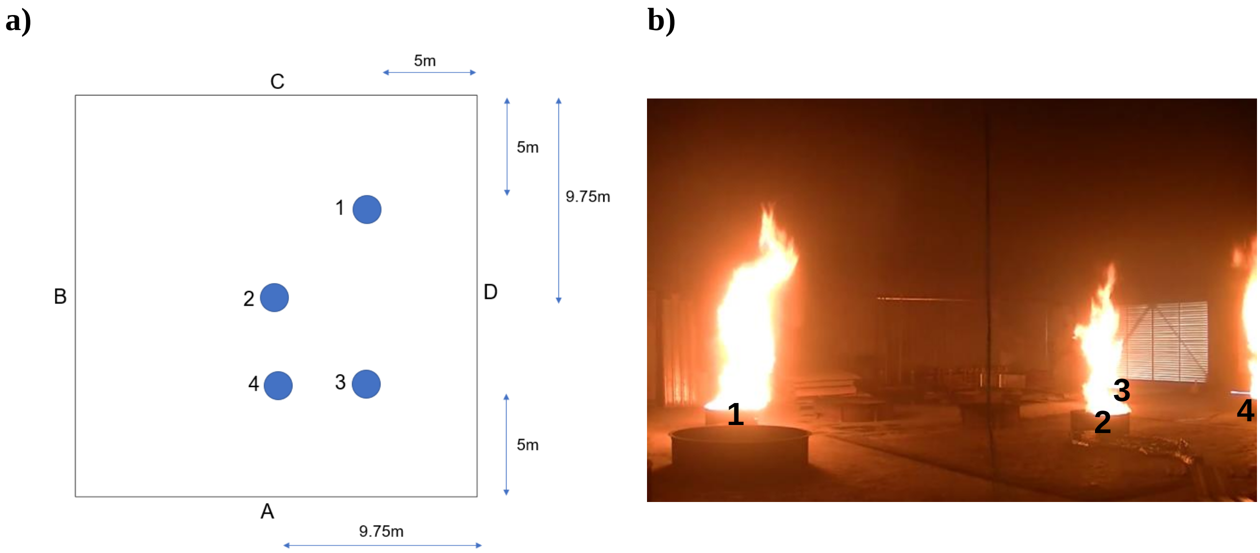

Figure 7 – Test #4FX: (a) sketch of the pan position, and (b) photo of the fires during the experiment.

The smoke layer interface was determined using the least squares method on the results given by the thermocouple tree [20,28]. As commented before, the temperature was measured by means of vertical trees, at the central section of the atrium, at a distance of 0.3 m from the walls A and C, and close to one of the diagonals of the facility. Moreover, five thermocouples were located at a height of 13.25 m but at different distances from the center, and another one under fan B. [15,20].

Table 5 – Summary of laboratory and ambient conditions during the set of fire experiments in #4FX.

Parameter	Fire1	Fire2	Fire3	Fire4

Pool diameter (m)	0.92	0.92	0.92	0.92
Fuel mass (kg)	18.8	12.0	14.1	14.2
Burning time (s)	662	488	730	783
Extract rate (m^3/s)	18.4 (0 to 360s), 27.6 (360s to end)			
Temperature (°C)	14.5			
Pressure (Pa)	101794			
Calculated average HRR (MW)	5.22			
Open vents	A1+A3+C1+C2 (each at 50%)			

The results of this experiment are disclosed in chapter 0, as well as the discussion and the conclusions that were drawn from these results.

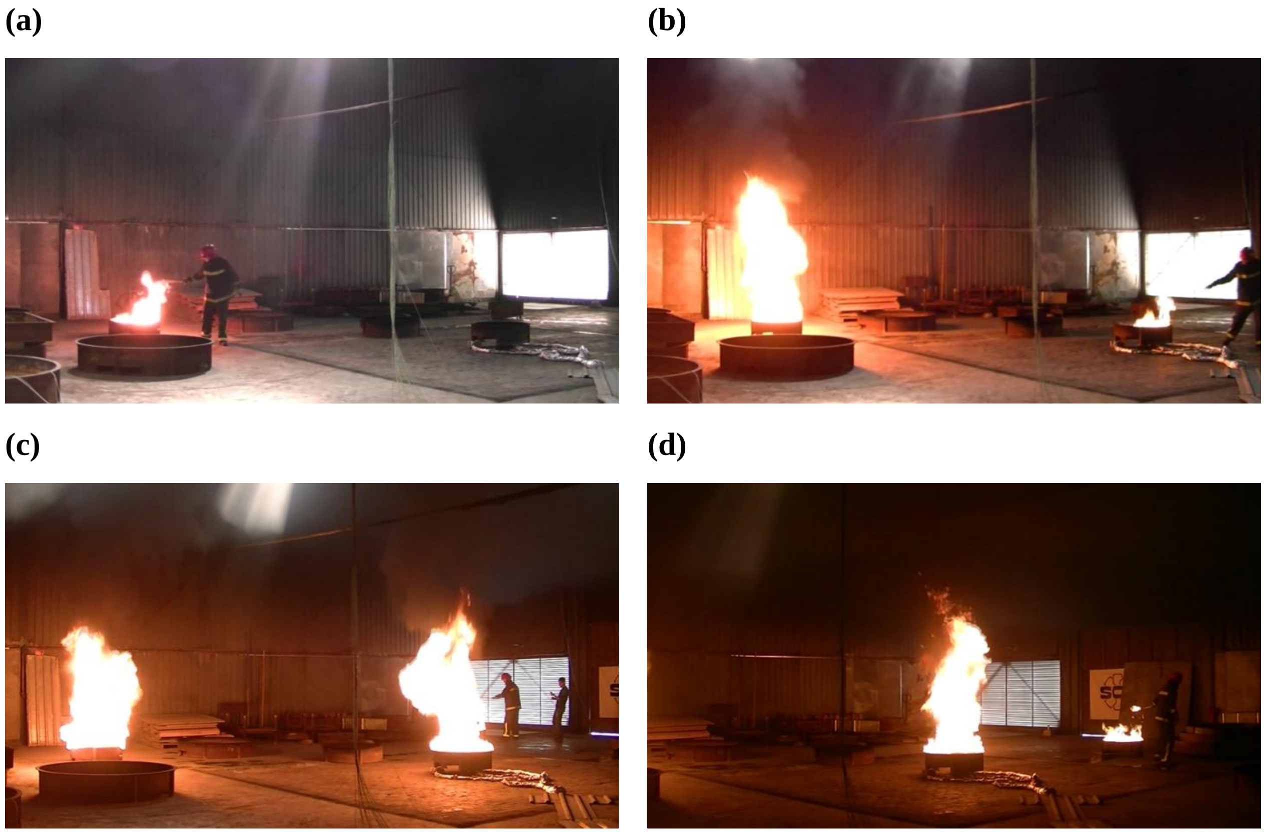

(e)

Figure 8 – Sequence of test #4FX showing the ignition of each pool fire (a-d) and when full regime is reached – i.e. all pool fire burning (e).

2.1.5 Additional experiments (#5)

Additionally, two full-scale fire experiments considering only one fire source placed at the center of the base and HRR of 5.2 and 5.3 MW (further referred to as #5_1 and #5_2, respectively) were conducted to complement results from #4FX. Table 6 shows the experimental and atmospheric conditions for these experiments.

Table 6 – Summary of experimental and ambient conditions during the set of fire experiments #5_1 and #5_2

Variables	#5_1	#5_2
Pool diameter (m)	1.67	1.67
Fuel mass (kg)	71	73
Burning time (s)	558	565
Extraction rate (m^3/s)	18.4	18.4 (0 to 270 s), 27.5 (270 to 360 s)[1]
Ambient temperature (ºC)	11.0	16.7
Pressure (Pa)	102022	102191
Calculated average HRR (MW)	5.2	5.3

Open vents	A1+A3+C1 +C2	A1+A3+C1+C2

1: Fans A, C: 4.6 m^3/s (0 to 270 s), 9.2 m^3/s (270 to 360 s). Fans B, D: 4.6 m^3/s

2.1.6 Calculation of the smoke layer height

Two different smoke layer computation methods have been used to determine the smoke layer from the thermocouple measurements, more specifically from the thermocouples near the walls A and C in tests #MX and the thermocouple tree placed at the diagonal of the atrium in tests #GV and #4FX, respectively: the N-Percentage method [29] and the least-squares method [20,28].

2.1.6.1 N-Percent method

In order to estimate the smoke interface position, Cooper at al. [29] defined a rule to be used with thermocouple arrays. This rule considers that at a specific time into a test run one computes a reference upper layer temperature difference $\Delta T_{ref}(t) = \max [T(z_{top}, t)] - T_{amb}(z_{top})$ where T(z, t) is the temperature at elevation, z, and time, t; z_{top} is the elevation of the top thermocouple, and max [T(z, t*)] is the maximum value of T(z, t) in the time interval $0 \leq t \leq t^*$. Then by the N percent rule the interface is defined as passing the elevation z_i,(t) at that time t when z_i, first satisfies

$$T(z_i,t) - T_{amb}(z_i) = \Delta T_{ref}(t) /100. \qquad (1)$$

2.1.6.2 Least Squares method

The least squares method, applied to the smoke temperature, determines the smoke layer interface in a way so that the deviations of the temperatures within each layer with respect to the mean temperature of each layer are the minimum possible. T_L and T_U (K) are the mean temperatures of the lower layer and upper layer respectively. They can be calculated using the following equations:

$$T_L = \frac{1}{H}\int_0^H T(z)dz \tag{2}$$

$$T_U = \frac{1}{H_T - H}\int_H^{H_T} T(z)dz \tag{3}$$

where H is the height of the layer interface (m), H_T is the height of the ceiling (m), z is a height measured from the floor (m) and T(z) is a temperature measured at a certain height above the floor (K).

The deviation of the temperature measurements within the lower layer with respect to T_L can be calculated using the following equation:

$$\sigma_L = \frac{1}{H}\int_0^H [T(z) - T_L]^2 dz. \tag{4}$$

The deviation of the temperatures within the upper layer with respect to T_U can be calculated using the following equation:

$$\sigma_U = \frac{1}{H_T - H}\int_H^{H_T} [T(z) - T_U]^2 dz. \tag{5}$$

The least squares method aims to find the smoke layer interface where the sum of these two deviations is the minimum

$$\sigma_T(H) = \frac{1}{H}\int_0^H [T(z) - T_L]^2 dz + \frac{1}{H_T - H}\int_H^{H_T} [T(z) - T_U]^2 dz. \tag{6}$$

$$\sigma_T(H_i) = min[\sigma_T(H)]. \tag{7}$$

where $\sigma_T(H)$ is the total deviation depending on the height of the layer interface and H_i is the height of the layer interface as determined by the least squares method (m).

2.2 Experiments at the Building Research Institute (ITB) in Warsaw, Poland

Full-scale fire tests were performed in the Building Research Institute (ITB) in Warsaw, Poland, to better study the impact of soot yield on visibility. The test facility includes a room with base cross-section of 10 x 10 m and a height of 4 m, equipped with a mechanical smoke exhaust system. Figure 9 shows different views of the test chamber and Figure 10 presents the images from the experiments performed. Results of the experiments are reported in chapter 0, along with the results from the numerical studies.

a) **b)**

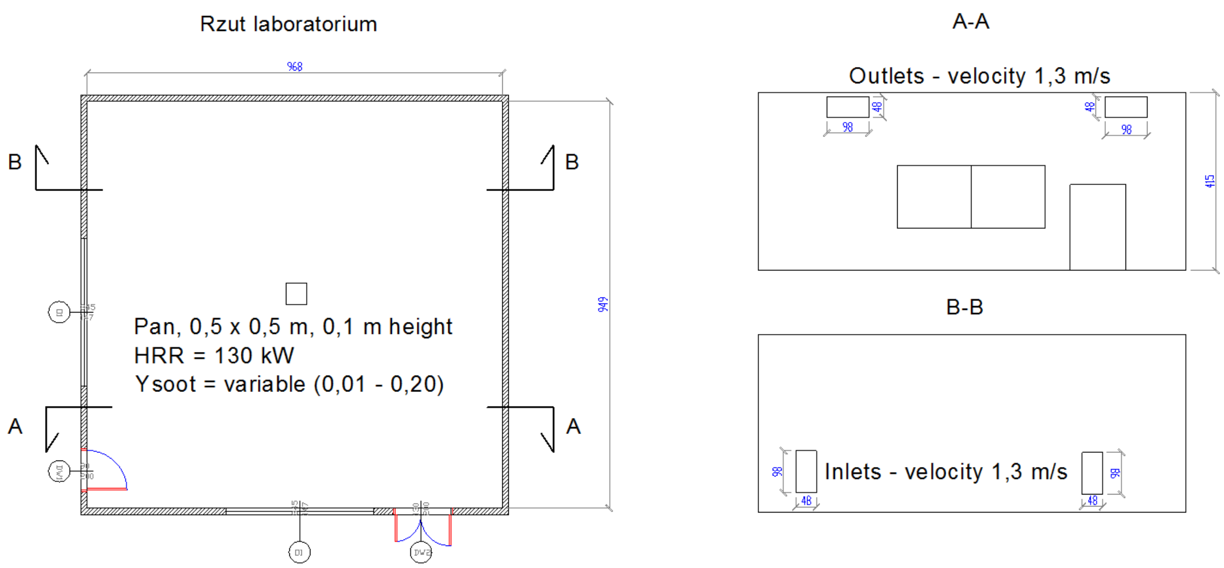

Figure 9 – Configuration of the test facility a) plan view of the chamber b) cross section of the chamber.

Previous experiments have demonstrated that a state of equilibrium was achieved in the chamber for fires with HRR ranging from 130 to 160 kW and approximately 2.00 m in diameter. This indicates that the same amount of smoke that enters the smoke layer is exhausted, so the height of the layer remains stable.

The latter is exploited to measure the obscuration within the smoke layer in longer time-span (close to a steady-state measurement in a homogenous smoke layer). Thus, different fires were examined, using fuels with a high diversity of soot yield values, varying from Y_s = 0.001 g/g to Y_s = 0.178 g/g, Figure 10 to Figure 13, measuring the density of the smoke layer with an optical densitometer. The following materials were chosen as burning fuels for assessment [5, 29]:

- Methyl alcohol (methanol), Ys = 0.001 g/g.
- Propyl alcohol (propanol), Ys = 0.015 g/g.
- Heptane, Ys = 0.035 g/g.
- Toluene, Ys = 0.178 g/g.

Figure 10 –ITB test chamber during each of the tests performed - Methanol, Y_s = 0.001 g/g

Figure 11 –ITB test chamber during each of the tests performed - Propanol, Y_s = 0.015 g/g

Figure 12 – ITB test chamber during each of the tests performed - Heptane, Y_s = 0.035 g/g

Figure 13 – ITB test chamber during each of the tests performed - Toluene, Y_s = 0.178 g/g.

3 Smoke Plume Entrainment Models for Large-Volume Enclosures

The design of smoke management systems in large-volume enclosures is of utter importance for life safety, property protection, and business continuity in case of fire. Despite the recent international trend in smoke control design towards the use of advanced fire models and performance-based codes, simple plume entrainment correlations are the basis of the discipline and are still a common practice, since they are often incorporated in technical documents for the design of smoke control systems. Different plume entrainment correlations have been developed over the years and are cited in different national codes and design guides [15]. These correlations have been widely investigated for fires in small enclosures, but their applicability and accuracy in large enclosures is not clear[15].

The present chapter studies the suitability and applicability of these approaches to properly predict the fire induced conditions within large volumes. Therefore, results obtained from the most commonly used plume entrainment correlations have been compared with full scale experimental data in an 8.000 m^3 enclosure[15]; these data were obtained from the experiments carried out in the Murcia Fire Atrium, as described in section 2.1.

As it well be demonstrated next, based on the results obtained by this analysis performed in a large-volume enclosure, the current correlations used to model fire and determine the smoke produced by the fire might not be suitable for these kinds of constructions.

3.1 Smoke control design and plume models

Engineers have a number of options available for evaluating the performance of a smoke management system. Depending on the jurisdiction, different design guides are used. The methods indicated in codes and design guides are usually empirical entrainment correlations, most of them originated from the plume[15] theoretical models of Yih [31], Morton et al. [32], and Yokoi [33]. These approaches have been improved in other studies through full-scale and reduced-scale fire experiments, as described in section 3.3. The resulting plume models are subsequently integrated as part of zone models. A summary of the research and practical recommendations on the use of such plume models can be found in [34]. The aforementioned plume models consider free axisymmetric smoke plumes. Further development of simple mathematical correlations describing the flow of smoke included the interaction of the plume and the building features, in form of adhered plumes [35–38], window plumes [39], and balcony spill plumes [40–45]. A thorough review of literature referring to complex flow of smoke in buildings can be found in [46]. In general terms, most correlations characterize the flow of smoke in a thermal plume as a function of three basic parameters: height of the plume (z, h), which is assumed to correspond with the height of the smoke-free layer; mass flow of the smoke in the plume ($\dot{m}_p$); and the temperature of the smoke in the plume (T_p), which is sometimes presented as the difference between ambient and plume temperature (θ). Additionally, some plume correlations consider also other parameters such as the flame height (L) or a virtual point of origin (z_o) in order to account for the flame region entrainment, which differs from the entrainment into the plume[15].

The importance of such plume models relies on the fact that they are often incorporated in technical documents for the design of smoke control systems, as a useful tool to dimension the fire protection system. Some of these documents are design guidelines or recommendations, and some of them are national guides that are considered to be the only ones valid in a given country[15].

Under the above conditions, it may happen that the same engineer needs to make similar calculations in different countries encountering a non-homogenous approach to the smoke modelling. Given the fact that every country has its history and traditions, methods used in one country may be questioned by authorities in another. As a result, there is not a single plume model used universally. Nevertheless, the most popular plume models used in design are the so-called Thomas (section 3.2.1) and Heskestad (section 3.2.4) plumes[15]. A summary of the approaches used in a wide range of chosen countries is shown in Table 7.

Table 7 – Plume models used in chosen codes and design guidelines

Code or design guide	Type	Country of origin	Plume entrainment correlations (relevant section of the paper)
NFPA 92 [47]	national code	USA	Heskestad (3.2.4)
EN 12101-5 [48]	international code	EU	Thomas (3.2.1) and Heskestad (3.2.4)
TM19 [49]	design guideline	UK	Heskestad (3.2.4), Thomas (3.2.1) as an alternative
NBS S21-208-1 [50]	national code	Belgium	Thomas (3.2.1)

BRE 368 [51]	design guideline	Europe	Thomas (3.2.1), Zukoski (3.2.2)
BS 5588-7 [52]	design guideline	UK	Redirect to BS EN 12101-5 [48]
BS 9999:2017 [53]	national code	UK	Redirect to BS EN 12101-5 [48]
AS 1668.3-2001 [54]	national code	Australia	Thomas (3.2.1)
Handbook of Smoke Control Eng. [2]	design guideline	USA	Heskestad (3.2.4)

As it has been previously commented, more advanced approaches include time-integration of the plume equation, in order to obtain the smoke layer height in the compartment as a function of time [51, 55]. Despite the dominant role of CFD calculations in the modern design process, zone models are still a valuable tool [17], and they are widely used for specific cases that lie within the limits of the empirical correlations on which they are based – such as the design of nuclear power facilities [56], warehouses (applying the empirical correlations to single smoke reservoirs), different types of atria, stadiums, etc[15].

Zone models [57] are simple models that divide the considered fire compartments into distinct gas zones (upper and lower layers), where the conditions in each zone are assumed to be uniform. The theoretical background of zone models is the conservation of mass and energy in fire compartments. After the ignition, the fire plume as a source of energy and mass is formed. It acts as a “pump” of mass from the lower zone to the upper zone [21, 34]. The zone modelling of compartment fires is more detailed, compared to that in parametric fires and time equivalence methods. As zone models were designed to enable transient evaluation of fire in a single (or series of) enclosure, they use time-integration of plume equations to predict the parameters of smoke layer in a prescribed domain. In many of the zone models available it is possible to choose different plume entrainment correlations, e.g. Heskestad and McCaffrey in CFAST, Heskestad, McCaffrey, Thomas and Zukoski in Ozone, or McCaffrey and Delichatsios in BRANZFIRE (see Table 8). This flexibility of zone models results in a great variety of results that not always help to find the right answer for a given scenario[15]. A comprehensive review of zone modelling of fire may be found in [58,59].

Table 8 – Plume correlations used in some important zone models.

Model	Author	Country	Plume entrainment correlations (relevant section of the thesis)
CFAST [60]	NIST	USA	Heskestad (3.2.4), McCaffrey (3.2.3) – removed in v7.0.0. (2015).
Ozone [61]	University of Liège	Belgium	Thomas (3.2.1), Zukoski (3.2.2), McCaffrey (3.2.3), Heskestad (3.2.4).
BRANZFIRE [62]	Branz	New Zealand	McCaffrey (3.2.3), Delichatsios.
B-RISK [63]	Branz	New Zealand	McCaffrey (3.2.3), Heskestad (3.2.4).

Comparison of plume correlations and of some design approaches in which they are implemented have been widely reported in the literature [55,64–68]. However, despite the profuse amount of studies, only few compare the modelling approaches with large-scale fire experiments. This is mainly due to the lack of high-quality experimental data. Large-scale fire experiments are essential in order to properly validate numerical models, given the fact that those models (in the present context the algebraic formulae) are normally the result of scaled experiments or experiments performed under particular conditions and extremely small fires[15].

Thus, with the intent of further understanding the aforementioned numerical models, they have been compared with large-scale fire experiments that have been described in Section 2, with HRR varying from 1.43 MW up to 5.3 MW, under different exhaust flow rates and make-up air supply configurations, with the smoke layer interface as the main outcome, both for the experimental and numerical analysis.

3.2 Plume entrainment correlations

In the following sections, the most relevant plume entrainment correlations will be presented and discussed, including how the convective HRR fraction is treated in them and how the time integrated approach was used in determining the smoke filling. A direct comparison between these models is difficult (when possible) due to the underlying theory behind them and the different treatment of important variables, such as HRR or the smoke layer interface height. Also, these models were validated with different experiments, considering different scales, and have different assumptions, which define their range of applicability[15].

In case of large-volume enclosures, the differences in the treatment of smoke layer height, which can also be considered as the difference in the calculation of air entrainment into the plume, can be very significant. The aforementioned reasons make necessary the validation of the plume entrainment correlations using large-scale experimental data.

The buoyant axisymmetric plume, generated by a diffusion flame formed above a burning fuel, is the most commonly used plume in fire safety engineering. An axis of symmetry is assumed to exist along the vertical centerline of the plume, and air is entrained horizontally from all directions [67,69] - see Figure 14. The assumption of central symmetry of the plume requires that there are no sources of disturbance to the plume (such as walls), that the fire source is uniform and that there are no air flows near the plume. Considering Cetegen et al. [70,71], the experiments behind the fire plume theory were done in the quiet atmosphere of a laboratory, and small ambient disturbances could provide a significant (20-50%) increase in the measured plume mass flows. Such conditions may be met only in the laboratory, where the experimental chamber is symmetric, and the sources of disturbance are under control[15].

Moreover, in the design of smoke control systems in atria, perfect plume symmetry may be difficult to achieve. However, in some cases where the air inlets are sufficiently large, thus not generating strong streams of air, and the potential fire sources are located far away from walls, plume symmetry is achievable. In such conditions, the spatial location of the plume in the compartment will not affect the dimensioning of the smoke control system [15,72].

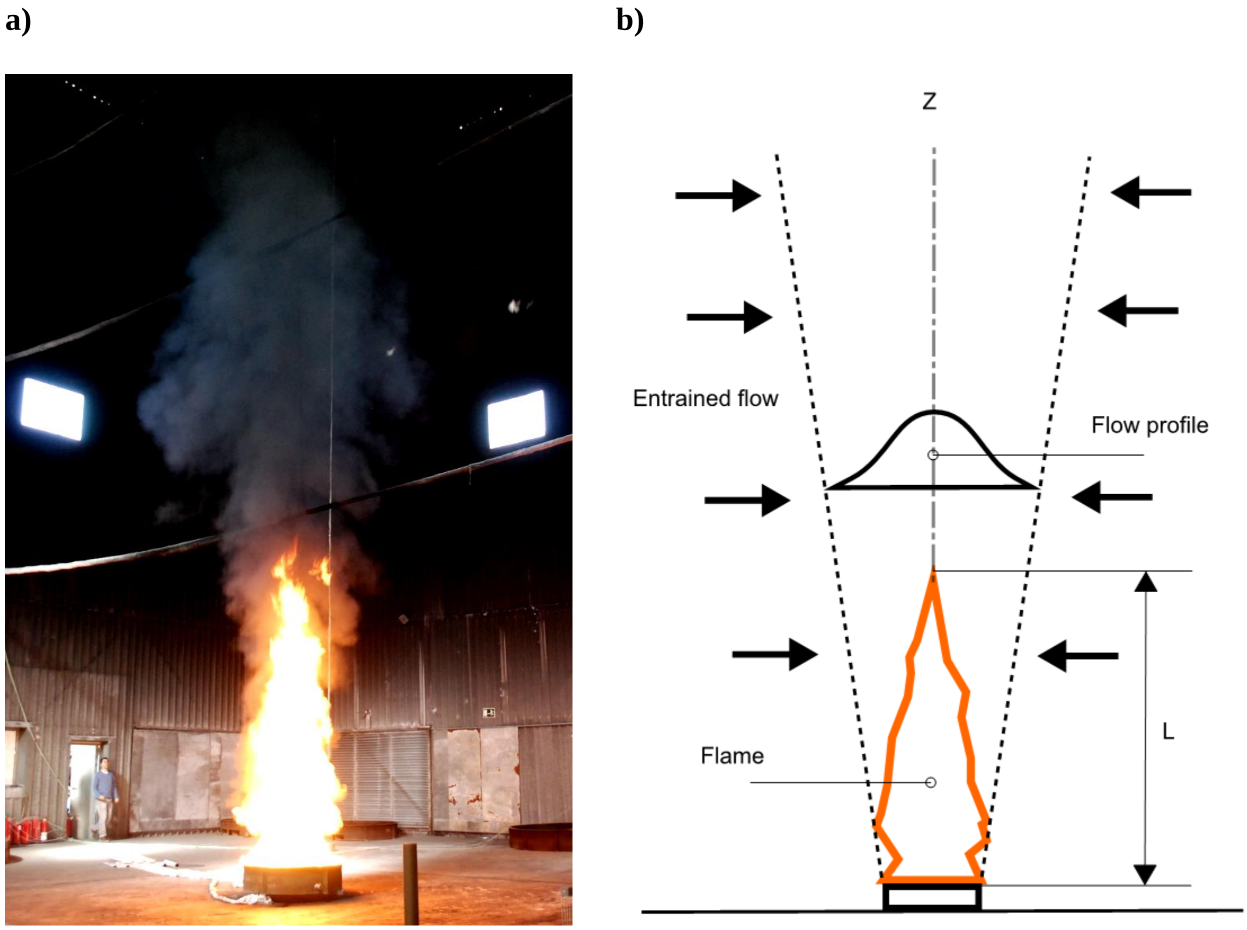

Figure 14 – Fire plume in one of the GX experiments (1a) and analytical representation of the fire plume (1b).

The first mathematical models of axis-symmetric buoyant plumes in fire are attributed to the work of Morton et al. [32], who often refers to earlier studies by Yih [31]. In this work, three main assumptions were made: (i) the rate of entrainment at the edge of the plume is proportional to the characteristic velocity at a given height; (ii) the velocity profiles of mean vertical velocity (and buoyant forces) are similar at horizontal sections in different heights; (iii) the local variations of density are small, compared to the difference between the average density of the plume and its surroundings. These assumptions were transferred to all further models of plumes based on the theory of Morton et. al [32]. Furthermore, the model by Morton et al. [32] assumed a point of line source, and conservation of mass, momentum and heat[15].

3.2.1 Thomas plume

One of the most widely adopted and cited plume models is the so-called Thomas plume model. The origin of the model is usually mistakenly attributed to the *Fire Research Technical Paper No. 7 (1963)* [73], when it was actually developed in the further work of its authors, reported for example by Hinkley [64].

The Thomas plume model can be considered as a landmark in the smoke flow theory. Thomas used buoyancy considerations in scaled fires to correlate the characteristic height dimension, the velocity and the temperature of the plume to the Energy Release Rate (Q). This technique is commonly used in modern fire safety engineering, and known as Froude-number based scale modelling [57,74]. However, in the work of Thomas the Froude number of the fire was not calculated explicitly. The base of the mathematical model presented by Thomas was the work of Yih [31] and Bernoulli's theorem. The fire was assumed as the source of the plume (point source), and the hot layer underneath the ceiling was considered as stagnant, and thermally uniform. An equilibrium between the smoke incoming to the layer, and removed through natural vents, was assumed. From these boundary data, the depth of the layer of hot gasses could be estimated, as well as the temperature and the flow rates[15].

This plume theory is applicable to plumes where the density of air in the plume varies only with height and where $\frac{\Theta}{T_\infty} \ll 1$, where Θ is the rise of temperature above ambient and T_∞ is the ambient temperature. This theory also requires the use of a virtual source point, at a distance r_y below the floor

$$r_y \cong 1.5 A_f^{1/2}. \tag{8}$$

$$r_b = r_y + h_c - D_b. \tag{9}$$

In the previous equations, A_f is the fire area (m^2), r_b is the vertical distance between the virtual source point and the bottom of the layer of hot gasses (m), h_c is the ceiling height (m) and D_b is the depth of the layer of hot gasses (m).

The use of this model is only valid for plumes at heights that are large compared with $A_f^{0.5}$. This means that the base of the smoke layer is at a height several times greater than $A_f^{0.5}$, which is possible if the smoke layer interface z is much larger than the fire diameter D ($z >> D$). The error of the method increases with $A_f^{0.5}/r_b$. Knowing the virtual origin, the mass flow of hot gases into the smoke layer may be calculated with equation (10)

$$\dot{m}_p = 0.043\ \rho_c r_b^{\frac{5}{2}} \left(\frac{2g\Theta}{T_\infty}\right)^{\frac{1}{2}}, \tag{10}$$

where ρ_c is the density of the air (kg/m^3), g is the acceleration due to gravity (m/s^2) and T_∞ is ambient temperature (K).

The original work of Thomas focused on the performance of natural ventilation of compartments and the methods used to design such systems. Later, it was further improved by Hinkley [64]. The form commonly used in design standards has only two variables – the perimeter of the fire, P (m), and the height of the layer above the seat of the fire, z (m).

$$\dot{m}_p = 0.188\ \mathrm{P}\ z^{3/2}. \tag{11}$$

Hinkley verified equation (11) against a series of full-scale experiments, with the most important being the work of Keough [75]. The parameter space of the experiments discussed by Hinkley included compartments of height from 0.70 to 15 m, fires from 8 kW to 30 MW, and heat output per unit area in the range of 250 – 630 kW/m^2 (in Keough experiments the convective heat output was greater, up to 1800 kW/m^2). The mass flow rate of smoke in the plume was in good agreement with equation (11). However, it was noted that Heskestad's model (see section 3.2.4) might be better for fires with small height and large heat release per unit area. This validation work was used as the justification to use equation (11) in smoke control design. As Hinkley pointed out, despite the purely empirical nature of this equation, its validity had been established for the parameter space described above.

3.2.2 Zukoski plume

The work of Zukoski et al. [22] focused on obtaining a correlation for axisymmetric plumes in the far field. The experiments assumed that the mass flow in the plume, $\dot{m}_p$, consists of a mass flow of fuel pyrolyzed by fire, $\dot{m}_f$, entrained air, $\dot{m}_E$, and recirculation at the area where the plume enters the layer, $\dot{m}_1$. They also considered that additional mass flow can occur at the interface between hot layer and cold air, referred as $\dot{m}_2$. Therefore, by maintaining the smoke layer at the height of the hood used in the experiment to extract the smoke, the measurement of the mass of smoke removed through the hood allowed the direct measurement of total mass flow in the plume. These results were further correlated into a mathematical model by Cetegen et al. [71]. By using ideal plume theory, the results of Zukoski can be approximated as equation (12) [15,67]

$$\dot{m}_p = 0.21 \left(\frac{\rho_\infty^2 g}{c_p\, T_\infty}\right)^{1/3} \dot{Q}^{1/3} z^{5/3}. \tag{12}$$

where ρ_∞ is the density of air (kg/m^3) at ambient temperature, g is the acceleration due to gravity (m/s^2), c_p is the specific heat capacity of air (J/kgK), T_∞ is the ambient temperature (K), $\dot{Q}$ is the HRR (kW) and z is the vertical distance above the base of the fire (m).

This equation is also commonly shown in the form below where the ambient air properties at normal conditions are assumed to be $T_\infty = 293$ K, $\rho_\infty = 1.1$ kg/m^3, $c_p = 1.0$ kJ/kg·K and $g = 9.81$ m/s^2

$$\dot{m}_p = 0.071\, \dot{Q}^{1/3} (z)^{5/3}. \tag{13}$$

3.2.3 McCaffrey plume

McCaffrey used experimental data and dimensional analysis to obtain plume correlations for upward velocity and temperature [24]. He divided the fire plume into three regions, the continuous flame region, the intermittent region, and the plume region[15]. The boundaries between the distinct regions were determined as a function of the fire HRR:

- $\frac{z}{\dot{Q}^{0.4}} < 0.08$ for the flame region;
- $0.08 < \frac{z}{\dot{Q}^{0.4}} < 0.20$ for the intermittent region;
- $0.20 < \frac{z}{\dot{Q}^{0.4}}$ in the plume region.

The corresponding mass flow rate calculations are given in equations (14), (15) and (16) [76],

$$\dot{m}_p = 0.011\,\dot{Q}\left(\frac{z}{\dot{Q}^{0.4}}\right)^{0.566} \text{ for } 0 < \frac{z}{\dot{Q}^{0.4}} < 0.08\,. \tag{14}$$

$$\dot{m}_p = 0.026\,\dot{Q}\left(\frac{z}{\dot{Q}^{0.4}}\right)^{0.909} \text{ for } 0.08 < \frac{z}{\dot{Q}^{0.4}} < 0.20\,. \tag{15}$$

$$\dot{m}_p = 0.124\,\dot{Q}\left(\frac{z}{\dot{Q}^{0.4}}\right)^{1.895} \text{ for } 0.20 < \frac{z}{\dot{Q}^{0.4}}\,. \tag{16}$$

The model was derived based on reduced scale experiments for fires with HRR varying between 14.4 kW and 57.5 kW. McCaffrey reported that, to obtain valid data for modelling, a time-averaged approach had to be used, through integration for a time of 100 s. This means that if one compares the model (averaged) results to results of CFD (instantaneous), large discrepancies may be noted. Further discussion on the time-averaging approaches used in plume modelling can be found in [24]. Moreover, some disagreements between the approach of McCaffrey and earlier plume theory can be found in [77].

The McCaffrey plume was used as one of the plume correlations in the zone model CFAST [60]. However, it was recently replaced by Heskestad's model. Karlsson and Quintiere [67] reported that for both plume temperatures and velocities the McCaffrey approach will give results roughly 10% higher than those by Heskestad.

3.2.4 Heskestad plume

Heskestad [66] compared existing plume models based on the theory of Yih [31], Thomas et al. [21] and Cetegen et al. [70], with entrainment predictions for strong plumes, that assume predetermined top hat profiles for velocity and temperature rise (density). The theory was later refined with the use of a flame height correlation [78]

$$L_{fl} = 0.235\,\dot{Q}^{2/5} - 1.02D. \tag{17}$$

where L_{fl} is the flame height (m) and D is the fire diameter (m).

A summary of Heskestad's assumptions with respect to the ideal plume theory of Morton [32] is given in [67], with the main changes being:

- The point source assumption is relaxed by introducing a "virtual origin" at height z_0 [23]. Also, account will be taken of the fact that some plume properties depend on the convective energy release rate, $\dot{Q}_c$. The "virtual origin" is computed as:

$$z_0 = 0.083\,\dot{Q}_c^{2/5} - 1.02D. \tag{18}$$

- The "top hat" profiles across the plume for velocity and temperature will be replaced by a more realistic Gaussian profile.
- The Boussinesq approximation ($\rho_\infty \approx \rho$) is removed.

Under the above conditions, the plume mass flow rate above the flame height ($z > L_{fl}$) is given by equation (19) [79]:

$$\dot{m}_p = 0.071\ \dot{Q}_c^{1/3}(z - z_0)^{5/3} + 1.92\ 10^{-3}\dot{Q}_c. \quad (19)$$

Finally, the plume mass flow rate below or at the flame height ($z \leq L_{fl}$) is given by equation (20):

$$\dot{m}_p = 0.0056\ \dot{Q}_c\ \left(\frac{z}{L_{fl}}\right). \quad (20)$$

3.2.5 Treatment of the convective HRR

Depending on the plume correlation, the total ($\dot{Q}$) or convective fraction ($\dot{Q}_C$) of the heat release rate (HRR) needs to be provided[15]. A summary of the needed HRR is shown in Table 9.

Table 9 – Inputs in different plume theories.

Approach	**$\dot{Q}$ (total)**	**$\dot{Q}_c$ (convective)**
Zukoski	YES	NO
McCaffrey	YES	NO
Heskestad	NO*	YES
Thomas	NO**	NO**

(*) In Heskestad's model, the total HRR is used only when estimating the mean flame height and the position of the virtual origin. (**) Thomas' formulae do not use the HRR as an input[15].

As it can be seen, Zukoski's model requires the total HRR, which can be explained by the origins of his theory, based on the works of Yih [31] and Morton [32], and the ideal plume theory. In Heskestad's model, the total HRR is used only when estimating the mean flame height and the position of the virtual origin. When estimating the other plume properties – such as the air plume entrainment – the convective energy release rate needs to be used. McCaffrey includes the convective fraction already into the formula, so the total HRR, $\dot{Q}$, must be used. In Thomas' formulae, the HRR is not used, as the user defines only the fire perimeter/diameter. However, the user must be aware of the model limitations, explained in section 3.2.1.

According to [67] the energy losses due to radiation from flames are typically in the order of 20% to 40% of the total energy release rate. The higher values represent the sootier and more luminous flames. For the calculations with the Heskestad model in this paper, a radiation value of 20% was assumed[15].

3.2.6 Time integrated approach

Smoke filling is a transient process, and as such the environmental conditions inside the protected space will vary in space and time. This process can be integrated in time with the use of a lumped-parameter mathematical model [80]. The investigation of these parameters as a function of time may be of importance when the Available and the Required Safe Egress Times (ASET vs RSET) are compared to determine the safety of the building [15,81]. The concept of time-integrated solution was presented in the past, e.g. by Morgan et al. [51] and Wu and Chen [55].

There are two parameters for which time integration is used and are important to this thesis – (i) the smoke layer interface height and (ii) the smoke production. The smoke layer interface height may be calculated using a time integration approach. Since the volume of the atrium and the mechanical volumetric exhaust are constant in time, the smoke that enters the reservoir causes a descent of the layer proportional to the difference between the volume of smoke that enters the layer and that which is removed from it[15]. This parameter is investigated in the experimental comparison presented in this thesis.

For the smoke production integration, the HRR of the fire is replaced with an unsteady function, out of which the most widely used is a parabolic curve known as a *t-squared fire*. T-squared fires are defined through a fire growth rate coefficient, α (kW/s^2), and the time of their growth. The standardized growth rates are described by NFPA 92 [47] and are widely used in various fire protection engineering applications [82,83]. The time change in HRR will also cause a change in the diameter of the fire (if heat release rate per unit area, HRRPUA, is assumed constant) or a change of HRRPUA (if the diameter of fire is assumed constant). The effects of these changes to the plume model were discussed in [55].

Figure 15 – Evidence of the smoke layer interface in one of the #GX tests.

3.3 Results and discussion

In order to assess the suitability of the previous plume models to characterize the smoke layer formation and growth in large-volume enclosures, these have been compared with full-scale atrium fire tests. This section presents and discusses the main results of the series of tests described in sections 2.1.2 and 2.1.3, which are, respectively, the first and second series of experiments carried out in the Murcia Fire Atrium – see Figure 15.

After the experiments, the results were plotted on graphs (one graph for each one of the three experiments) and compared to the four empirical plume models that have been investigated. The graphs show the smoke layer height against time; the moment at which the smoke layer reached 15 m, 10 m and 5 m above the floor were recorded and plotted on the graph. The same graphs include plots of the relationship between the smoke layer height and time given by each of the four plume models investigated: the Thomas model, the Zukoski model, the Heskestad model and the McCaffrey model. For more information about these models see section 3.2.This way, the results could be easily compared with the predictions given by each model. To see the results of the experiments, the comparisons with the empirical models and the discussion, see section 3.3.

Initially, the different phases of the smoke filling are discussed in order to provide with a correct interpretation of what is subsequently presented. Finally, a discussion of the results together with the impact of them on design are presented. As the discussion is based on the smoke layer interface height, it is important to define how this has been evaluated. The models estimate how much smoke is traveling into the smoke reservoir and, based on that, an assessment of the smoke control performance is carried out. We consider that if a model predicts that the smoke layer interface is higher than it was in the experiment, it is an over-prediction. On the other side, if a model predicts a smoke layer interface lower than it was in the experiment, it is considered an under-prediction[15].

For each presented experiment, relevant important parameters, such as HRR and exhaust fan flow rate, were accordingly fed into the analytical models. For the Heskestad model, an additional assumption made was that the radiative fraction of HRR is 20% (see chapter 3.2.5). For the Thomas model, two different scenarios have been analyzed – one in which the fire perimeter is equal to the perimeter of the pan used in the experiment, and one in which the fire perimeter is calculated based on the value of HRRPUA = 1000 kW/m²[15]. Further discussion on the impact of HRRPUA in the Thomas approach is presented in section 3.3.4.

3.3.1 Interpretation of the results

All of the performed experiments show similar smoke layer behavior in relation to the change of layer height, z(t). In the early phase of the experiment (first 200 s – 300 s) the layer interface changed fast, but after that period of time it stabilized and remained at a constant height until the end of the fire. This behavior can be divided into two distinct regimes – a transient regime, when the layer height is changing as the compartment is filling up with smoke, and the steady state phase, when a state of equilibrium is reached between a steady source of firepower and the exhaust. As the layer height will fluctuate through the fire, the transition between transient to steady state phase is blurred[15]. For the purpose of comparison of the methods, the authors have considered that after 300 s of the experiment, the smoke layer height remains constant. The illustration of these two regimes is shown in Figure 16.

As the experimental results were compared to time-integrated smoke plume formulae, it is possible to assess their validity separately for both regimes – the time-dependent smoke filling phase, and the stabilized layer phase (which corresponds to the minimum layer height obtained with steady-state formulae)[15].

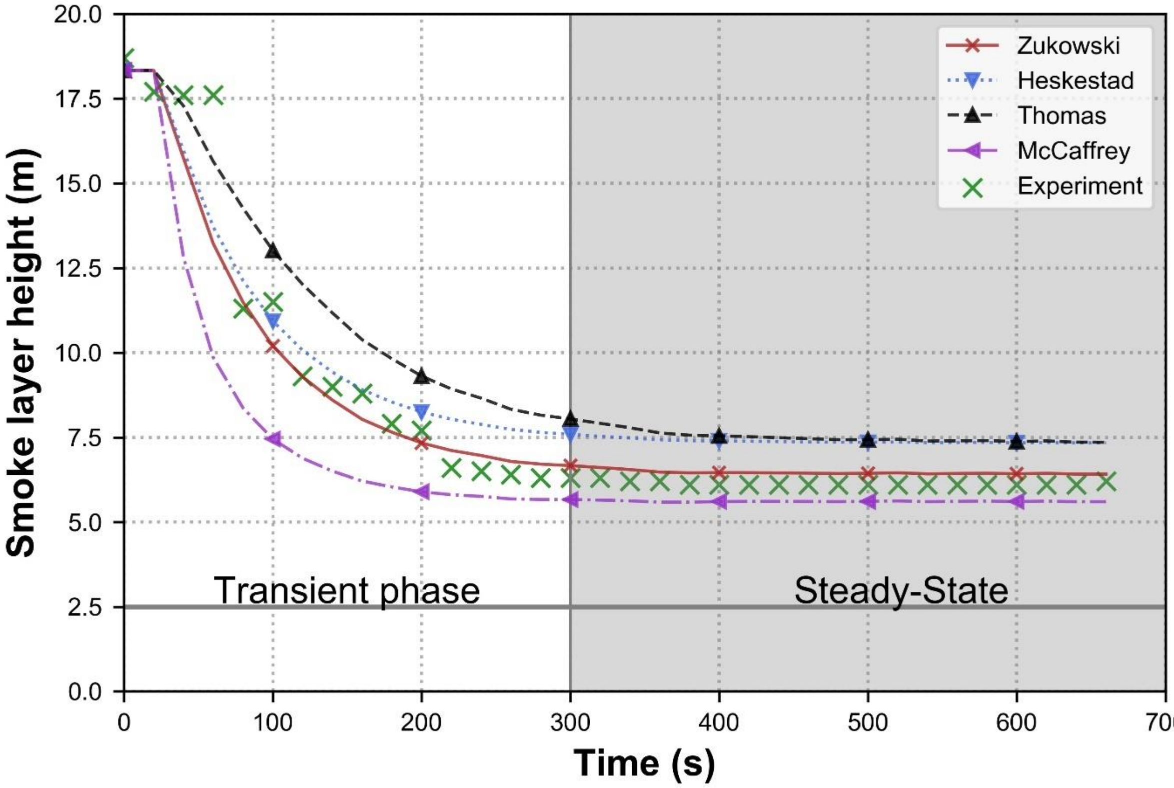

Figure 16 – Smoke layer height measurements versus model predictions with visible regimes of transient and steady-state phases (corresponds to experiment #G1).

It should be emphasized that the way in which the smoke layer interface height is assessed during the experiments is important in order to understand the phenomenon being studied. The smoke layer interface can be defined as the horizontal plane that separates the top layer of hot gasses in the compartment from the bottom layer of relatively cooler and cleaner air [67]. Clearly, the bottom layer will contain fire products as well, but usually there is a threshold height at which the concentration of smoke species increases substantially. This threshold height, i.e. the smoke layer interface height, is not always easy to define from the raw experimental data.

Several methods exist to determine the height of the smoke layer interface, each method giving providing with different definitions of the interface. Usually, the interface is evaluated in the literature by means of CO_2 concentration [84,85], as well as temperature measurements [1,29,86–88], the latter being the most used due to the ease of its measurement. There are many different temperature methods to evaluate the smoke layer interface in the literature, such as the N-percent method proposed by Cooper et al. [29], the upper zone averaging and mass equivalency by Quintiere et al. [29], the maximum gradient by Emmons [89], the Janssen method [21] or the least squares method by He et al. [25]. For the first series of experiments, the N-percent method was utilized. This methodology, and how it was used during the first series of experiments, is explained in section 2.1.6.

As it has been already commented, except the least squares method, present a certain component of empiricism. For that reason, the least squares method was used to determine the smoke layer interface height during the second series of experiments [20]. This method and the specific way in which it was used during the second series of experiments are explained in section 2.1.6.

3.3.2 First series of experiments (#MX)

As shown in Table 3 the first series of experiments considered 0.92 m diameter pans containing 44 to 52 l of n-heptane as fuel. These yielded HRR between 1.43 and 1.77 MW. The experimental data relevant to the layer interface height is limited for this series, thus the comparison between experiments and analytical methods is possible only for a few points, Figure 17 to Figure 19. Due to scarcity of data in the transient phase, the evolution of the layer height in the experiments may not be precisely determined, although it can be considered valid for the steady-state phase. Furthermore, the measurements presented in Figure 17 to Figure 19, represent the time values in which the smoke layer interface reached height values of 15, 10 and 5 m in each of the experiments. The last measured point in the experiments can be considered as within the steady-state regime. Thus, these results can be compared with the respective steady state predictions from the analytical models. It must be noted that for this comparison the N30% method was chosen, based on [27] and the discussion presented in [26]. Figure 17 to Figure 19 show the comparison between experimental measurements and results from the four models assessed, namely the Zukoski, Heskestad, Thomas and McCaffrey models.

In general terms, when the fire ignites, a smoke plume forms and generates a smoke layer. This layer rapidly lowers due to the significant air entrainment into the plume and, as the fire evolves, subsequently, the mass flow of air entering the plume is reduced. This reduction leads eventually to an equilibrium between the mass flow of hot gas feeding the smoke layer and the exhaust mass flow rate through the fans at the ceiling. This is better appreciated in the predicted results.

In the transient phase of the smoke layer development, the models predict a faster growth of the layer than that estimated from the experiments (in relevant points in time). Among the models, the Thomas model predicted a smoke layer height evolution closer to the measurements at 15 m, i.e. at the initial stages. This trend remains for the 10 m measurement point, where the Thomas model with 1000 kW/m² yielded a value close to the experiment. However, for larger times, i.e. near the steady-state phase, both calculations with the Thomas model were significantly off, compared to the measurements at 5 m height.

Based on the measurements with the thermocouple tree, and using the N30% method, the final layer height was estimated as close to 5 m above the floor in all cases. The time to reach this point in experiments #M2 and #M3 was sufficient to assume this height is reflecting the steady-state phase and could be compared with the results of analytical modelling. Based on the data from these experiments, the McCaffrey model yielded the closest value of smoke layer height, followed by Zukoski and Heskestad. The prediction of the Thomas model was significantly different from the results of the experiment and the predictions of the rest of the models. Moreover, most models predicted higher layer heights (over-predicted) than that from the experiments, which can be dangerous if implemented in a smoke exhaust system design[15]. The discussion of the significant discrepancy between the Thomas model and the experiment is reported in section 3.3.4.

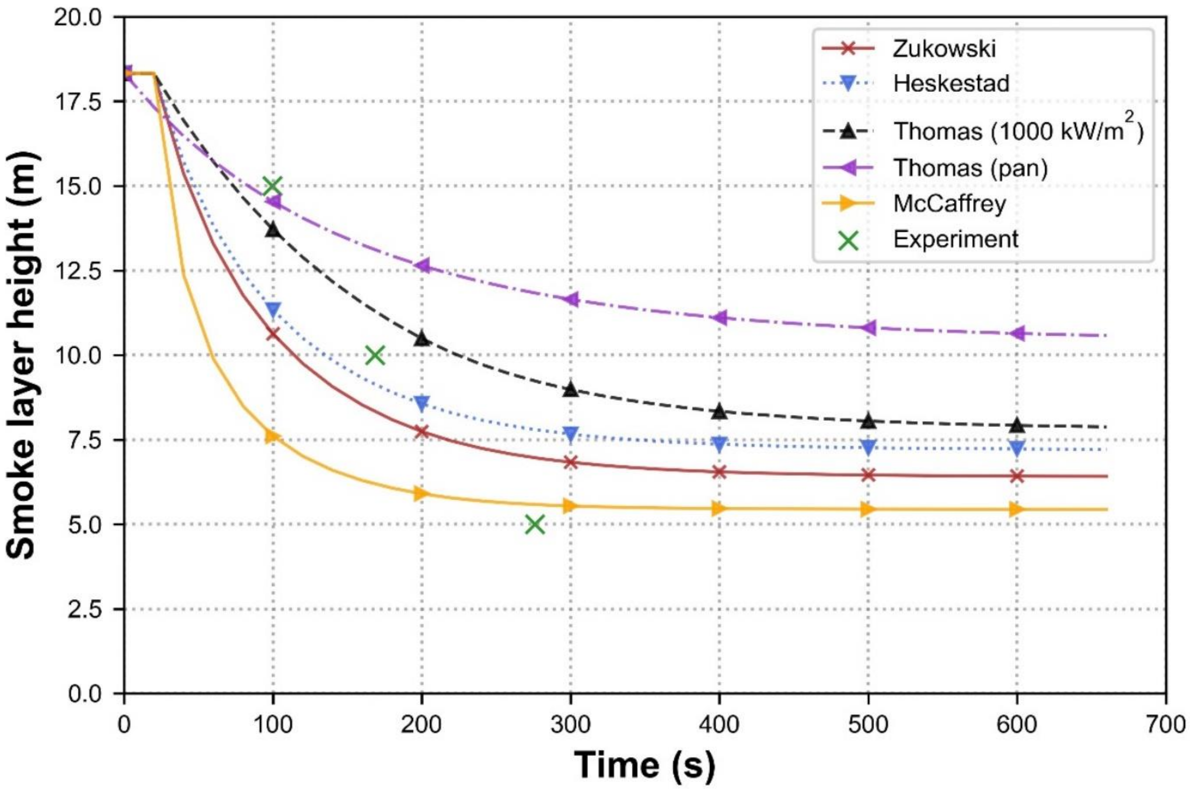

Figure 17 – Measured (30 N% method) and predicted smoke layer interface height for experiment #M1.

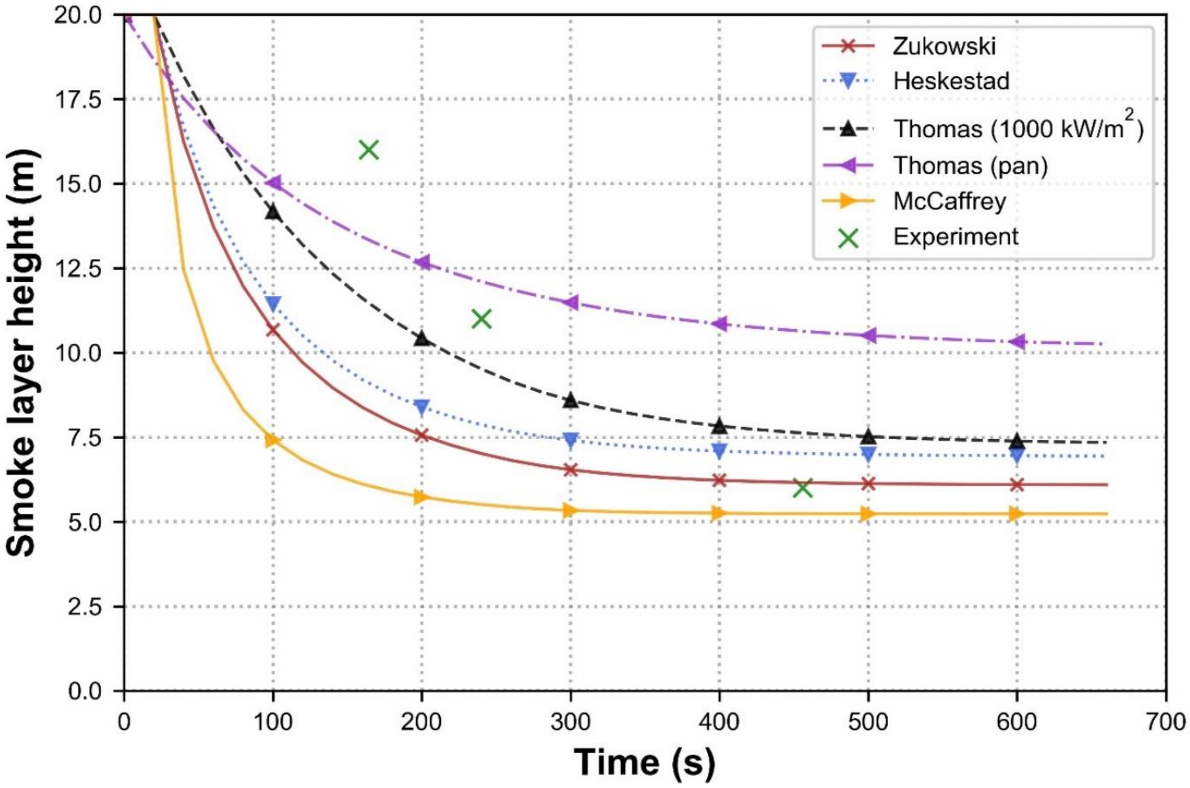

Figure 18 – Measured (30 N% method) and predicted smoke layer interface height for experiment #M2.

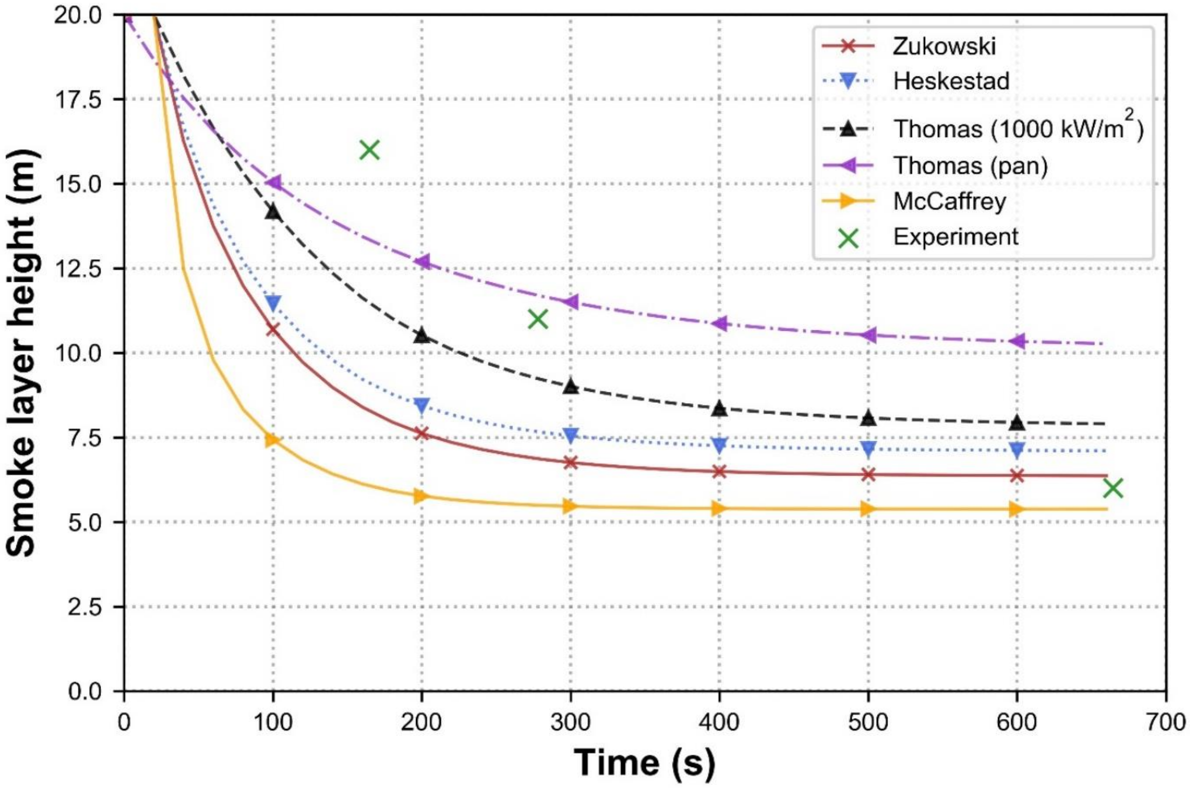

Figure 19 – Measured (30 N% method) and predicted smoke layer interface height for experiment #M3.

3.3.3 Second series of experiments (#GX)

Figure 15 to Figure 17 show an insufficient spatial resolution of the smoke layer evolution, only valid to roughly assess the models' performance at three locations. Therefore, the temporal resolution of measurements in the second series of experiments was significantly improved compared to the first series. As it has been commented in section 2.1, a vertical rack of thermocouples was used - see Figure 3. This allowed for more detailed analysis of the transient phase of the smoke layer evolution in the atrium. Another improvement over the first series was the use of the least squares method for the definition of the layer boundary. Discussion on this choice has been presented in sections 2.1.6 and 3.3.1, as well as in [20]. The fires used in the experiments and the exhaust ventilation rates were comparable with those in series one. However, due to the changes in the data processing, the results of both experiments should be analyzed separately.

As it was done with the results from the first series of experiments, these results were plotted on a graph of smoke layer height against time, and they were compared against the smoke layer height predictions given by the different plume models derived Thomas, Zukoski, McCaffrey and Heskestad.

Figure 20 to Figure 22 show the results obtained from tests #G1, #G2 and #G3, respectively. The experimental measurements show more clearly the smoke layer evolution previously described, i.e. a fast growth in the early stages followed by a slower smoke layer thickness increase as the height is reduced, to finally achieve a quasi-steady state of equilibrium.

When comparing the temporal evolution of the layer height predicted by the models, it may be noted that the Zukoski and Heskestad approaches yielded the closest results to the experiments. In the transient phase, the McCaffrey model yielded a lower layer height and the Thomas model yielded a higher layer height compared to the measurements in the experiments. It should also be noted that the McCaffrey model predicted the quickest transition to steady state of the layer.

The steady-state phase was reached between 220 and 260 s, while the remaining models and the experiment showed a state of equilibrium between plume and smoke exhaust after 260 to 320 s, approximately.

To compare the steady-state results, the layer height measured or calculated between 300 and 600 s was averaged with respect to time. Table 10 shows detailed results on this matter. In the steady-state phase of the experiments the Zukoski model presented the best agreement with the prediction of layer height in experiment #G1. However, the McCaffrey model was the best model for experiments #G2 and #G3. The worst predictions were obtained with the Thomas model, with relative error to the experimental results ranging from 36.5% to 101%.

Table 10 – Comparison of the average layer height for different experiments and calculation methods.

Model	**#G1**		**#G2**		**#G3**	
	Height [m]	**Relative error vs exp. [%]**	**Height [m]**	**Relative error vs exp. [%]**	**Height [m]**	**Relative error vs exp. [%]**
Experiment	6.13		6.08		5.75	
Zukoski	6.47	5.5%	7.13	17.2%	6.62	15.1%
Heskestad	7.40	20.5%	8.15	34%	7.48	30%
Thomas (HRRPUA=1000 kW/m²)	9.67	57.7%	8.90	46.3%	7.85	36.5%
Thomas (P = pan perimeter)	10.43	70.1%	12.23	101%	10.43	81.3%
McCaffrey	5.61	-8.4%	5.96	-1.9%	5.69	-1%

In most cases, the models over-predicted the smoke layer height, i.e. delivered heights higher than the experimental ones. This constitutes the worst-case scenario, since those results could lead to unsafe designs that can endanger building occupants.

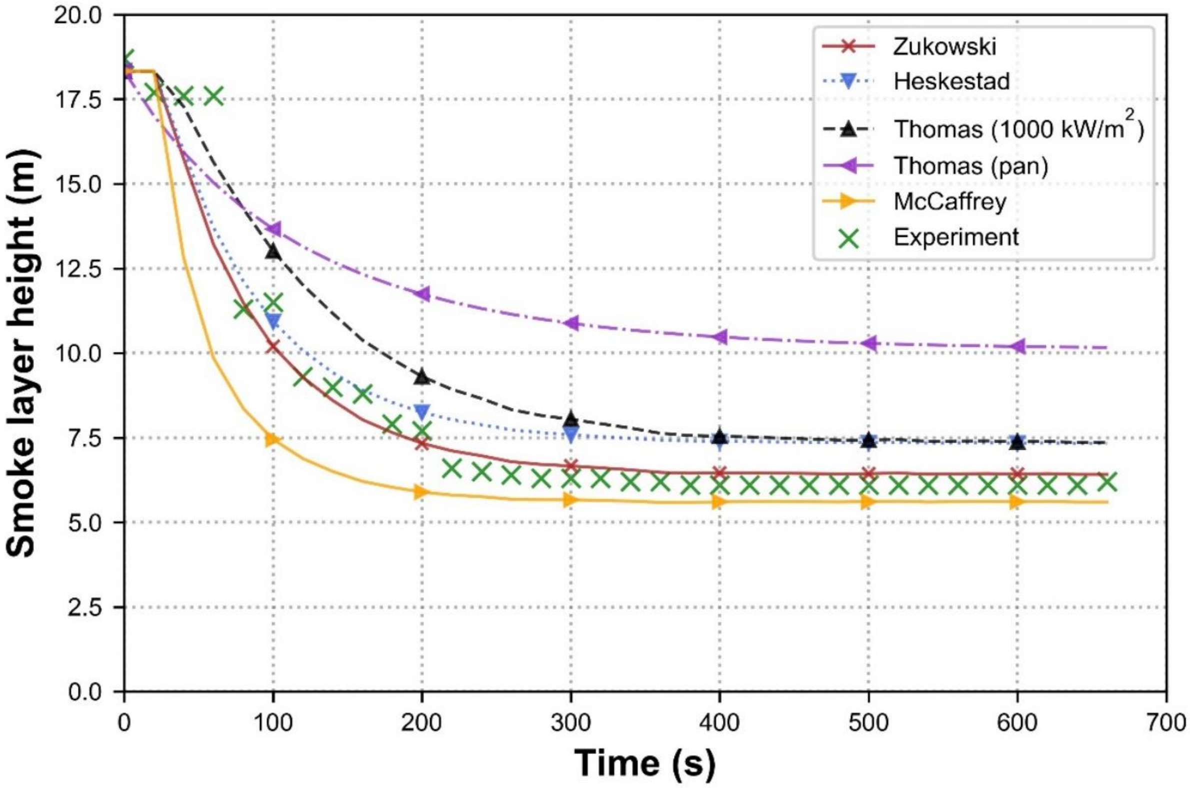

Figure 20 – Measured (least squares method) and predicted smoke layer interface height for experiment #G1.

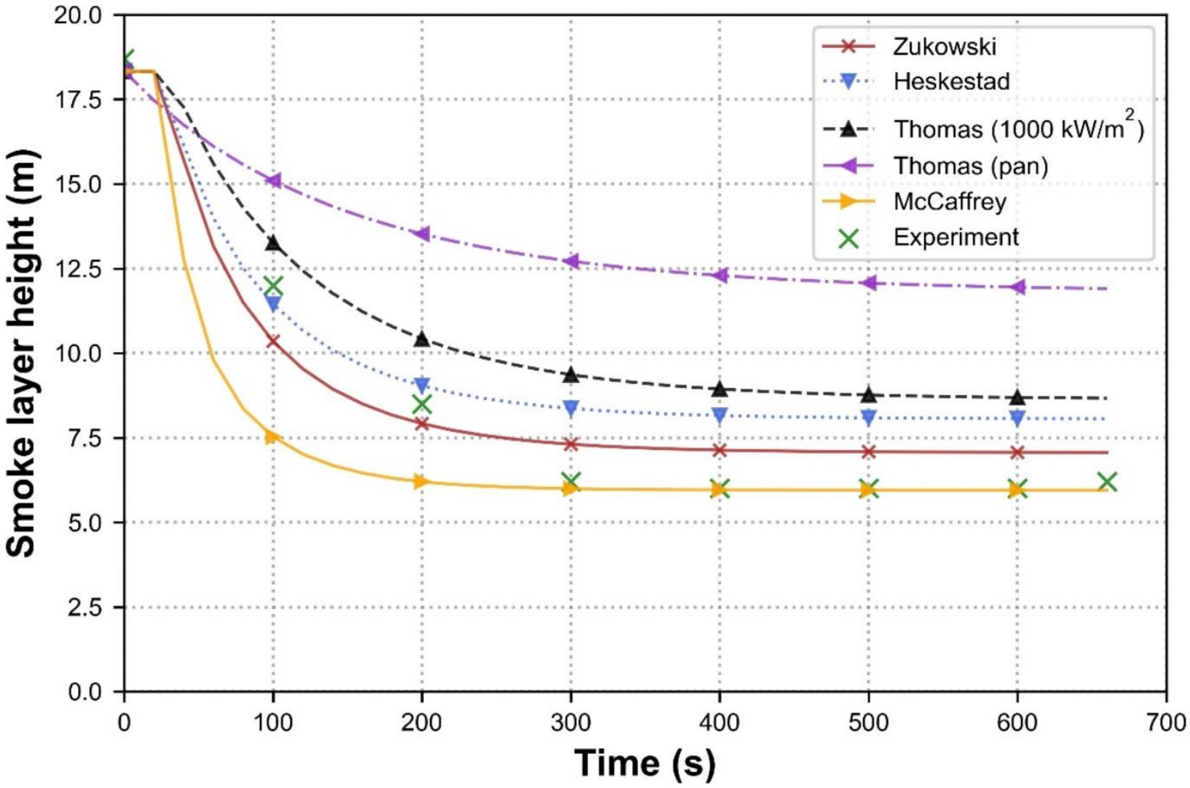

Figure 21 – Measured (least squares method) and predicted smoke layer interface height for experiment #G2.

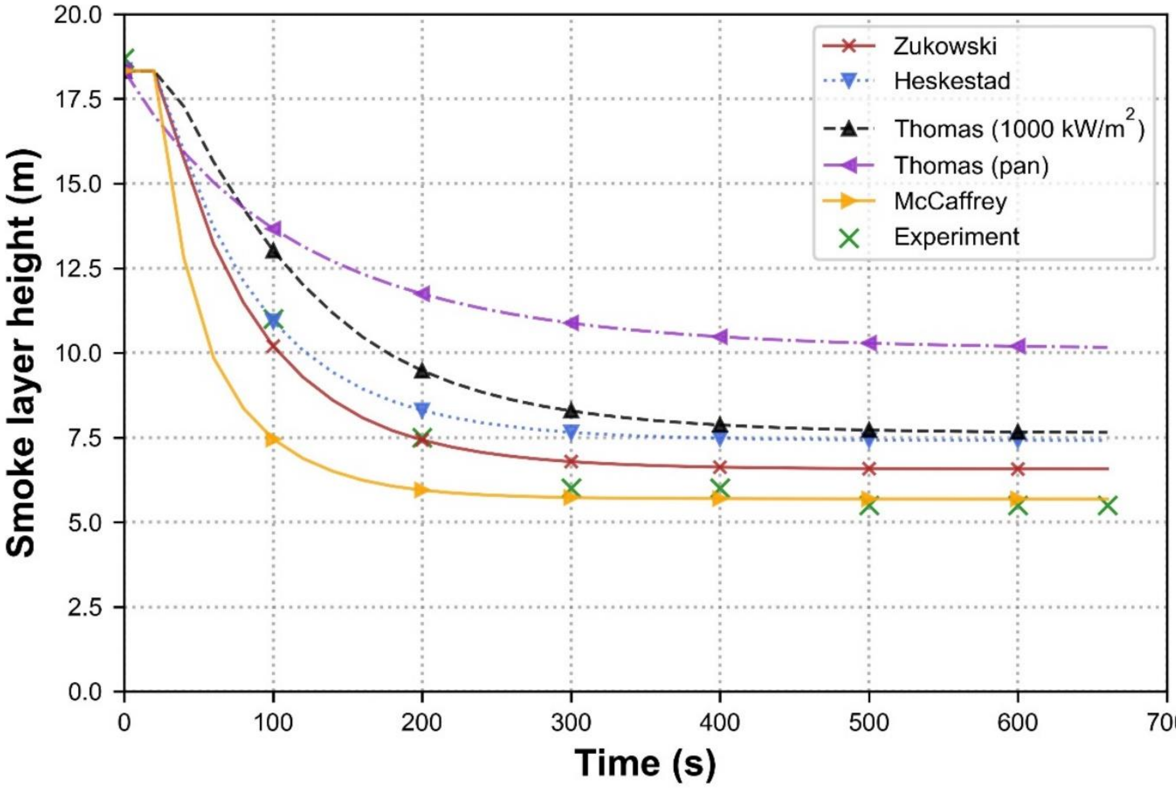

Figure 22 – Measured (least squares method) and predicted smoke layer interface height for experiment #G3.

3.3.4 Discussion of the results

In the six fire scenarios analyzed, the McCaffrey approach is the one that best fits the experimental data in the steady-state phase overall, while the Zukoski model provides with the best agreement in the transient phase. In this regard, it may be argued that the transient evolution of the layer is less valuable in engineering practice since the steady-state value is commonly used in designing the smoke control systems and thus, based on the results shown, the McCaffrey model is the better overall solution[15].

An important observation of the study is that in all of the experiments the Thomas model predicted results significantly different from the experimental data, with relative errors of up to 101%. As this model is widely used in Europe and Australia for the design of smoke control systems in atria - see Table 7, the observed discrepancies between measurements and model must be further discussed. The latter might be mainly attributed to how the fire is introduced into the model, i.e. through the fire perimeter. The fuel used in the experiments was n-heptane, which is known to have high values of HRRPUA, due to its high heat of combustion. The perimeters of the pans used in the experiments were 2.89 m (for D = 0.92) and 3.67 m (for D = 1.17 m). The measured HRRPUA in the experiments varied between 2140 kW/m² (#G1) and 3190 kW/m² (#M2), while the Thomas model was widely validated by Hinkley in a range between 225 kW/m² and 625 kW/m²[15].

Since one of the main assumptions for the use of the Thomas approach is that the fire flames are considerably smaller than the diameter, this matter needs further investigation. One of the most used equations to calculate the mean flame height, L_{fl}, is presented by Heskestad [34], which provides good results for the different flame regimes, except for the jet flame regime[15].

Although Heskestad's equation is shown to be reliable to calculate the mean flame height [34,78], there is a lack of experimental data where the mean flame height is significantly smaller than the fuel source diameter, D. Thomas found that in the continuous flame region or in the near field the plume mass flow rate was more or less independent of the HRR and more a function of the diameter of the fire and the height above the fire source, z. This has been found to be particularly valid for fires where the mean flame height, L_{fl}, is considerably smaller than the diameter [15,41], which was not the case during the experiments conducted for this study, Figure 23.

In order to explore Thomas model's validity, a brief analysis has been performed for typical design fires used in fire engineering, i.e. involving cellulosic and/or plastic materials. For localized fires it is very unlikely to find a design fire where the diameter is significantly larger than the flame height, since the HRRPUA is usually higher than 1000 kW/m^2. Figure 23 shows the relationship between mean flame height and diameter for a 1000 kW fire using Heskestad's equations, equations 20 and 21, to determine the minimum D and maximum L_{fl}. The point where the diameter is equal to the flame height has been indicated with a red circle, i.e.

$$D_{min} = L_{fl\,max} = \frac{0.235\,\dot{Q}^{2/5}}{2.02}. \quad (21)$$

The Thomas theory is valid only after that point (to be rigorous, significantly after that point). The result of equation (21) for a 1000 kW fire is $D_{min}=L_{fl\,max}=1.844$ m. Using the resulting D_{min}, assuming a circular fire and thus an area of 2.67 m², the HRRPUA would be 374.64 kW/m², which is far below the 1000 kW/m² suggested for a fire involving cellulosic and/or plastic materials.

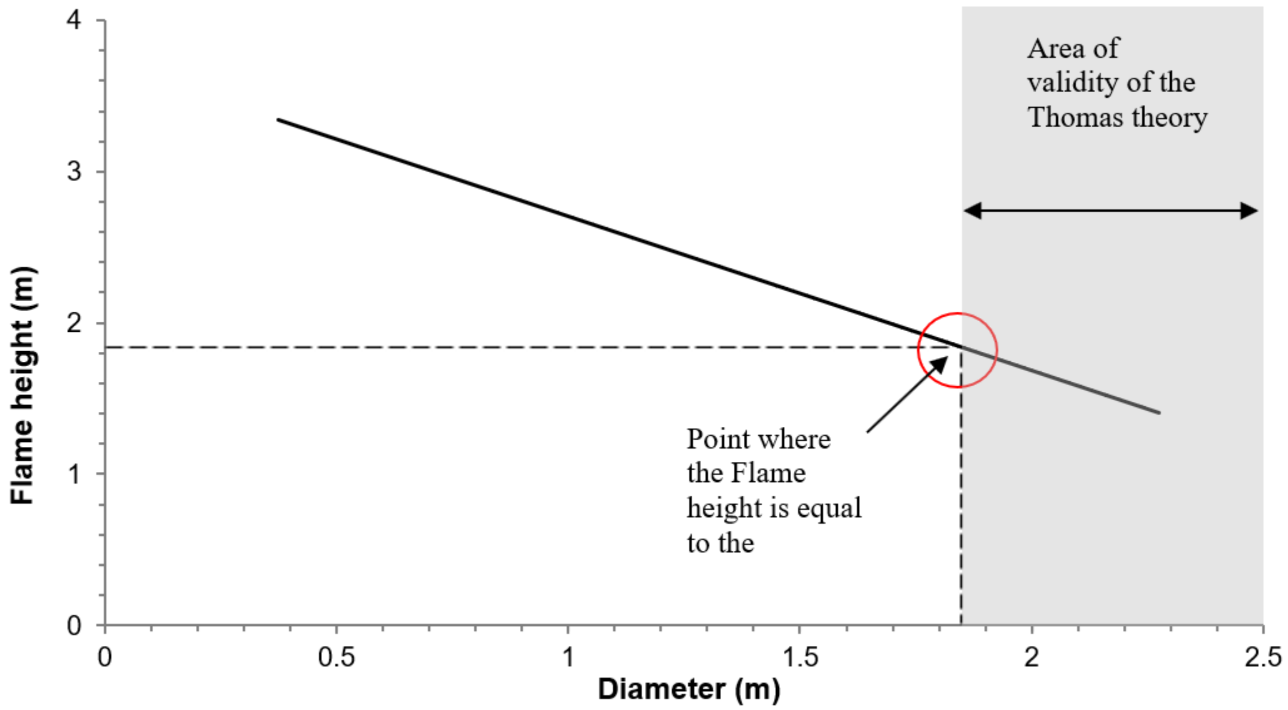

Figure 23 – Mean flame height vs Diameter for a 1MW fire with emphasis on the area of applicability of the Thomas theory and the point where the flame height is equal to the diameter.

The Thomas model can give predictions of layer evolution close to the measured for a certain value of the HRRPUA parameter of the design fire. An example of such a posteriori data fit to the results of experiment #G1 is shown in Figure 24. It can be noted that the Thomas model with a HRRPUA = 500 kW/m² provide with results very close to the experiment. This HRRPUA is significantly smaller than the actual value. However, it must be noted that the value of 500 kW/m² does not meet the flame height requirement described above – this is explicitly met by the 250 kW/m² scenario, in which the smoke generation is over-predicted. Furthermore, it must also be noticed that the values of HRRPUA for design purposes presented in standards and national codes are often misused. Fire codes often assume that the HRRPUA is the average of the total HRR generated by the fuel divided by the area of the whole compartment and that the fire burns uniformly in the area of the compartment. However, this approach does not consider at all a localized fire. In reality, a fire can easily exceed 1000 kW/m^2 (as for example the heptane fire, ~3000 kW/m^2) resulting in flame heights considerably bigger than the perimeter of the fire, which clearly contradicts the hypothesis on which the Thomas theory is based[15].

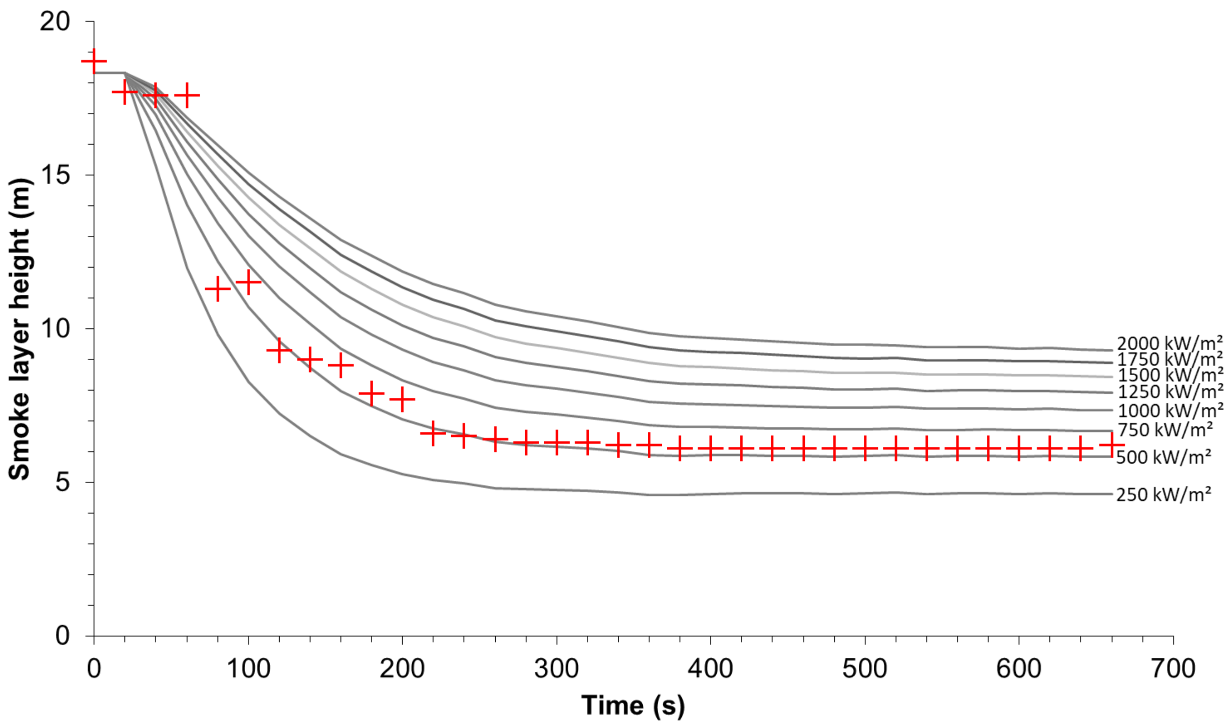

Figure 24 – Transient analysis of smoke layer height with Thomas equation for different values of HRRPUA. Red crosses mark the results of experiment #G1

Under the above conditions, the following section evaluates three different case studies. The results demonstrate that fires with HRR larger than 1 MW are likely to occur in buildings.

3.4 The Heat Release Rate per Unit Area (HRRPUA)

In Fire Engineering practice, the HRRPUA is one of the key factors in defining the design fire for a given scenario, since, based on a given area, it determines the total HRR of the fire.

The geometry of the fire and the correlations between flame height and diameter have a considerable influence on the HRRPUA. In this section three relevant case fires are described. As conclusion, it becomes evident that fires of HRRPUA ≥ 1MW/m^2 are likely to occur very commonly in buildings. The three case fires are the following:

- Single workstation fire.
- Stack of wooden pallets fire.
- Kiosk fire.

3.4.1 Single workstation fire

A workstation is a mixture of a great deal of diverse materials such as wood, cellulosic materials, polymers and other combustible materials. Those materials present different heats of combustion, chemical reactions, etc. Among others, the National Institute for Standards and Technology (NIST) have conducted fire experiments to characterize this kind of fires. The workstation experiments (NIST NCSTAR 1-5C, Fire Tests of single office workstation [90]) show that a single workstation with an area of 6.25 m^2 releases a HRR of approximately 7.7 MW (data extrapolated from 5 tests), which corresponds to a HRRPUA value near 1.23 MW/m^2.

3.4.2 Stack of wooden pallets

Cellulosic/wooden materials are the most commonly found ones in all types of buildings. Although the hazards from these fires are considered as relatively low because of the low heat of combustion, the fires can easily exceed 1 MW/m^2, thus resulting in a substantial risk to the occupants in a building.

A stack of wooden pallets of dimensions of 1.07 m x 1.07 m and height of 0.76 m can generate a HRR of 1430 kW (16% of moisture) and 2340 kW (5% of moisture), which gives HRRPUA of 1249.017 kW/m^2 and 2043.847 kW/m^2 for 16% and 5% moisture, respectively [1]. Table 11 shows the results of peak HRR and HRRPUA for different heights of storage of wooden pallets. These values were calculated using Babrauskas's equation:

$$Q = 919 \cdot L \cdot W(1 + 2.14 \cdot H) \cdot (1 - 0.03 \cdot M) \qquad (22)$$

Where:

- Q = peak HRR [kW].
- L = pallet length [m].
- W = pallet width [m].
- H = stack height [m].
- M = moisture [%].

In the calculations a net heat of combustion of 12000 kJ/kg was assumed. The stack of wooden pallets represents a good match of cellulosic/wooden items stored on 1 m^2 with good ventilation and an oxygen-rich environment.

Table 11 – Peak HRR and HRRPUA of stack of wood pallets [1]**.**

Length [m]	**Width [m]**	**Height [m]**	**HRR at 16% moisture [kW]**	**HRR at 5% moisture [kW]**	**HRRPUA 16% [kW/m^2]**	**HRRPUA 5% [kW/m^2]**
1.07	1.07	0.76	1430	2340	1249.017	2043.847
1.07	1.07	1.52	2320	3790	2026.378	3310.333
1.07	1.07	2.29	3200	5240	2795.004	4576.819
1.07	1.07	3.05	4090	6690	3572.364	5843.305
1.07	1.07	4.57	5860	9590	5118.351	8376.277
1.07	1.07	5.33	6750	11040	5895.711	9642.764

3.4.3 Kiosk

Another example of a possible fire exceeding 1 MW/m^2 is a kiosk fire. A kiosk fire with merchandise (t-shirts) has been evaluated. Fire experiments of small kiosks selling clothes, e.g. t-shirts, also show that fires with power larger than 1MW/m^2 can easily occur. Table 12 shows the average peak HRR and the HRRPUA for this specific case [2].

Table 12 – Peak HRR and HRPPUA of small kiosk.

	Length [m]	**Width [m]**	**Height [m]**	**HRR [kW]**		**HRRPUA [kW/m^2]**
test 1	1.2	1.2	2.13	1440		1000.00
test 2	1.2	1.2	2.13	1519		1054.86
test 3	1.2	1.2	2.13	1760		1222.22
			average	1573	average	1092.36

3.5 Conclusions

Based on the results obtained by this analysis performed in a large-volume enclosure, the current methods available (and recommended by the national regulations) to model fire and determine the smoke produced by the fire might not be suitable.

The best agreement in the prediction of the steady-state layer height were consistently obtained with the McCaffrey model. As for the evolution of the smoke layer the best agreement was obtained with the Zukoski model. The popular Thomas model under-predicted the smoke generation in the atrium, yielding significantly higher smoke layer heights than the measured one. It was further shown that this result may be improved by carefully choosing the value of the HRRPUA parameter to fit the results with experimental data. However, in practical design, the engineer is not able to choose reliable values for this parameter, thus being exposed to a significant error.

The results presented in this study show that the smoke layer height and its temporal evolution may be predicted with satisfactory accuracy with simple methods. This prediction improves the whole design process as the first approximation is often considered as a boundary condition for further costly numerical modeling. Use of simple plume models should be further investigated by the fire safety engineering community as they can still be considered as a valuable tool. However, the use of such models to predict the smoke production of a given fire shall be only a first approximation and not a design tool, especially using those models that have not shown a good match to the experimental data[15].

4 Influence of Fuel Soot Yield on the Visibility in Smoke

Many parameters exist that can be used to describe the smoke properties, e.g. temperature, mass density of products, obscuration density, transmittance, toxic gases concentration, etc. Among these numerous variables, when conducting Fire Safety Engineering (FSE) analysis, one of the most important is the "visibility in smoke". It is very common in FSE analysis to consider the visibility to be the first parameter that meets its critical value (tenability criteria). Visibility in numerical modeling is a result of modeling the transport of combustion products within the model, especially the soot aerosol. The soot is introduced into numerical domain through a source model, and its amount is directly affected by the effective heat of combustion of the fuel ($\Delta H_{c,eff}$) and the soot yield (Y_s). The visibility sub-model is also dependent on the visibility factor (C) and the mass extinction coefficient of the smoke (K_m). Previous research [91] has shown, that among these parameters, the soot yield has the greatest influence on the value of visibility. Nonetheless, in Fire and Smoke Modelling, despite the importance of this parameter, the value of the soot yield is often selected without proper justification. For example, some engineers may assume the materials that could act as fuel for a fire without really being sure if that material will actually be present in the building they are designing. During the design phases of a building, the engineers might not know, for example, what type of furniture will be placed inside the building. The possible materials of the furniture could be wood, plastic, metal or fabric, just to enumerate a few. All these materials having very different soot yields, the final selection of the material may have a considerably large effect on the visibility evolution, and on the Available Safe Egress Time (ASET), in any potential fire scenario.

The aim of this study to further investigate the impact of soot yield on visibility was pursued through full-scale fire tests performed in the Building Research Institute (ITB) in Warsaw, Poland. Different fires have been examined, using fuels with a high diversity of soot yield values, varying from $Y_s = 0.001$ g/g to $Y_s = 0.178$ g/g. The density of the smoke layer has been measured with an optical densitometer. For a full description of the experiments that were carried out and of the facilities that were used, see section 2.2.

The results have been compared to numerical models implemented in ANSYS® Fluent® and Fire Dynamics Simulator. The numerical analysis shows a hyperbolic trend of the visibility when increasing the soot yield. The hyperbolic relationship has a cut-off point where the soot yield is around 0.10 g/g. From the critical value, slightly decreasing the soot yield can produce a very relevant change in visibility. On the other hand, using a larger value of soot yield a negligible change in the visibility and therefore in the ASET is observed.

Determining the way in which the soot yield influences visibility through smoke is very important for CFD analysis. As it was mentioned before, visibility is normally the critical criterium for determining the ASET. CFD users must know how important the soot yield is. In cases where the materials are not known, or where it is possible that the materials be changed in the foreseeable future, the CFD user must select a soot yield above the aforementioned cut-off point in order to be conservative. Ultimately, a case study has been included to show how critical the soot yield is in the determination of the ASET in a real building.

4.1 Optical properties of smoke

The optical properties of smoke aerosol in the air are comparable with other dispersive systems. The intensity of light passing through the smoke depends on scattering, absorption, diffraction and other smaller effects, which are dependent on the parameters of the smoke and the light. Black smoke is highly absorbing, while white smoke is highly light-scattering. As smoke contains condensed water particles, additional light refraction is observed. As it is not possible to measure the absorption and scattering effects separately, their combined damping effect is measured. In engineering calculations, these effects are simplified even further, as the optical properties of smoke and their influence on the light are not modeled at all, but rather evaluated with simplified mathematical models of visibility within the smoke as a function of the local smoke concentration.

Figure 25 shows a graphic example of a local visibility plot, which is a typical method to represent results of visibility through smoke in CFD analyses. The local visibility range plot is created as an array of visibility values of individual cells. The value within each cell represents the distance from which a certain object (e.g. a sign, a light) could be seen in a room with a uniform smoke concentration corresponding to the mass concentration within that cell. In this plot, the blue represents the best visibility (30 m) and the red represents the worst (< 5 m).

Points (a), (b) and (c) are relatively close to each other but have radically different values of visibility. This does not mean that a subject in point (a) would see at 30 m distance, while one at (c) only at 5 m. The physical meaning is that an object would be visible from 30 m, 20 m or 5 m if a whole room was filled with a uniform smoke layer, as dense as in points (a), (b) or (c), respectively. To realistically determine the visibility through a non-uniform smoke, more advanced methods such as ray-tracing should be used.

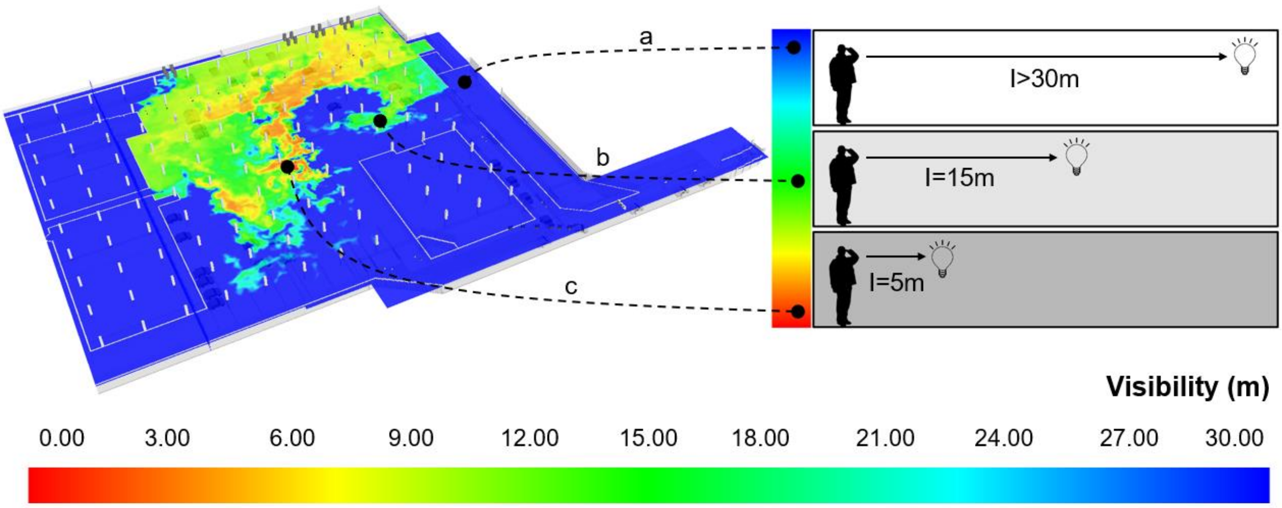

Figure 25 – Example of a local visibility range plot

4.2 Introduction of the smoke into the numerical model

In complex models, the fire is usually represented by one of three typical approaches, each of them can be implemented either as a 2D source (surface) or a 3D source (volume), depending on the solver:

a) A fixed source of heat and smoke, which is described by its volume or area, and by the amount of energy and mass of combustion products emitted from within. The yields and their change in time are predefined, and chemistry models are not used. Complex phenomena such as pyrolysis, self-extinguishing or under-ventilated combustion are not explicitly modeled.

b) A source that emits fuel or a mixture of fuel and oxygen, which is further burned using simple chemistry models (e.g. 2-eq. Arrhenius models [2], or pre-mixed burning models [3]). The yields are dependent on the chemistry and local oxygen concentration, which allows the inclusion of self-extinguishing or under-ventilated burning phenomena, but, due to the yield being predefined, the time to burnout is not explicitly modeled.

c) A model of materials that have a mass and are the source of fuel through pyrolysis or evaporation. The chemistry of the combustion model is similar to model b). This approach allows modeling of the fuel depletion and the spread of the fire, but it is the most computationally expensive and it does not have sufficient validation for complex materials, thus it is rarely used in practical engineering applications.

Models a) and b) are a prescriptive representation of a fire, which can be considered explanatory, but not predictive. Once the smoke is released into the model, to estimate the smoke density in particular control volumes (cells) of a CFD model, continuity, momentum, and mass transport equations, along with the turbulent flow sub-model, are solved. The smoke is generated within the source of fire, represented as soot particles introduced to the convective stream of air also produced by the source. This representation heavily relies on the main parameters relevant to the soot production, $\dot{m}_s$ (kg/s) – effective heat of combustion, $\Delta H_{c,eff}$ (kJ/kg), heat release rate, $\dot{Q}$ (kW), and the soot yield parameter, Y_s (g/g). The mass of smoke introduced into the model can be presented as:

$$\dot{m}_s = Y_s \frac{\dot{Q}}{\Delta H_{c,eff}}. \tag{23}$$

The amount of soot, often referred to as the "mass smoke concentration", is known in every control volume of the model, in every discrete time-step.

4.3 Light dampening by the smoke

The basic interaction between light and an aerosol is described by the law of Bouguer-Lambert-Beer, eq. (24), which describes the relation between light dampening and the light extinction coefficient K (m^{-1}) [6]

$$I = I_0 e^{-\mathrm{KL}}, \tag{24}$$

where I is the luminous intensity through smoke (cd), I_0 is the luminous intensity through clear air (cd) and L is the length of the light path (m).

The application of the Bouguer-Lambert-Beer law for smoke has the following limitations:

a) the smoke layer should be homogenous. If visibility is estimated for an heterogeneous mixture it must be referred to as “local visibility” parameter and related separately for each control volume for which the calculation is performed.
b) the mechanism of light dampening is absorption and not scattering – while in fire smoke, both phenomena occur at the same time.
c) a single light source exists, or light sources are parallel – while in buildings, there are multiple sources of light.
d) the source of light is monochromatic – while in buildings both natural and artificial light sources are polychromatic.

As Mayerhöfer et al. stated [92], taking simply the negative decadic logarithm of a singular transmittance measurement does not compute the absorbance and the results cannot be quantitatively evaluated and will not linearly depend on concentration or thickness. However, some solutions for optimizing the use of Bouguer-Lambert-Beer law exist, and are used for computing photometrical data in the context of fog and other atmospheric phenomena [93–95].

Despite its limitations, the Bouguer-Lambert-Beer law is still the most common approximation of the effect of smoke on the light passing through it. To describe the smoke layer with a mathematical model, the obscuration density parameter, also known as the optical density of the smoke, is introduced. This parameter relies on the size of smoke particles, their distribution, diameter, absorption and scattering coefficients and the length of lightwave. As a simplification of this, a mass extinction coefficient can be introduced, K_m (m^2/kg), which was discussed in depth in [96,97]. Introducing this coefficient into the Bouguer-Lambert-Beer equation results in:

$$I = I_0 e^{-K_m m L}, \tag{25}$$

where m is the mass concentration of the smoke aerosol (kg/m^3).

The values of mass extinction coefficients for various flammable materials can be found in the literature, ranging from 7600 to 9800 m^2/kg. For example, the standard value implemented in FDS v.6 is 8700 m^2/kg.

A comprehensive discussion on the values of mass extinction coefficient can be found in [96,97]. Detailed information on how this parameter is derived from thermal decomposition and combustion of polyester materials is presented in [98,99]. A different approach, not directly connected to the material but to the light, is presented by Widmann [100]. A power-law correlation is introduced for the mass specific extinction coefficient dependent on the wavelength of the light, λ (nm). This correlation allows estimating the K_m coefficient for a well-described source of light with constant wavelength.

$$K_m = 4808\lambda^{-1.0088}. \tag{26}$$

The Bouguer-Lambert-Beer law can answer the question of whether the light can pass through the layer of smoke, but it is not an indicator of visibility of an exit door or a sign.

4.4 Modeling the visibility in smoke

The human eye can distinguish a shape (such as an evacuation sign) when the difference between the luminance of the object, L_t (cd/m^2), and of its background, L_b, exceeds the critical contrast value, δ_c, at which the object is visible. This critical contrast value will rely on the light intensity. As an example, for mist conditions, this value is $\delta_c = 0.02$ [5], while some sources present this value in a range from 0.01 to 0.05 [101]. This parameter is also obviously dependent on the individual eyesight characteristic of a person.

$$\left|\frac{L_t - L_b}{L_t}\right| > \delta_c \ . \tag{27}$$

By combining this theory with the mathematical model of light dampening effect, Jin [102,103] derived a mathematical model that allows estimation of visibility through a homogenous layer of smoke, V (m)

$$V = \frac{1}{\mathrm{K}} \ln\left(\frac{L_t \pi}{\delta_c a E}\right). \tag{28}$$

Both the luminance of the sign, L_t, and its illuminance from all directions, E (lx), will influence the visibility value. K is the light extinction coefficient (m^{-1}) and *a* is a dimensionless coefficient that depends on the scattering coefficient and the absorption coefficient. To simplify this equation, based on a test program in a small chamber filled with white smoke produced by pyrolysis of wood, most of the variables were combined into a single coefficient, the visibility factor, C.

$$V = C\left(\frac{1}{K}\right). \tag{29}$$

The widely used values of C are 3 for light reflecting signs and 8 for light emitting signs, although, in the original work of Jin in the 1970s [102,104,105], this is a variable dependent on the dimensionless brightness of a sign (L_t/E), Figure 26. In the SFPE Handbook of Fire Protection Engineering (3rd edition, 2002), this value is presented as a range between 2-4 for light reflecting signs and 5-10 for light emitting signs. In the last edition of the SFPE Handbook of Fire Protection Engineering (5th edition, 2016), a comment was included in the chapter relevant to visibility in smoke:

"It should be noted that the constant C in Equation 61.4 tends to be larger than the previous data indicated by Jin (...)."

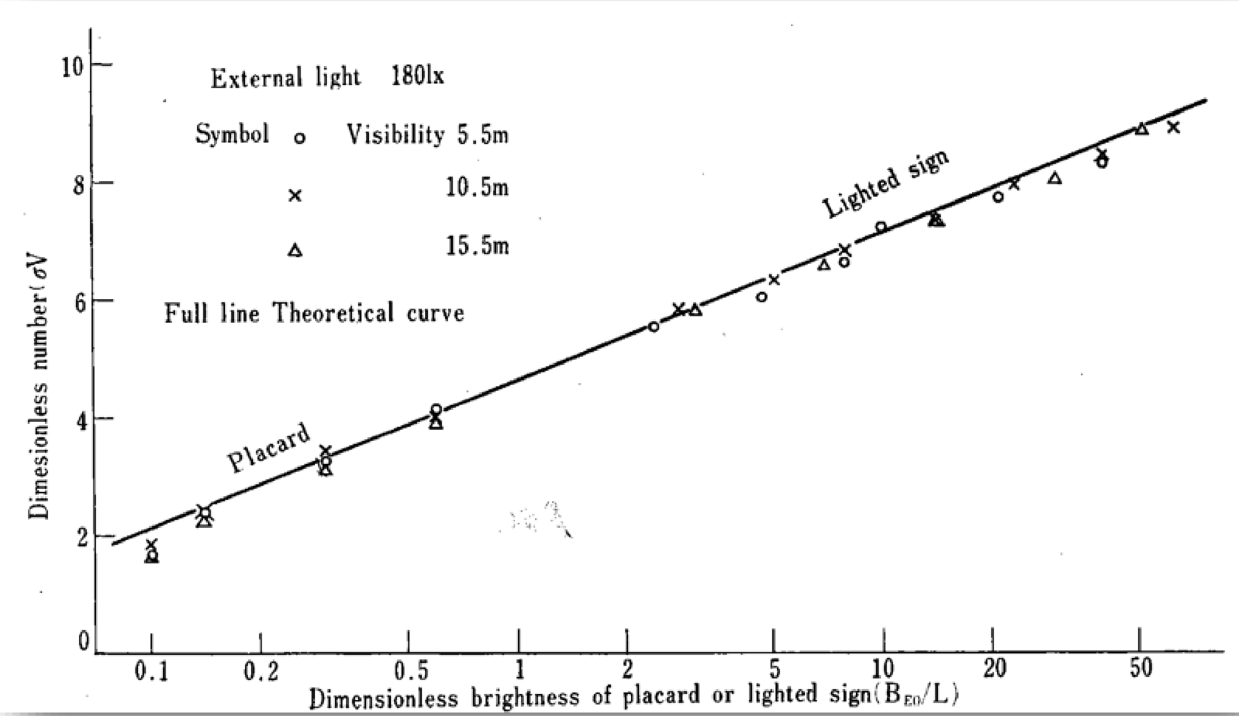

Figure 26 – Dimensionless number C as a function of dimensionless brightness of an evacuation sign, as printed in original paper by T. Jin [102] **(σV in the graph)**

When applying the theory of Jin into modern CFD models, the user has to be advised that this theory was derived by Jin in the early 1970s, before the development of two-zone models [59], the ASET/RSET concept [106] or early CFD models [89] developed for Fire Safety Engineering applications. This means that the theory may be expanded beyond its original area of application, and as such, it has to be taken with necessary caution. Application of the theory of Jin directly into modern CFD models, for each control volume, has taken the form

$$V = \frac{C}{K_m m}, \tag{30}$$

where K_m is the mass extinction coefficient (m^2/kg) and m is the mass concentration of smoke (kg/m^3).

4.5 Validation of numerical model of visibility in CFD

The Warsaw ITB experiment was recreated in numerical models ANSYS® Fluent® (v.17.0.0) and Fire Dynamics Simulator (v.6.4.0) to validate these models for further parametric studies. Two different approaches were used:

a) ANSYS® Fluent® package, second-order numerical scheme (segregate model), with Realizable RANS k-ε turbulence model and P1 radiation model. Solution convergence was measured at each discrete time step. Space discretization with unstructured tetrahedral mesh. The fire was modeled as a volumetric source of heat and smoke [107].
b) FDS package, Low Mach, explicit, second-order solver. LES turbulence model and DO gray gas radiation model. Structured uniform Cartesian mesh. Eddy dissipation model (fast chemistry) for the single-step reaction between fuel and oxidizer [108].

In both models, the fire source has been modeled as a source of heat and smoke. The HRR was defined a priori based on the burning time and mass loss rate of the experiments. Authors are aware of the existence of sub-models which allow to predict the evaporation of the fuel and therefore the HRR. However, predicting the HRR in such way would add a source of uncertainty that would move the focus of this study. Previous studies have shown a high level of uncertainty comparing real scale tests and predicted HRR in several heptane pool fires [109]. In order to check the performance of the numerical models used, a preliminary validation analysis has been performed comparing the measured and predicted temperature in test data obtained from different tests (in particular, tests with heptane, propanol, toluene and methanol). The results show a relatively good agreement between modeled and experimental temperature data for heptane and propanol with a maximum discrepancy of about 20%. Higher discrepancies have been found for methanol and toluene, which can be attributed to the uncertainty of HRR measurement in the model. The resulting smoke layer, Figure 29, in CFD analysis was close to homogenous and stable, as observed in the full-scale experiments, Figure 10 to Figure 13.

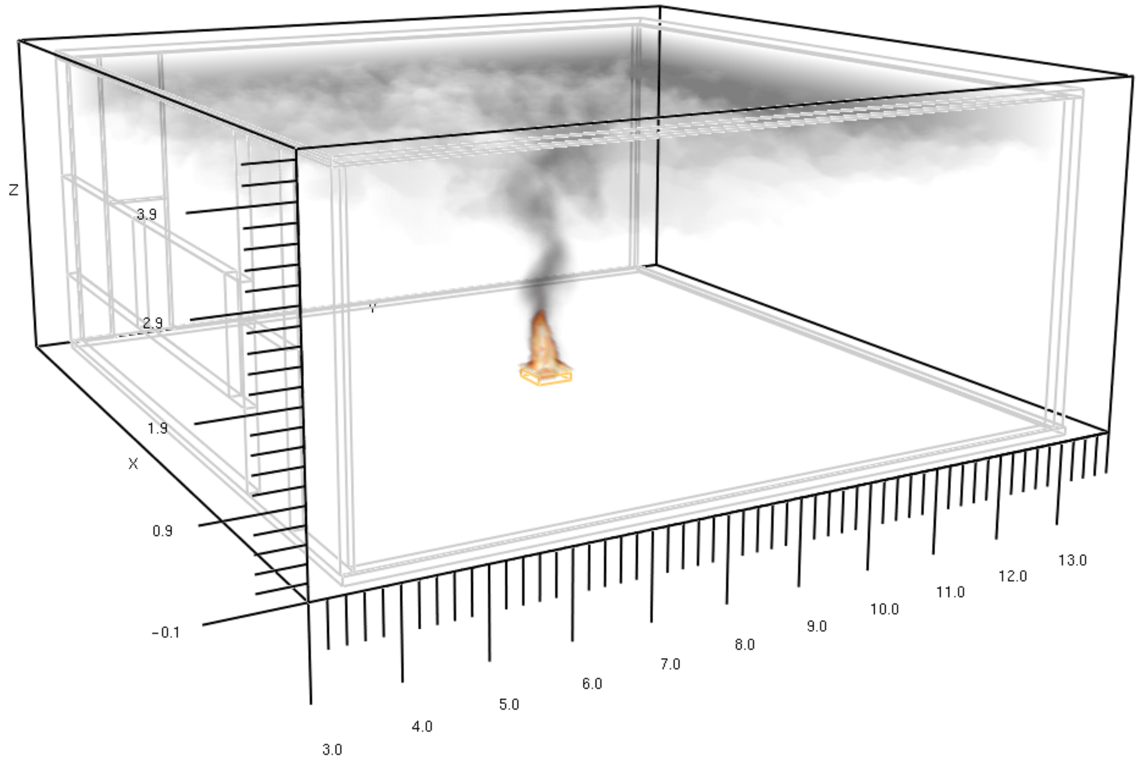

Figure 27 – Visualization of the FDS model results with Smokeview.

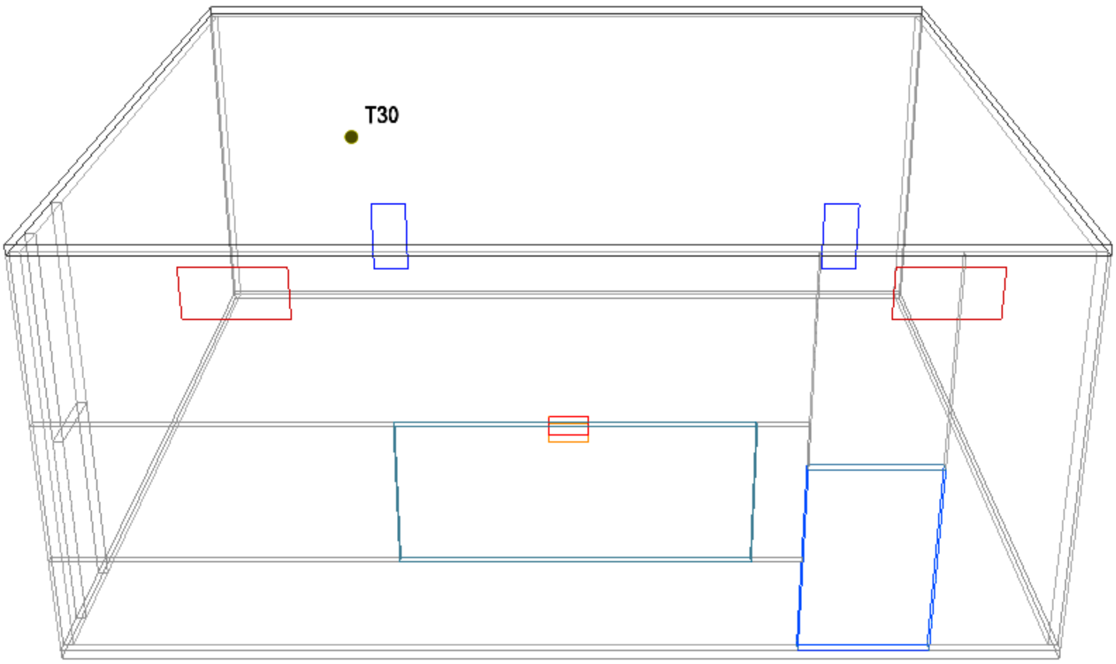

Figure 28 – Position of the Thermocouple T30 employed in the analysis (FDS model), next to the optical densitometer, used as the presented reference for model validation.

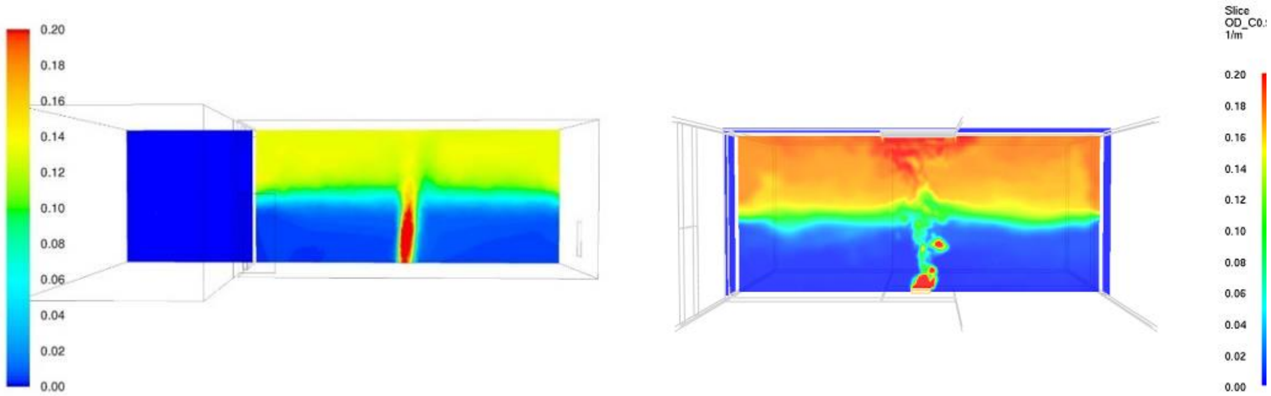

Figure 29 – Sample results of reference studies performed in ANSYS Fluent (left) and FDS (right). Besides the plume, ceiling jet and zone transition regions, the layer can be considered homogenous. The colors represent different values of soot optical density (m^{-1}).

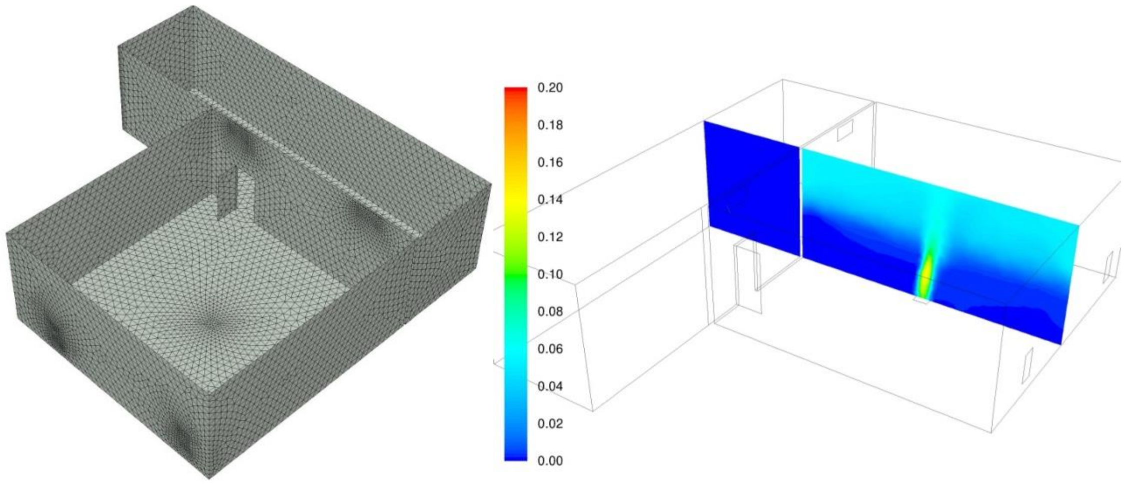

Figure 30 – Numerical model used in a preliminary study using ANSYS Fluent (left) and mass density of smoke in preliminary study of propyl alcohol fire (right).

Figure 31 and Figure 32 show the comparison between experimental and numerical data (FDS and Fluent) for a specific thermocouple (T30, in Figure 30 above) which was reasonably away from the fire plume and sufficiently immersed in the smoke layer. Several thermocouples were installed in the chamber and defined in the model, but only this one was used in this validation since it was in a relevant position and it was not affected by the fluctuation of the flame.

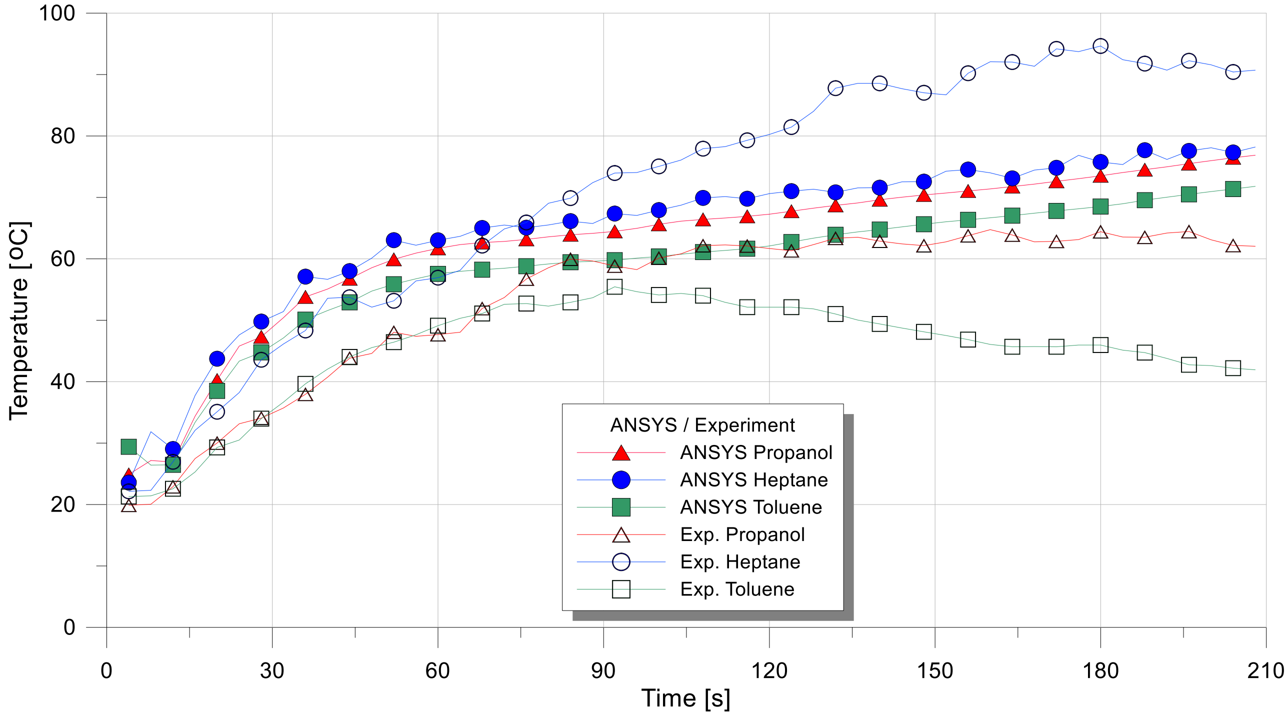

Figure 31 – Experimental validation – temperature comparison in the optical densitometer proximity, ANSYS Fluent.

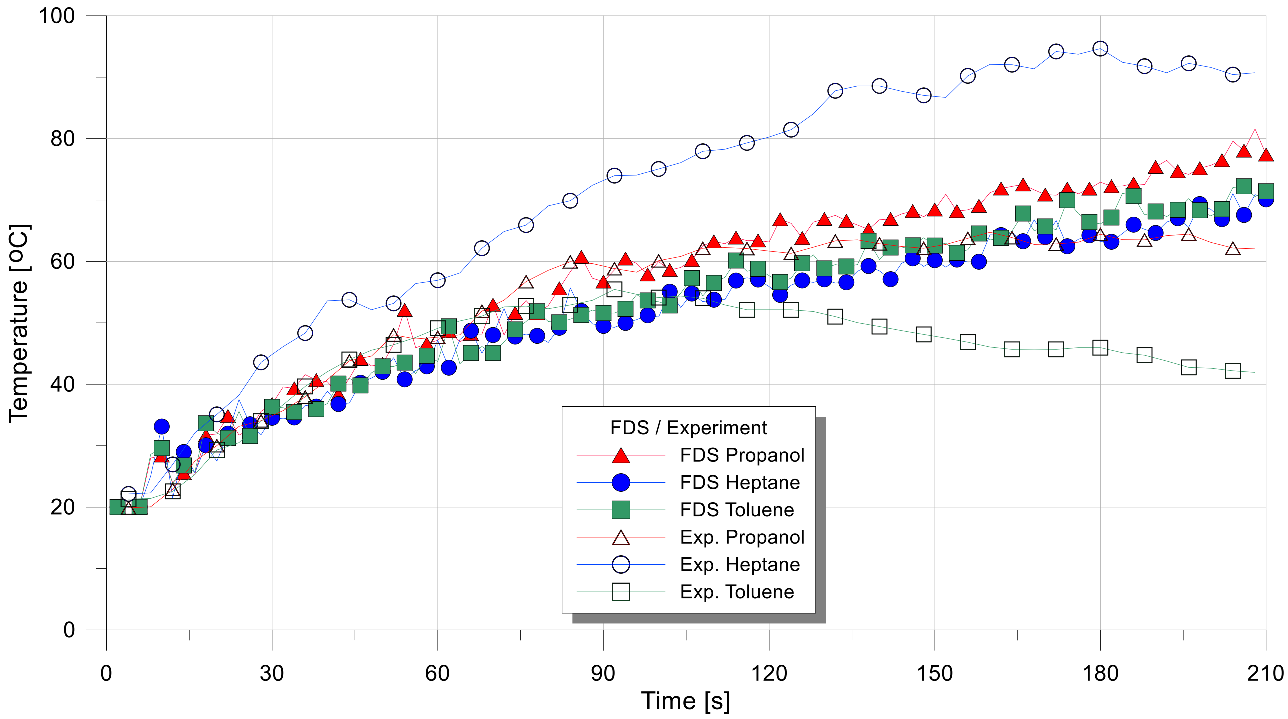

Figure 32 – Experimental validation – temperature comparison in the optical densitometer proximity, FDS.

4.6 Parametric Studies

One of the purposes of both the empirical and the computational experiments was to compare different parameters related to smoke and evacuation, and to explore how varying one parameter affects the others. In order to find out which parameter is the most important in the determination of the visibility through smoke, a basic mathematical analysis was carried out before the parametric studies. This pre-analysis compared the three main parameters that are considered when the visibility through smoke is calculated: soot yield (Y_s), light extinction coefficient (K) and the visibility factor (C)[110].

4.6.1 Pre-analysis

Estimates of visibility through smoke, V (m), can be made by using the following equation, equivalent to equation (31):

$$V = \frac{C}{K}, \tag{31}$$

K, the light extinction coefficient (m^{-1}), can be calculated using the following equation:

$$K = K_m \rho Y_s \, , \tag{32}$$

where K_m is the mass extinction coefficient (m^2/kg), ρ is the density of the smoke (kg/m^3) and Y_s is the soot yield of the fuel (g/g).

Combining equations (31) and (32), one can obtain equation (33):

$$V = \frac{C}{K_m \rho Y_s} \, . \tag{33}$$

A simplified analysis was performed by Alonso [110] to determine which of the parameters in equation (33) (except density) has the greatest influence on visibility through smoke. Various graphs were produced where the visibility was plotted against each of these parameters. Figure 33 and Figure 34 show plots of visibility against soot yield and against the extinction coefficient. These graphs are solely based on the equations, i.e. on the theoretical mathematical relationship between the parameters. In Figure 33, the existence of a cut-off point around 0.10-0.12 g/g is evident.

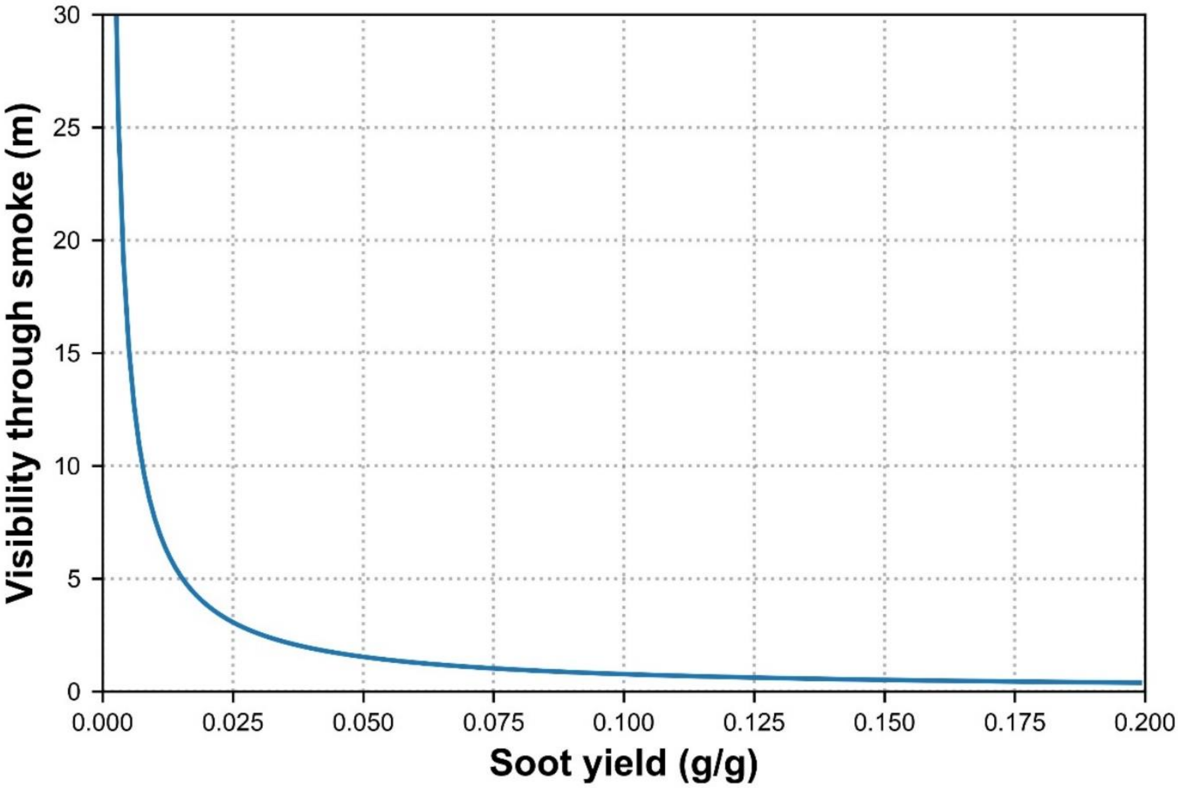

Figure 33 – Influence of soot yield on visibility through smoke based on the theoretical equation.

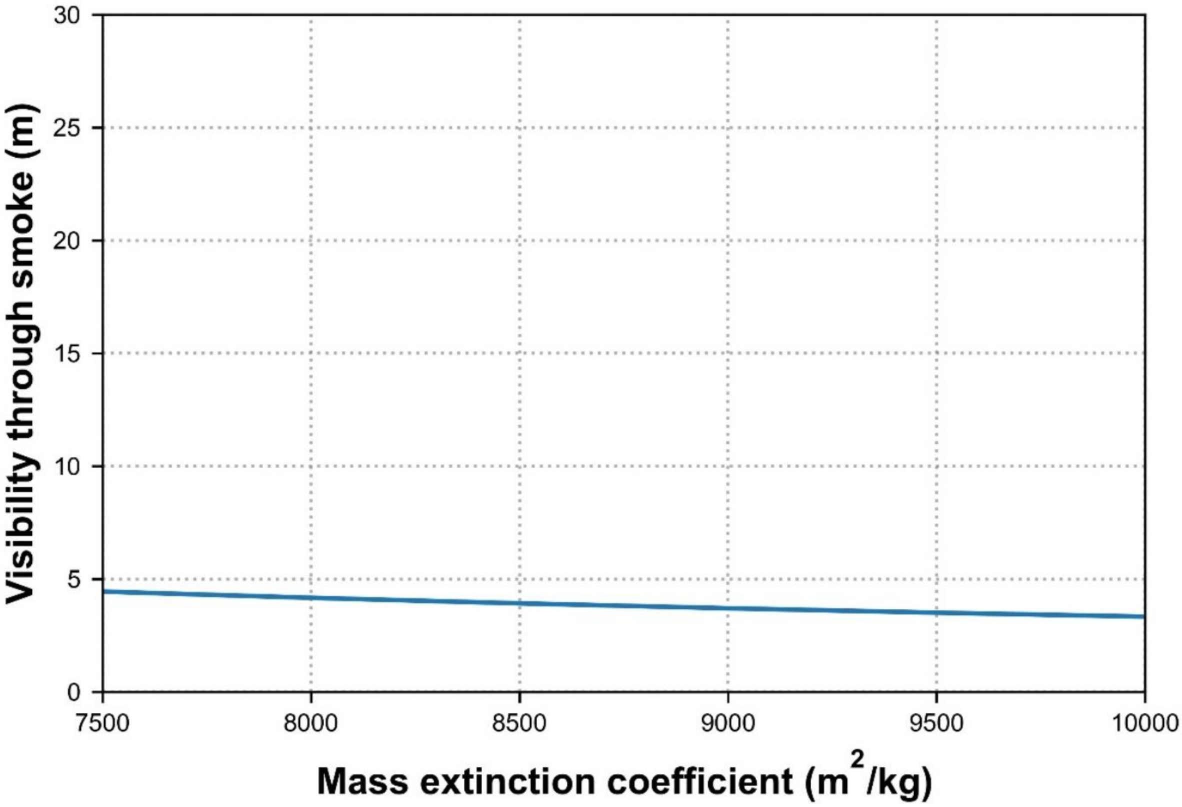

Figure 34 – Influence of the extinction coefficient on visibility through smoke based on the theoretical equation.

After the analysis it was concluded that the soot yield is the most important parameter provided by the user of a CFD model because of the huge influence it has on the visibility through smoke. The soot yields of usual fuels vary vastly, and it makes a huge difference whether the soot yield is 0.005 g/g (visibility would be around 13 m) or 0.015 g/g (visibility would be around 4m).

It is true that the extinction coefficient influences the visibility through smoke, although not nearly as much as the soot yield. This parameter does not vary as much as the soot yield, since its typical values range from 7600 m^2/kg to 9800 m^2/kg. Nonetheless, it is encouraged that future research investigates empirically the relationship between the extinction coefficient and the visibility.

Regarding the visibility factor, C, it was concluded that it was not as interesting to investigate as the soot yield. Usually, only two values are used for this factor, 3 or 8. On the other hand, soot yield is extremely variable, being 0.01 g/g for methanol, 0.15 g/g for propanol, 0.035 g/g for heptane and 0.178 g/g for toluene, just to name a few fuels. However, once again, it is encouraged that future researchers investigate this parameter experimentally as well.

4.6.2 Impact of the Soot Yield on Visibility

Twenty (20) models based on the “Warsaw experiment” have been processed both in Fluent and FDS [111] with a soot yield range between 0.01 g/g and 0.2 g/g using the Heptane reaction as a base. Despite the possible error with the use of Bouguer-Lambert-Beer law, the same mathematical model was also applied to the transmittance measurements of the “Warsaw experiment” and presented in the plots along with the results of the numerical study. The results for both Fluent and FDS (and the experiments) show a linear trend for obscuration density (a representation of the mass concentration of smoke - Figure 35 - and a hyperbolic trend of the visibility when increasing the soot yield, confirming the previous work undertaken by the author.

As expected, the increase of the amount of soot introduced to the model increases the amount of the soot within the steady-state smoke layer. For the visibility in smoke, a cut-off soot yield value exists at about 0.10-0.12 g/g. Under that value, visibility changes considerably, while, above that value, the variation is almost unsignificant. Figure 36 and Figure 37 show the visibility trend against soot yield calculated with Fluent and FDS both for reflecting and emitting signs. It can also be noted that the measurements of the obscuration density (and the visibility) differ between experiment and both numerical models substantially. This difference could be attributed to the uncertainty of the choice of extinction coefficient (K) which was taken directly from the literature. It was not possible to measure this value for the smoke generated in the experiment, as this requires dedicated, sophisticated apparatus. The use of Widmann’s equation (26) provided a better correlation, but for the purpose of this study, the default values of the CFD software were used, to illustrate the practical aspects of the change in soot yield.

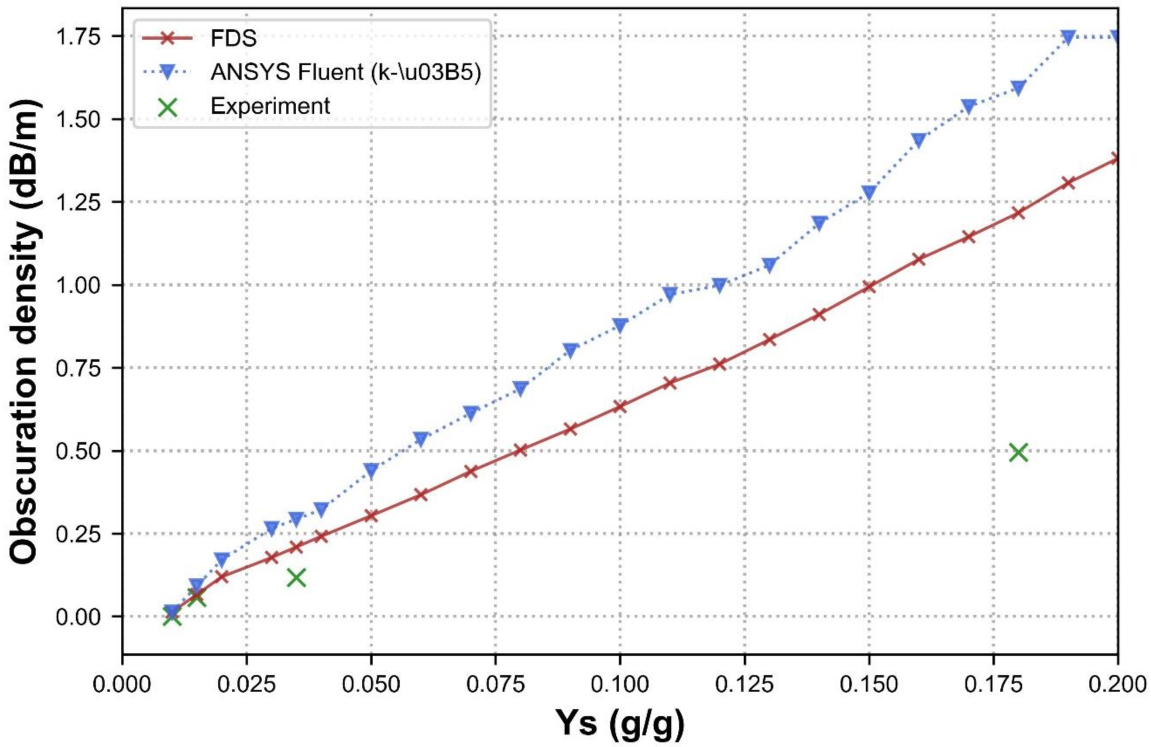

Figure 35 – Obscuration density vs. Soot Yield

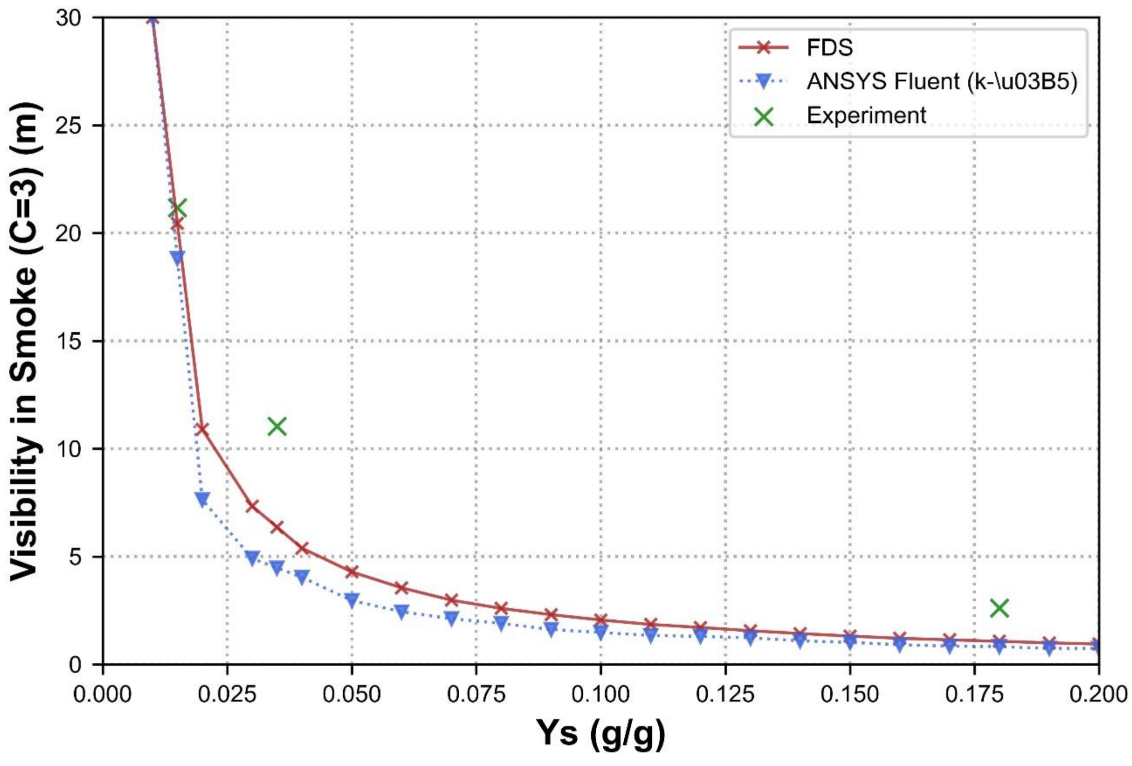

Figure 36 – Visibility range vs. Soot Yield for C=3

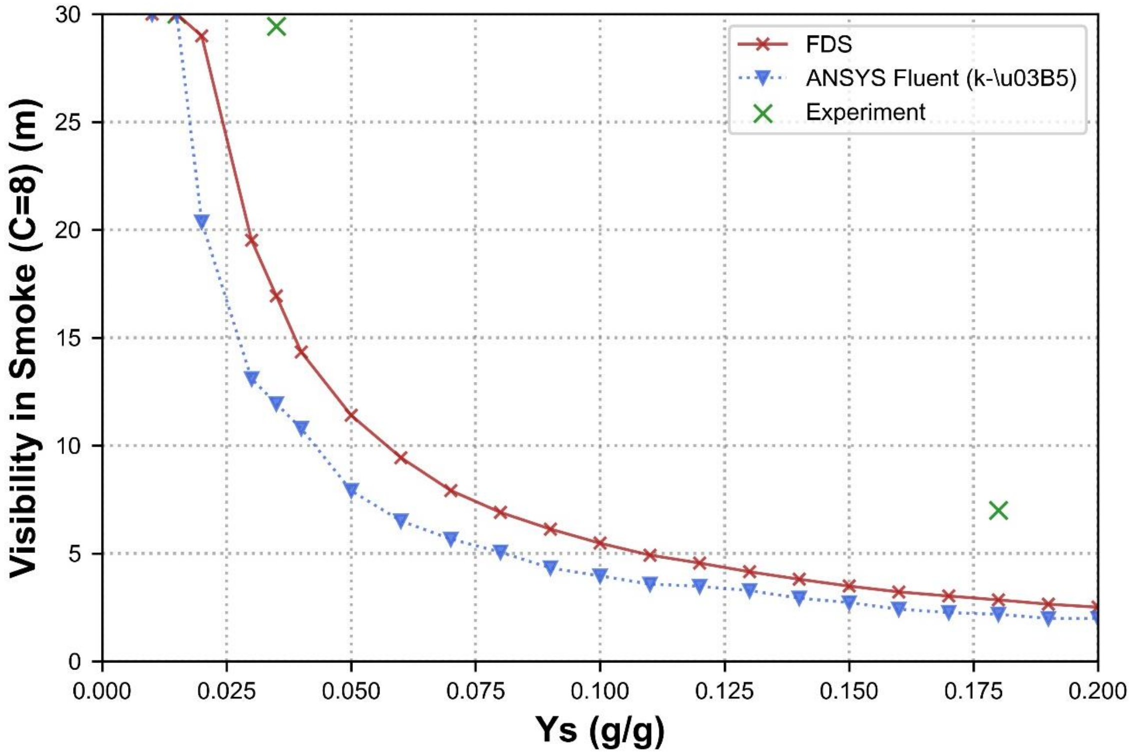

Figure 37 – Visibility range vs. Soot Yield for C=8

4.6.3 Soot yield vs. ASET

Using previously described the results were investigated to find the time at which the 10 m visibility criterion was exceeded in the model within the homogenous smoke layer (for visibility factor C=3). The 10 m visibility criterion was chosen as a representative due to its popularity among Fire Safety Engineers, and it is mentioned in various guidelines: [112–115]. It must be noted that some sources give higher values than 10 m (e.g. 16 m in [116], 13 m for unfamiliar users [104]).

For the time to reach a visibility of 10 m, a similar cut-off value existed, at approximately 0.10 and 0.12 g/g. For soot yield values below the cut-off point, the time to reach 10 m visibility was significantly shorter. For soot yield values above this point, the time to reach 10 m visibility did not differ more than the resolution of time measurement (for subsequent steps in soot yield value). It is important to note, that with the conservative assumption, the time to reach 10 m visibility was close to 10 – 15 seconds, while for values under 0.03 it was more than one minute.

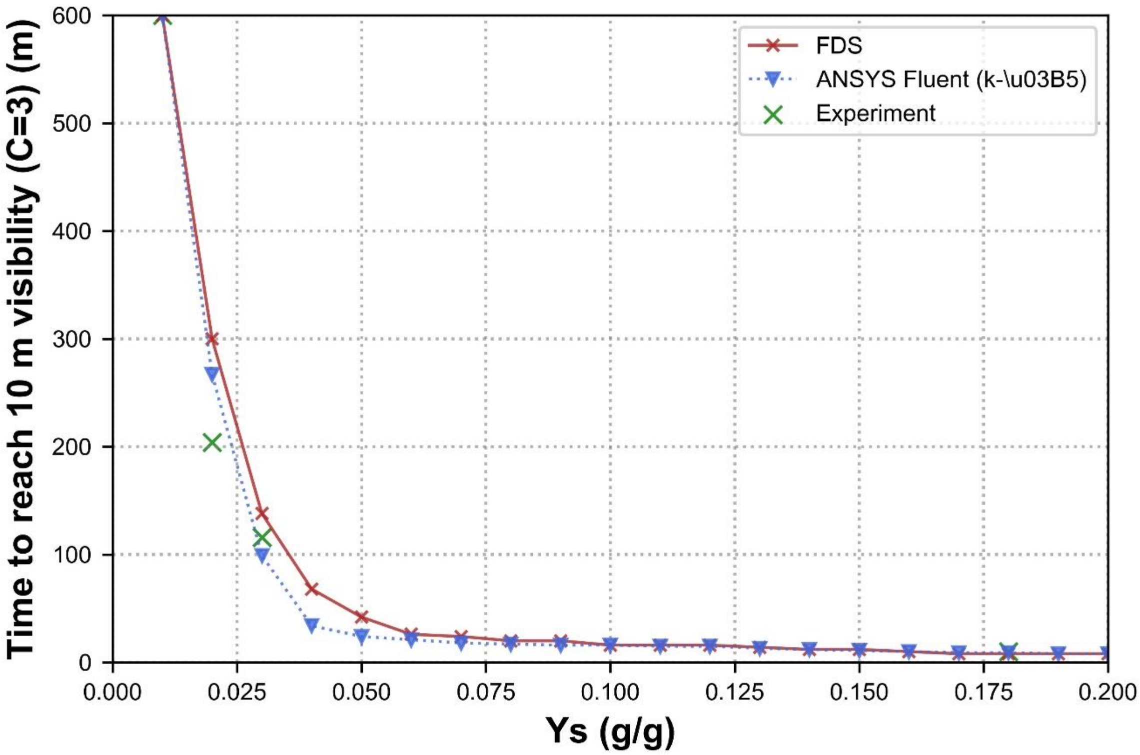

Figure 38 – Time to reach 10 m visibility (C = 3) in experiment, ANSYS Fluent, and FDS

4.6.4 Example of application in a large-volume compartment

A real case has been included to show how the observations from the previous studies can be translated into the Fire Safety Engineering design process. This exercise is concerned with determining the concentration of smoke and the visibility in smoke in a real building through a series of numerical simulations using ANSYS Fluent software. The analysis was conducted for a compartment with dimensions of 20.00 m x 25.00 m x 5.00 m, and a volume of 2500 m^3. The compartment was connected with a fragment of the adjacent space (a corridor of a shopping mall) through an opening dimensioned 8.00 m x 3.50 m. The smoke and heat exhaust system in the compartment had a volumetric flow rate of 60000 m^3/h, and the air was exhausted through two ducts with 11 inlets on each of them (22 in total). The fire was modeled as a frustum with a height of 1.75 m and the total volume of 3.2 m³. The total heat release rate of the fire was limited to 2.50 MW, and it was described with αt^2 growth function, with $\alpha = 0.0469$ kW/s² - see Figure 40. $\Delta H_{c,eff}$ was equal to 20.00 MJ/kg, and the Y_s was a variable ranging from 0.02 g/g to 0.16 g/g (0.02 step). This set of boundary conditions and mathematical models was previously validated using the experiments shown previously.

The following physical sub-models were used:

- Realizable RANS k-ε turbulence model;
- P1 radiation model;
- Wall boundaries – gypsum plasterboard, a third type of b-c.

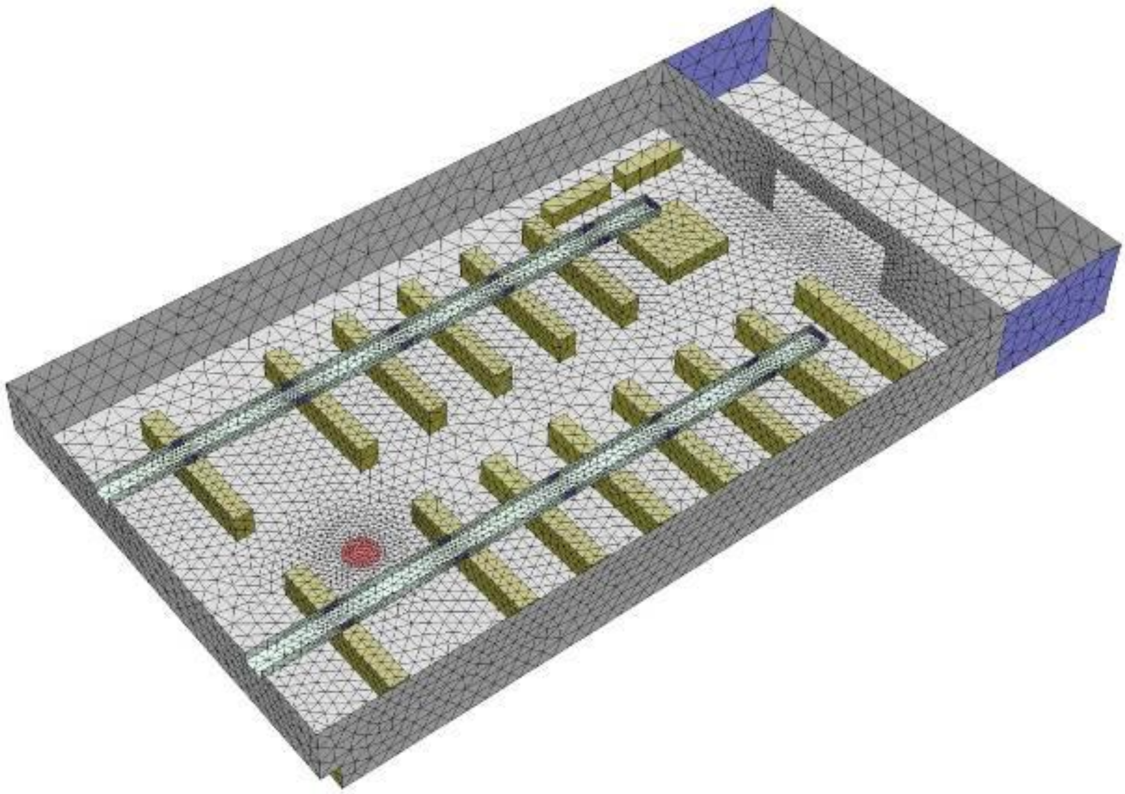

Figure 39 – Numerical model of the volume compartment.

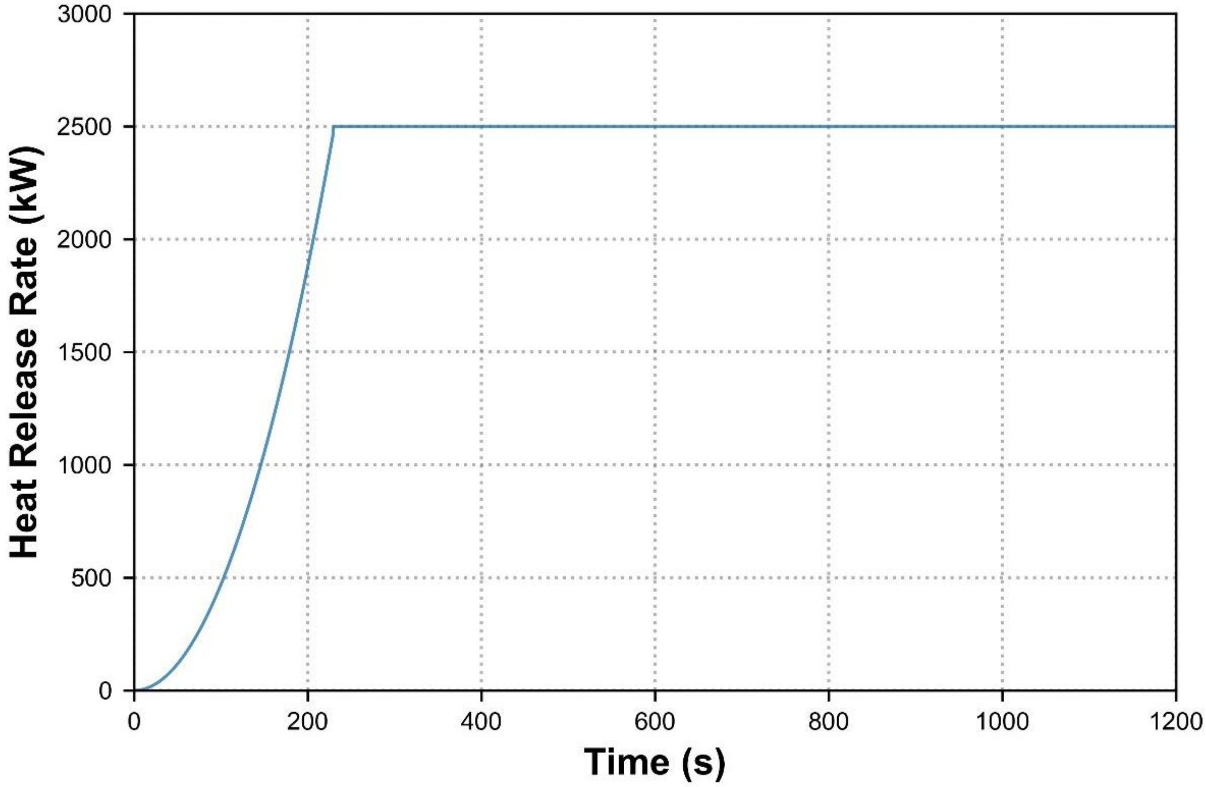

Figure 40 – HRR of the fire used.

The results were assessed with respect to:

- The mass density of smoke and visibility in smoke (C=3), in a point in the middle of the room (x = 12.5 m, y = 10 m, z = 2.00 m) - Figure 41.
- The mass density of smoke and visibility in smoke (C=3) in a plot (axis y = 9.00 m) through the fire, in the 420th second of the analysis, Figure 42.

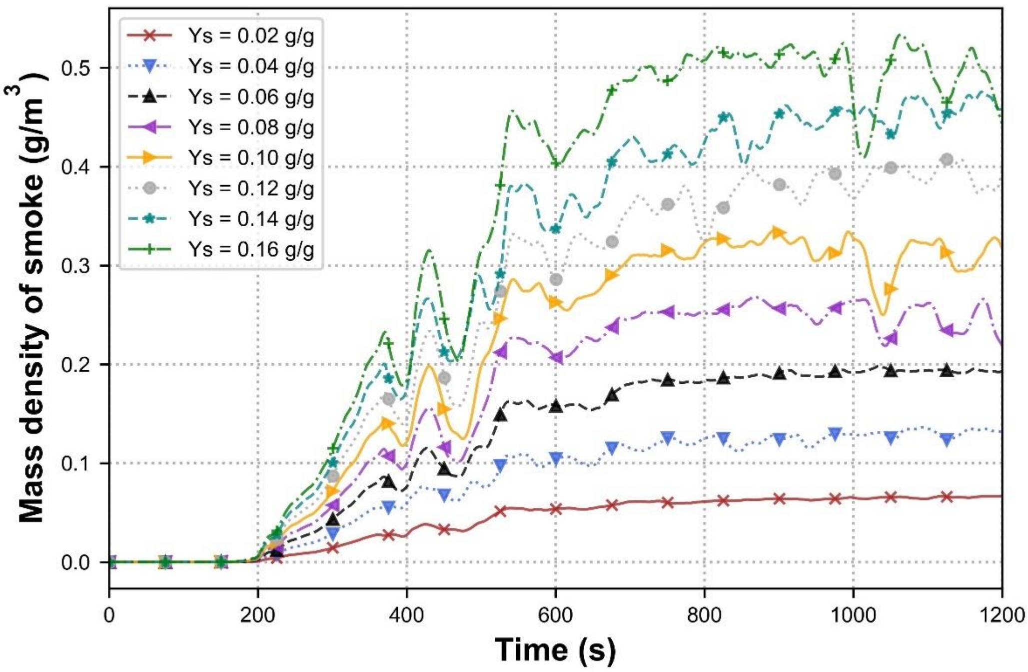

Figure 41 – Plot of the mass density of smoke.

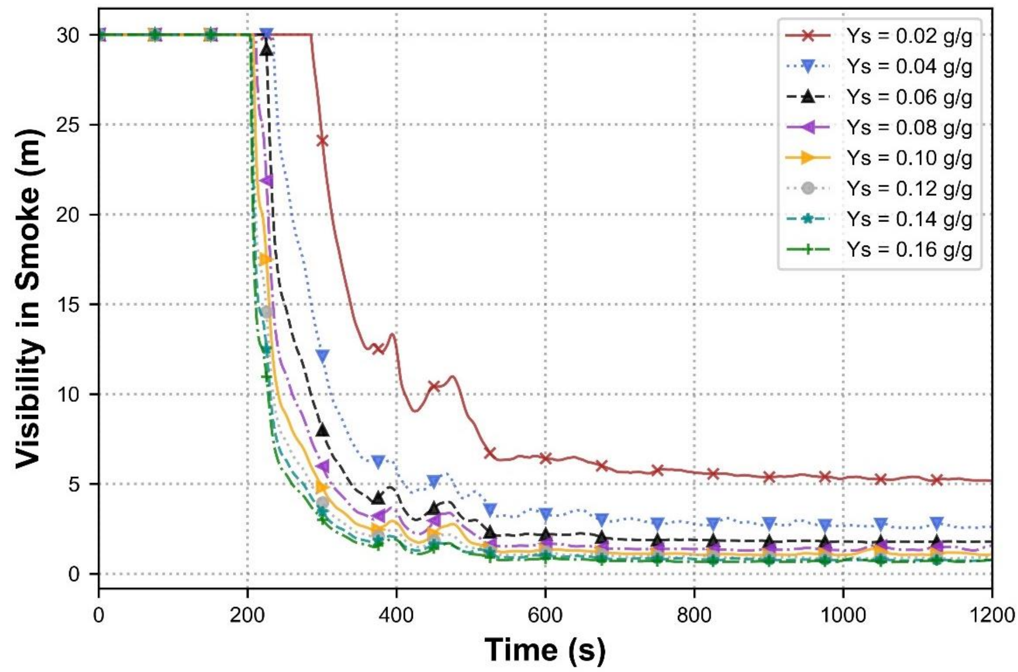

Figure 42 – Visibility in smoke in a point in the middle of the compartment.

Quantitative assessment of the results shows that the mass density of smoke between subsequent models differed by a close to constant value - i.e., the difference between Y_s = 0.02 g/g and Y_s = 0.04 g/g was approximately the same, as between Y_s = 0.04 g/g and Y_s = 0.06 g/g). The only significant differences were observed in the late stage of the simulation when the flows within the compartment differed between the scenarios. Despite the fact that the mass concentration of smoke within the room was proportional to the change of the soot yield value, the visibility in smoke differed substantially. The times to reach 10 m visibility in the chosen point was: 410 s for Y_s = 0.02 g/g; 312 s for Y_s = 0.04 g/g; 285 s for Y_s = 0.06 g/g; 260 s for Y_s = 0.08 g/g; 227 s to 237 s for Y_s = 0.10 – 0.16 g/g. It can be noted, that with Y_s between 0.02 – 0.10 g/g, the time to reach 10 m visibility ranged from 410 s to 260 s, while for Y_s between 0.10 – 0.16 g/g, this time, varied between 227 s and 237 s. This shows, that if the user chooses $Y_{s\,=}$ 0.10 g/g, it can be considered as a conservative assumption that will not negatively influence the qualitative analysis of the results.

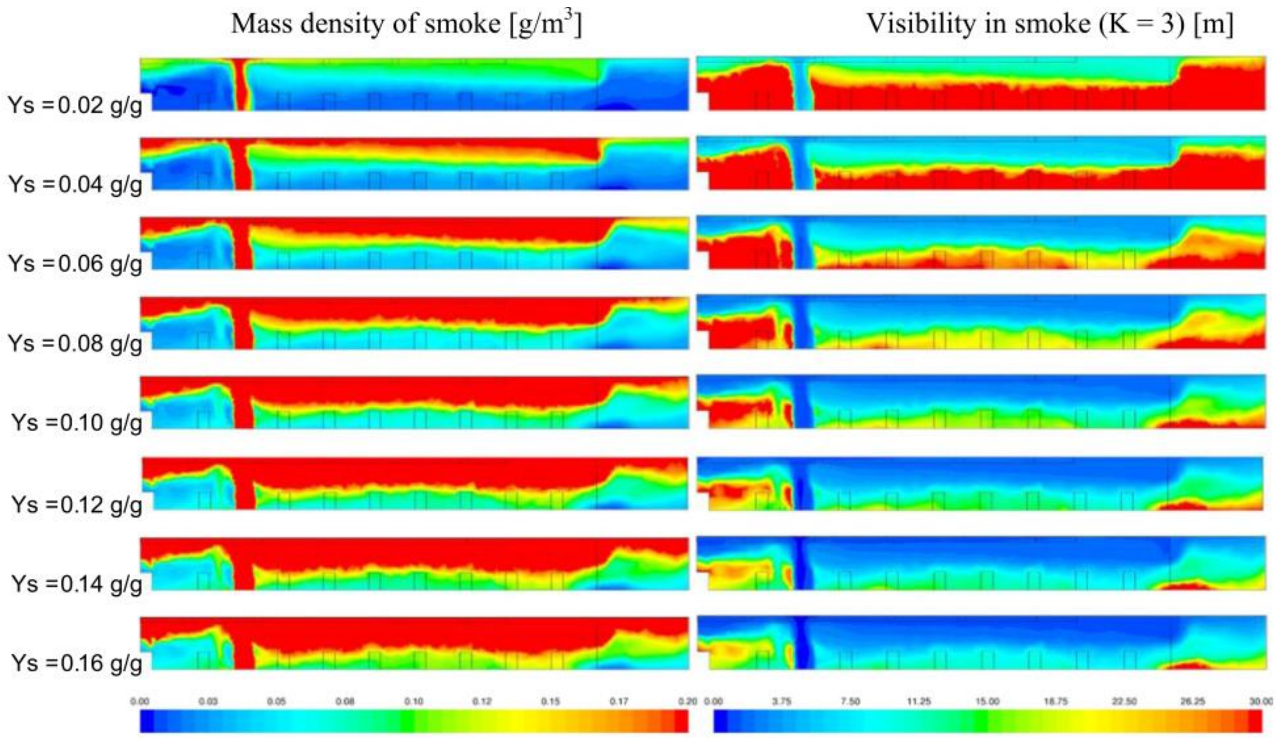

Figure 43 – Mass density of smoke and visibility in smoke in a plot through the compartment, t = 420 s.

The qualitative assessment of the results differs substantially among the five cases with Y_s < 0.10 g/g, while for cases with $Y_s \geq$ 0.10 g/g the results were similar, Figure 43. In the two lowest soot yield value cases (Y_s 0.02 and 0.04 g/g) the smoke exhaust system was effective, while for cases with Y_s between 0.04 to

0.08 g/g the system did not manage to maintain a smoke-free layer in the compartment. For soot yield values below 0.06 g/g, a smoke lodging in the bottom layer of the room is not observed (especially in the visibility plots), while for higher soot yield the smoke is observed in the whole height of the room. Additionally, with the Y_s lower than 0.08 g/g, the conditions outside the compartment can be considered tenable, while at higher Y_s they are not. The differences between the scenarios have severe consequences on the assessment – for $Y_s < 0.04$ g/g the system could be considered correct, at 0.04 – 0.08 g/g the conditions inside the room were untenable, but outside it was correct, and at $Y_s \geq 0.10$ g/g a large amount of the smoke was observed in and out of the room. If the CFD user relies on a low Y_s value ($Y_s < 0.10$ g/g), his assessment may be invalid, and potential problems with the smoke control system can be overlooked.

4.7 Conclusions

Four (4) experimental tests have been performed in the ITB Research Centre of Warsaw, Poland, using different fuels with a broad range of soot yield values (from 0.001 g/g for methanol to 0.178 g/g for toluene). The description of the tests and of the facility where they were carried out can be found on section 2.2. The results have been compared to four (4) numerical models processed with both ANSYS Fluent and Fire Dynamics Simulator. The numerical models were over-predicting the temperature, which may be connected to the non-perfect modeling of the HRR – in the experiments the burning process was non-uniform, while in the CFD models steady-state heat and smoke generation were used. After the validation, a numerical study looking at 20 different cases was carried out, each one with a soot yield difference of 0.01 g/g (from 0.01 g/g to 0.20 g/g).

It is difficult to compare optical densitometer measurements (experimentally) with measurements in CFD software. The main reason behind it is that transmittance measured with a monochromatic light source of optical densitometer has the limitations of Bouguer-Lambert-Beer law, described in section 4.3. In numerical modelling, this value is not a result of light ray-tracing, but a mathematical description of the phenomena using many approximations (e.g. mass extinction coefficient, K_m value). Despite this, the change in visibility caused by a change in fuel soot yield may be considered as valid, if subsequent cases were estimated with the same mathematical approach, and the only variable was the soot yield value. This approach was chosen for this analysis.

The numerical analysis, both for ANSYS Fluent and FDS, shows an hyperbolic trend of the visibility when increasing the soot yield with a cut-off point at around 0.10 g/g, around which a variation of the soot yield can produce a relevant (below 0.10 g/g) or a negligible (above 0.10 g/g) change in the visibility.

One of the major findings of this study is that, unless the materials (and thus the chemical reactions) in the building to be assessed by a Fire Engineering analysis are well known, values of soot yield below approximately 0.10 g/g should be used with extreme cautiousness when performing an ASET/RSET exercise. In cases where the materials are not known, or where it is possible that the materials be changed in the foreseeable future, the CFD user must select a soot yield equal to or above 0.10 g/g in order to be conservative.

5 CFD Validation of multiple-source full-scale experiment

This chapter presents the results of the new full-scale fire tests, #4FX, which was described in section 2.1.4. The test was performed with four pool fires igniting at subsequent times, with a total HRR of 5.2 MW, under a transient exhaust flow rate. The investigation concerned mainly the smoke temperature in the near field (fire plume) and in the far field (close to the walls), as well as the smoke layer interface.

These experimental results could be also used as a benchmark to validate numerical models. In fact, a numerical–experimental comparison using FDSv6.7.1 is also presented, validating the numerical model.

Section 2.1.4 described the experimental set-up completely, including the devices used in the fire tests. Sections 5.1 introduce the numerical model. After that, section 5.2 will present the results of the experiments and of the modelling, as well as their discussions. Section 5.3 includes the conclusions drawn from this analysis.

5.1 Numerical Analysis

5.1.1 Numerical Setup

The numerical simulations have been carried out using Version 6.7.1 of Fire Dynamics Simulator (FDSv6.7.1) [117,118]. FDS is a computational fluid dynamics (CFD) model of fire-driven fluid flow. FDS solves a form of the Navier-Stokes equations appropriate for low-speed (Ma < 0.3), thermally-driven flow with an emphasis on smoke and heat transport from fires numerically, [118]. The model used to account for combustion was the Eddy Dissipation Concept (EDC) model with a thermal extinction model, flow turbulence was modelled with Large Eddy Simulation (LES), Deardorff model (Cv = 0.1), and the radiation was solved with Discrete Ordinates model in a Finite Volume Method with 100 radiation angles [118].

The pool fire was modelled setting the estimated individual HRR curves from the experiment as an input. The resulting HRR curve for the simulation is shown in Figure 44. The radiation fraction used for heptane was 0.35 [118].

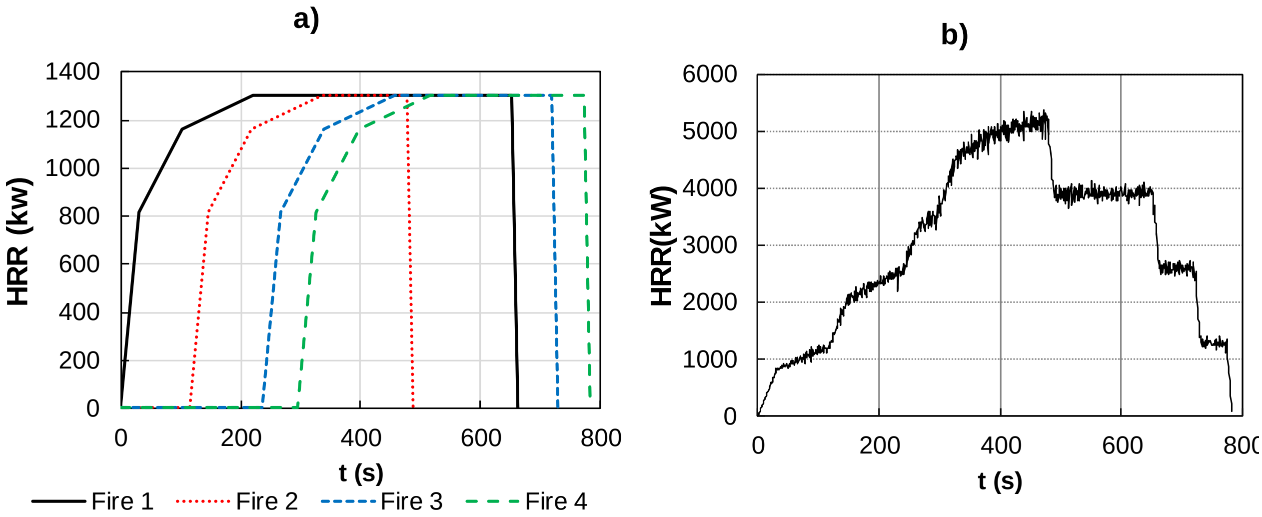

Figure 44 – HRR assigned to each fire (a) and (b) Total HRR as a result of the FDS model for the #4FX experiment.

The atrium geometry was built in PyroSim preprocessing tool [119] and has been modelled using 11 different meshes with a total of 4.582.656 cells. Cubic cells (with an aspect radio 1:1:1) with a resolution of 0.125 m were used. Each mesh has been assigned to a CPU core using the MPI (Multi Processors Indexing) feature of FDS through a designated cluster. The computational domain was extended where fluid dynamics connections were expected to be relevant, such as in the proximity of the make up air and on above the roof (where the temperature of the smoke layer could be influenced by the ambient temperature more than other regions). The boundary of the computational domain was set as open to outside, in order to include a fluid dynamics connection between the computational domain and the rest of the environment. The walls and the pyramidal roof were modelled with 6 mm thermally thick galvanized steel, see table 3, and the floor was simulated as a thermally thick layer of concrete, table 3. The fans were modelled as flow rate curves corresponding to the temporal exhaust flow rates, and their status in the simulation is shown in Figure 45. The make-up air inlets at the bottom of the atrium as open vents. The model of the atrium is shown in Figure 46.

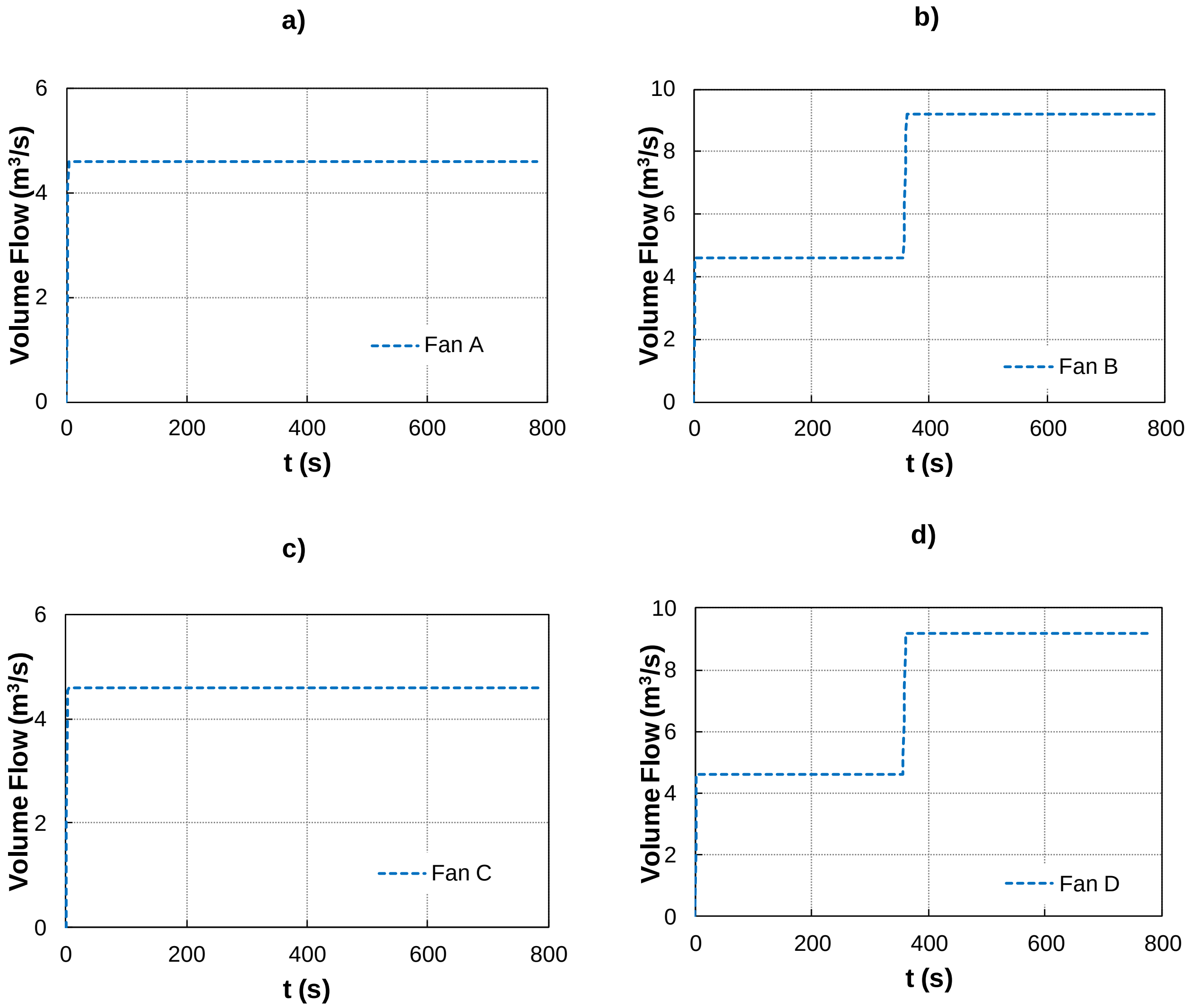

Figure 45 – Volume flow through the fans as a result of the FDS model for the #4FX experiment a) Fan A; b) Fan B; c) Fan C; d) Fan D.

Table 13 - Walls and roof material properties.

	Density (kg/m^3)	Thermal conductivity (W/K·m)	Specific heat at constant pressure (J/kg·K)	Emissivity
Steel	7800	45	460	0.3 - 0.4
Concrete	1860	0.72	780	0.9

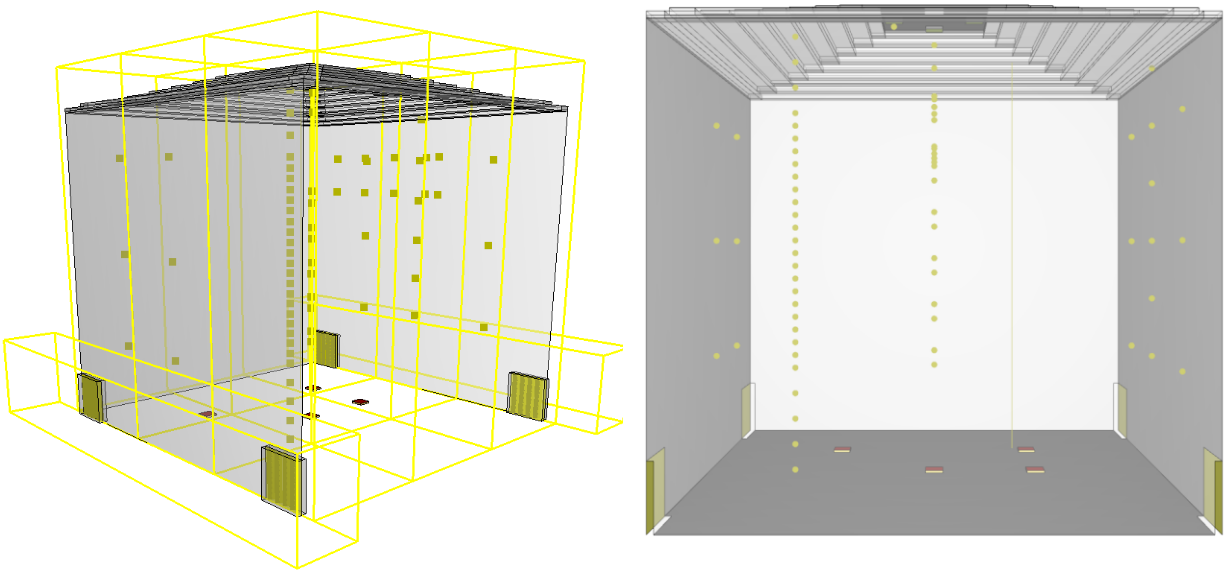

a) b)

Figure 46 – FDS model of the atrium for the #4FX test (a) 3D view with the computational domain outlined in yellow (b) front view of the model.

5.2 Sensitivity analysis

The grid size must be small enough to accurately model the turbulence and other effects relevant to the plume entrainment. When undertaking a simulation of a large fire (i.e. larger than 1 MW), in order to better capture the air entrainment from the fire and to properly model the flame, the fire is often divided into different burners, given the fact that the fire will not start covering the entire area of the design fire, i.e. the fire will start from the ignition and then move based on the actual fuel and ventilation available. As such, for the experiment #4FX, with an HRR of approximately 5.2 MW, splitting the fire into 4 different burners would have followed this approach. In that concern, when looking at the features of the fire as a whole, it is not clear whether to choose a D^*/δ ratio, where δ is the cell size and D^* the characteristic diameter of the plume, for the entire HRR (D^*= 2.00) or the HRR of the smaller fire (D^*= 1.15), in order to describe the fire dynamics of the fire, flame and plume.

For the LES method (Large Eddy Simulation), a spatial resolution of $4 < D^*/\delta < 16$ is commonly considered as a reasonable assumption [118]. The characteristic diameter of the plume is obtained from the fire Froude number [1], calculated as

$$D^* = \left(\frac{\dot{Q}}{\rho_\infty C_{\rho,\infty} T_\infty \sqrt{g}}\right)^{2/5} \quad (34)$$

where $\dot{Q}$ is the HRR (kW), ρ_∞ is the air density (kg/m^3), $c_{p,\infty}$ is the air specific heat at constant pressure (J/kg K), T_∞ is the air temperature (K) and g is the gravity acceleration modulus (9.81 m/s^2) [120]. A sensitivity analysis has been performed and the results showed a small discrepancy (less than 10 % for the plume without considering the thermocouple directly above the flame for the central fire and less than 5% overall) when using a D*/δ ratio for the overall fire or for the singular burners. This can be appreciated in Table 14.

Table 14 - D*/ δ for different mesh resolutions where D* is based on the overall HRR or the HRR of one single burner.

	Mesh size 0.125 m	Mesh size 0.250 m	Mesh size 0.375 m
D*/ δ (based on total HRR)	16.00	8.00	5.33
D*/ δ (based on single burner HRR)	9.20	4.60	3.07

As can be seen in Figure 47, when moving away from the fire, the sensitivity analysis shows that there is a minor difference in the temperature results using the mesh resolutions indicated before. In particular, the sensitivity analysis result shows similar performance when moving away from the fire plume, even with a coarse mesh resolution, with a D*/ δ=5.33 based on the total HRR and a D*/ δ=3.07 based on a single fire. In the "flame" region though, the differences are above 50% when using a resolution of 0.125 m and 0.375 m. The latter might be expectable since close to the flame region many factors influence the results, such as the fluctuation or twist of the flame. Consequently, mesh resolutions within the range 4 < D*/ δ < 16, based on a single fire, are proven to be suitable to properly predict the overall fire induced conditions. However, finer grids are expected to be necessary to accurately predict local effects or interactions within the flame regions or between flames [121].

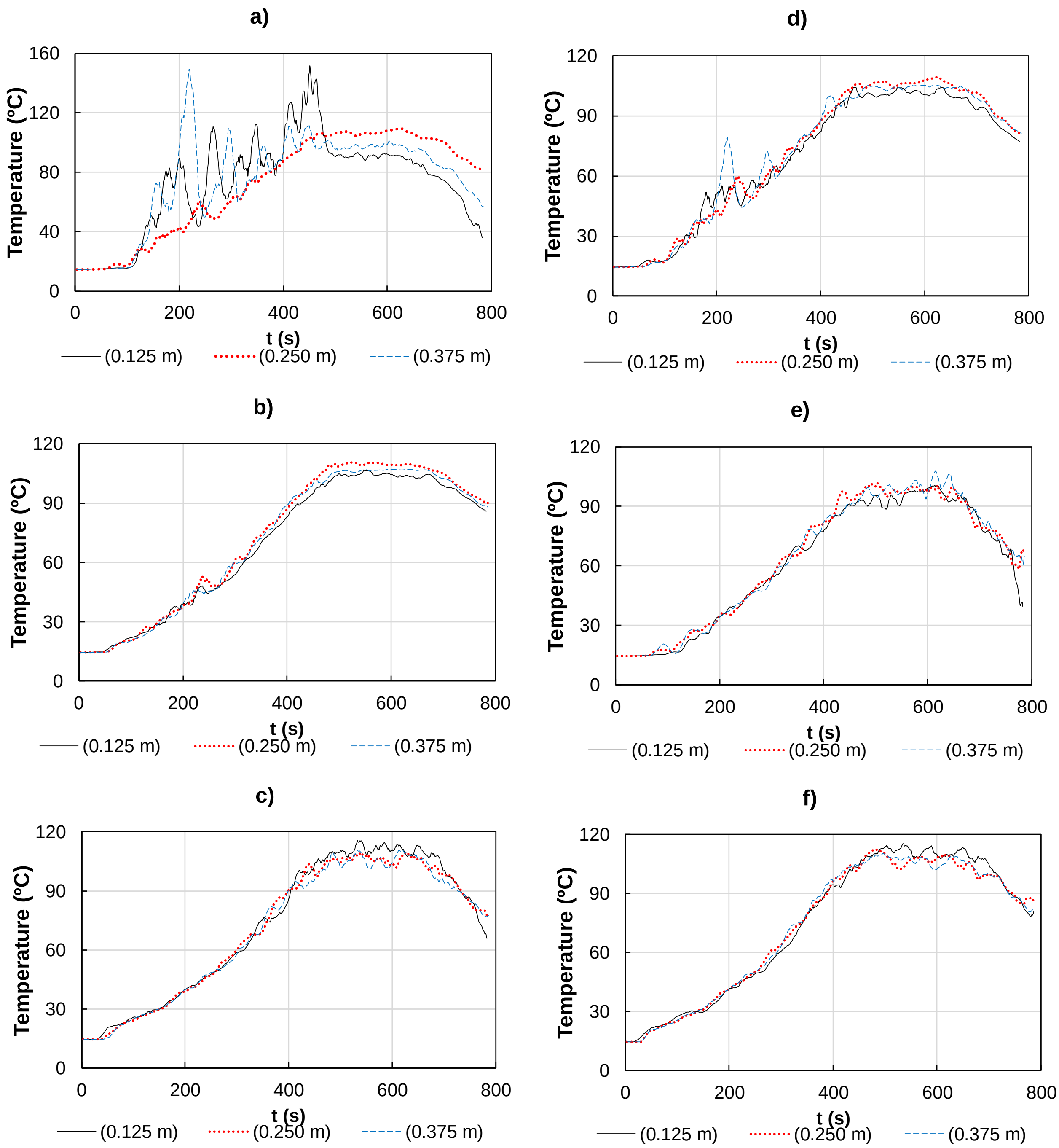

Figure 47 – Temperatures with different mesh resolutions at Fire plume for the pool fire n.2 (central pan) at (a) h = 5.25 m (sensor 2), (b) h = 7.25 m (sensor 4), and (c) h = 13.25 m (sensor 6). At 30 cm from Wall A at (d) h = 5 m (sensor 14), (e) h = 10 m (sensor 16) and (f) h = 15 m (sensor 18).

5.3 Results and discussion

The experimental measurements (Appendix A) have been compared with the corresponding predictions from simulations using absolute and relative differences, the latter being calculated with respect to the experimental results. To that aim, Pyrosim Results [122] has been used as a post-processor to show graphical results of the FDS simulation (such as slice files, smoke 3D and HRRPUV).

Let us first make a close inspection of the overall fire induced conditions, as predicted by the numerical model, in terms of smoke movement and thermal field. Figure 48 shows the visualization of the smoke layer, with its visible decline, in chosen time-steps of the analysis. As visible on the illustration, the smoke does eventually reach the bottom of the compartment, which was not observed to such an extent in the experiment. Such discrepancies can be explained as a result of an overestimation of the loss of visibility in the post-processing model, compared to the obscuration density measured in experimental setups of similar smoke, which was previously discussed in [123]. Furthermore, although symmetric venting conditions were considered, the fire sources disposition and the fire time development caused local fire deviations. Figure 49 presents the evolution of the temperature in chosen cross-sections of the compartment (5.375 m, 9.75 m and 14.00 m planes parallel to the wall A). It can be observed how the inner temperature rises fast, provoked by the two first fires, to unsafe values above 80 ºC, first row of Figure 48. Moreover, temperatures higher than 100 ºC are reached and maintained through a significant period of time, due to the high global HRR of the fires and the insufficient smoke extraction rate, second row of Figure 49. Only for moderate HRR (first and last row of Figure 49) tenable conditions can be found at the lower levels of the atrium.

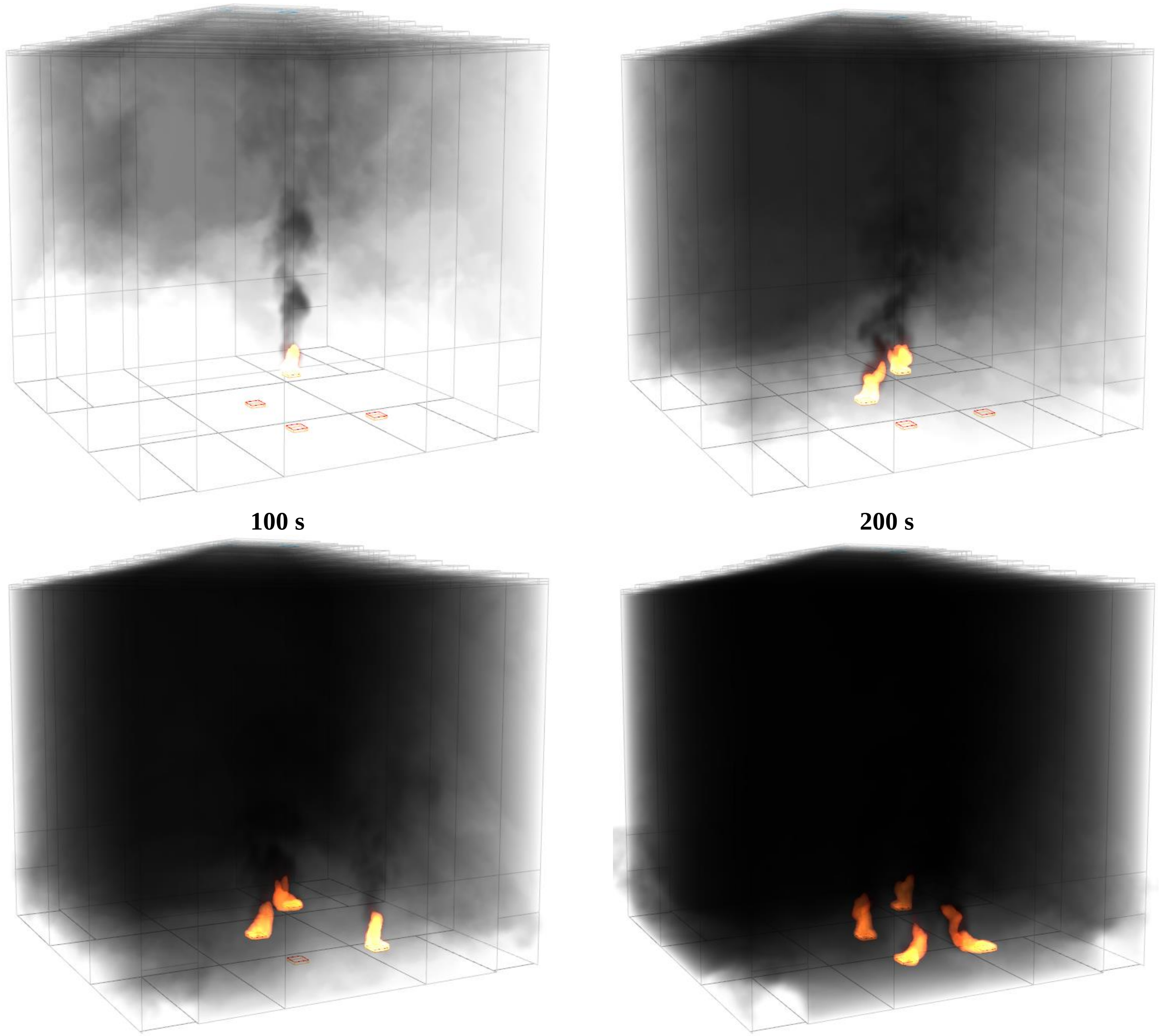

100 s 200 s

280 s 360

Figure 48 – Evolution of the fires and visible decay of the smoke layer in the FDS model of the atrium for the #4FX test.

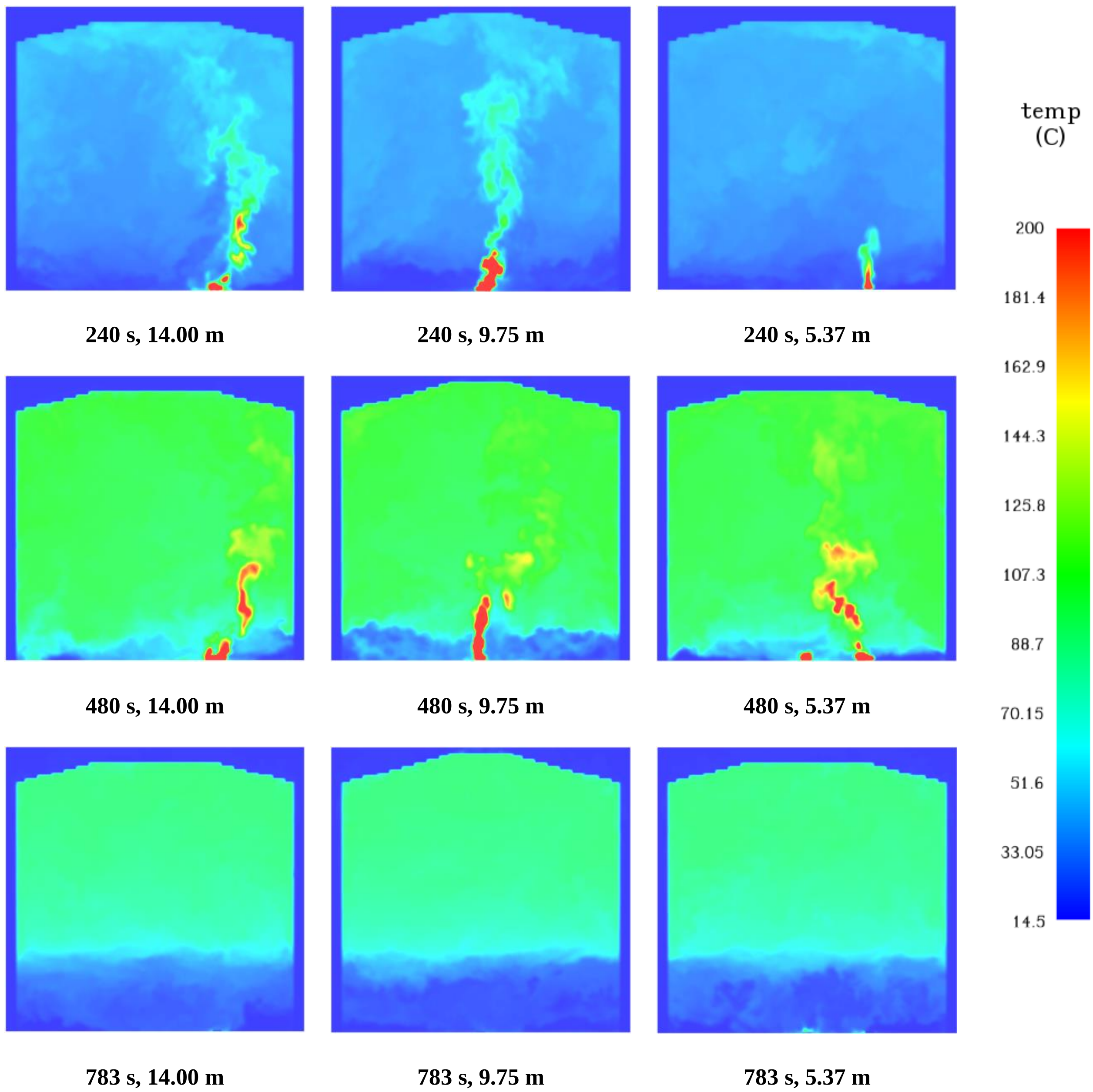

Figure 49 – Test #4FX. Temperature profile (through slice files) across the 4 fires in chosen points of time. The distance indicates the distance of the plane from the Wall A. The leftmost column presents a slice through fire 1, middle column the slice through fire 2 and the right column the slice through fires 3 and 4

Focusing on the experimental measurements and corresponding numerical predictions, Figure 50a–c show the near-field temperature, specifically the fire plume temperatures at h = 5.25 m, 7.25 m and 13.25 m (sensors 1, 3 and 5) for the pool fire n.2. The temperature in this region is very high due to the proximity to the flame and the combustion products are not diluted with air, above all at

5.25 m (Figure 50a). The temperature decreases as the height increases due to the make-up air entrainment to the fire plume, Figure 50b, c. These measurements are highly affected by flame local effects, e.g. flame inclinations. The latter explains the discrepancies observed at h=5.25 m above pool 2. When the flame leans, the plume deviates from the vertical axis, and, thus, lower temperatures than the measured ones are predicted, Figure 50a. On the other hand, the results of the simulation for the plume temperature at 5.25 m from the ground start to match after 500s from the ignition, when the central fire is over, and the thermal contribution comes from the other 3 fires. At h=7.25 m, Figure 50b, the plume has enlarged, which reduces the flame deviation effect significantly to be negligible. At higher locations, Figure 50c, good agreement is found between measurements and numerical results. Furthermore, at the lower locations, i.e. h=5.25 and h=7.25 m, four experimental temperature peaks can be appreciated, at t=180, t=210, t=300, and t=430 s, approximately, which are caused by flame deviations provoked by the cross make-up air supply distribution. As it has been above mentioned, these peaks are hardly noticeable at h=13.25 m.

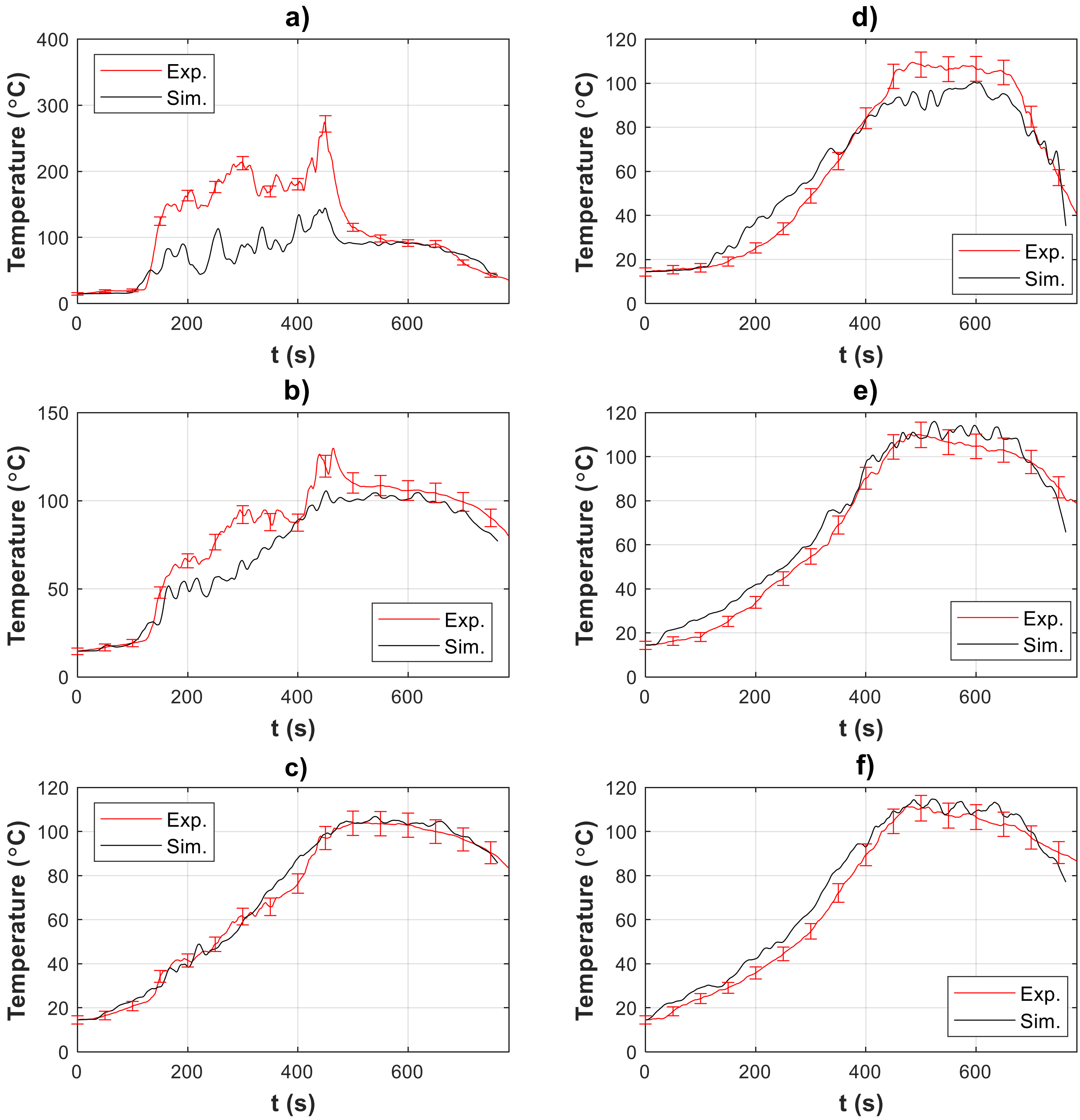

Figure 50 – Test #4FX. Temperatures and experimental uncertainty bounds. Fire plume for the pool fire n.2 (central pan) at (a) h = 5.25 m (sensor 2), (b) h = 7.25 m (sensor 4), and (c) h = 13.25 m (sensor 6). At 30 cm from Wall A at (d) h = 5 m (sensor 14), (e) h = 10 m (sensor 16) and (f) h = 15 m (sensor 18).

With regard to the far field, Figure 50d–f show the temperature measurements at three sensors close to wall A (sensors 14, 16 and 18). The temperature at this region is lower and starts to rise later as a consequence of the travelling time of the smoke from the fire plume to the smoke layer and its subsequent growth. In general, the same trends are noticed in the experiments and the simulations, with a good match for the sensors at 10 m and 15 m height from the ground (Figure 50e and Figure 50f) and a small underprediction of the peak temperature for the lower thermocouple (at 5 m from the ground, Figure 50d).

Fire induced thermal and flow fields are highly affected not only by the venting conditions, but also by the fire layout. Thus, Figure 51 shows the evolution of the flows at the ground level changing with additional fires ignition. The velocity field time sequence highlights the complexity of the flow structure introduced by the multiple fire scenario, compared with the fairly simple flow when just 1 fire, Figure 51a (even 2, Figure 51b), is present in the atrium. Figure 51c and d show how high air velocity regions and recirculating patterns form when the 4 fire sources are active. Consequently, larger mixing at the smoke layer interface is expected to occur, which can invalidate the efficiency of the designed smoke management system. Therefore, in a real fire event, it results of key importance the design of flexible smoke management strategies which account for such variable effects, allowing further control over the fire evolution, as well as over the inner induced conditions and the smoke movement.

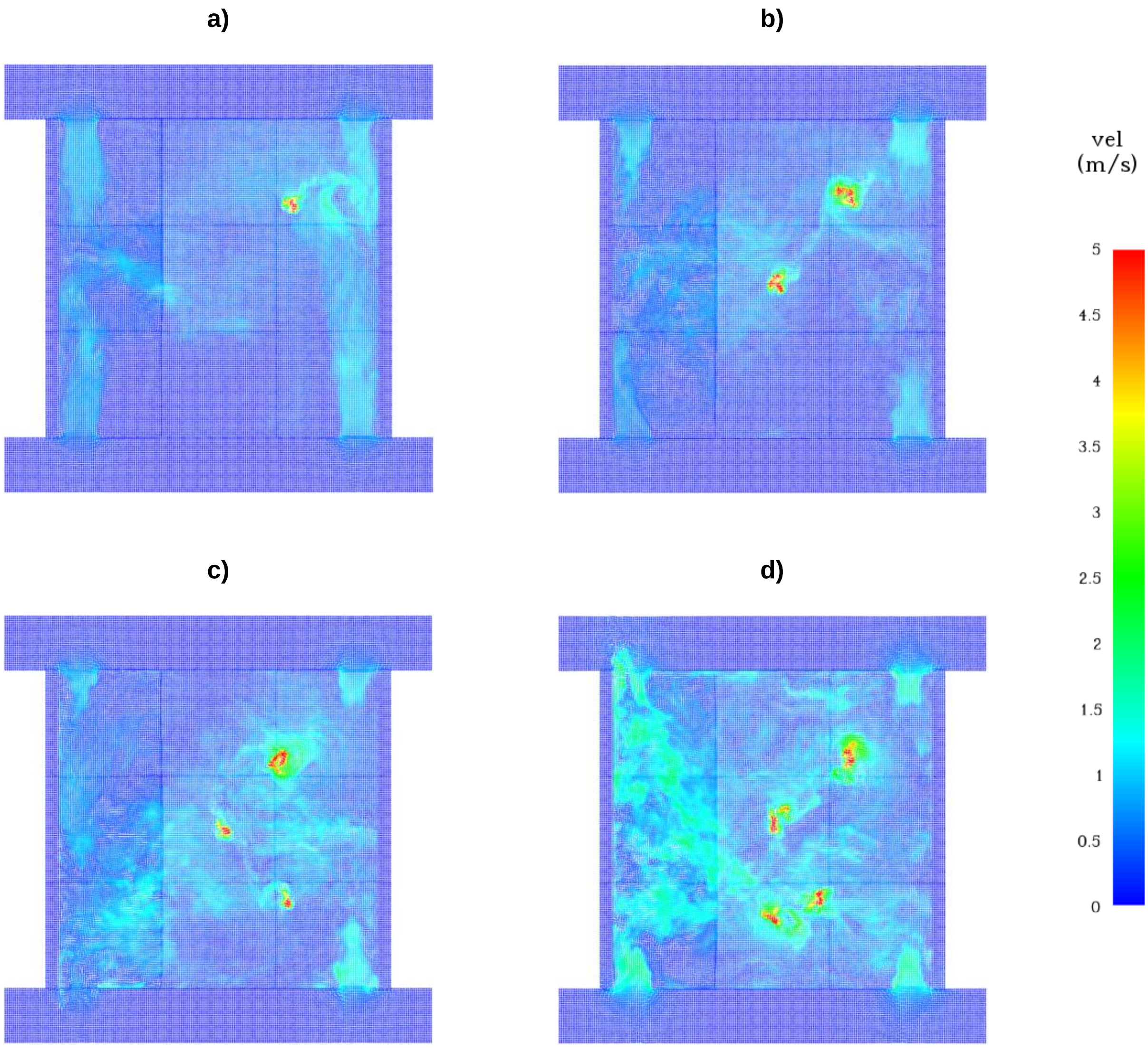

Figure 51 – Evolution of the velocity at 1.25m from the ground (horizontal slice files) in the FDS model of the atrium for the #4FX test. 100s (a), 200s (b), 280s (c), 360s (d).

Finally,

Figure 52 shows the smoke layer drop and the experimental vertical temperature profiles every 100 s. The smoke layer height has been studied using the "Smoke Layer" thermocouple tree (Figure 3). The least-squares method [124], as well as the N-percent (N = 30%) method [23], have been used and the error was estimated by means of absolute and relative discrepancies. The latter error was calculated with respect to the total atrium height (20 m). These two methods have been used to assess their accuracy in representing the smoke layer height. The N-percent method has been one of the most extended methods to determine the free smoke height, due to the ease of calculation. On the other hand, the least-squares method is not dependent on any parameter or empirical correlation [88]. Both these methods require to be updated every time step to obtain the smoke layer descent. To improve the prediction of the interface layer height with both of the methods, virtual thermocouples have been introduced every 10 cm by means of interpolation the measurements between the neighboring thermocouples. The height of the smoke layer has also been numerically evaluated using the least-squares method applied to the same thermocouple locations as in the experiments. Experimentally, the N-percent method predicts a slightly more conservative smoke layer height than the least-square method, detecting the initial smoke layer drop earlier, even though the difference is not significant. From then on, a maximum difference of 1.8 m (10%) is obtained at the end, with average discrepancy of 0.6 m (3%). When compared to the simulation, the smoke layer interface shows the same trend with an overall substantial underprediction of the smoke layer interface. More specifically, the difference with respect to the experimental measurements is minimal during the smoke layer drop (from the ignition to approximately 150 s). However, after 150 s, the difference between the smoke layer determined by the model and the experiments reaches a difference of up to 1.8 m (at approximately 550 s). Such differences might be caused in part by a larger mixing process at the smoke layer interface predicted by the simulation, as it has been previously shown.

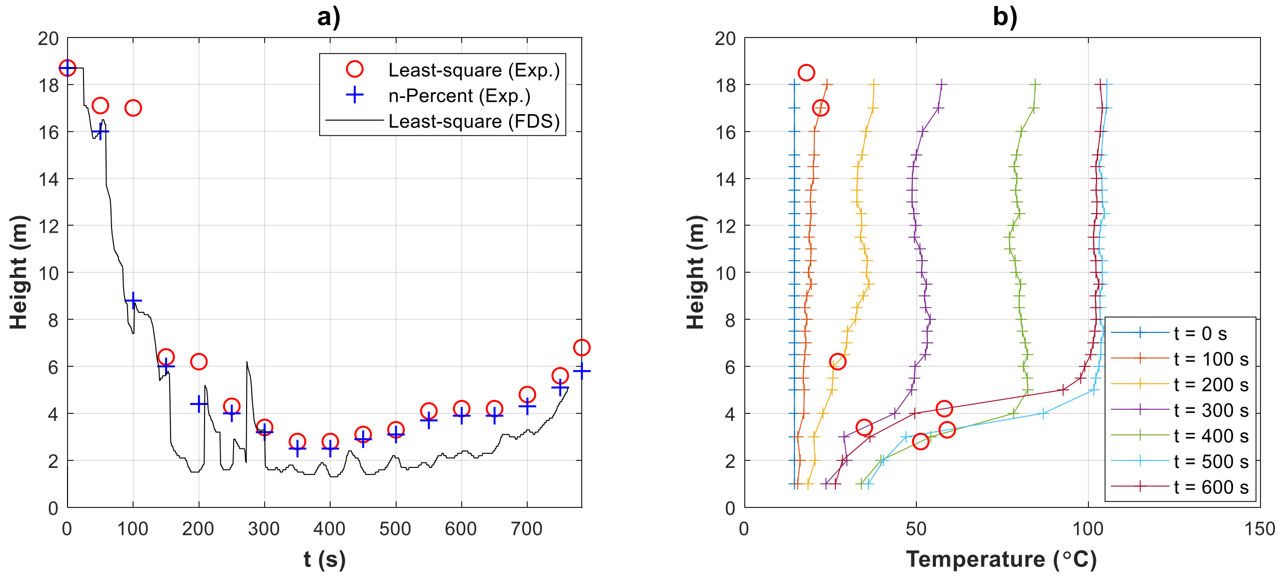

Figure 52 – Test #4FX. (a) Smoke layer drop. (b) Experimental smoke layer temperature profiles every 100 s. The red circles on figure (b) indicate the location of the smoke layer interface height calculated with a given profile. It is necessary to comment something on figure 15 b.

The experimental vertical temperature profiles in Figure 52b shows how the temperature is not very uniform through the smoke layer as it grows, mainly caused by the ignition of the fires at different locations. At 360 s, the smoke exhaust is increased and the smoke layer interface starts to rise. It can be observed how the ventilation system also homogenizes the temperature through the smoke layer, reaching a very uniform maximum value. Then, the smoke layer starts to decrease its temperature, in the same way, very homogenously.

5.4 Comparison with single pool fire experiments

With the aim to verify the importance of these full-scale experimental data with different sources of fire, this case has been compared with other two other fire experiments, but with only one source of fire. These experiments, #5_1 and #5_2, present a calculated average HRR of 5.2 and 5.3 MW, respectively, very close to the peak value measured for the #4FX experiment. In addition, only during the first 270 s, the three experiments have the same extraction rate, which will allow us to compare the fastest period of the smoke layer growth. As it has been commented previously, FDSv.6 was validated for single pool fires, placed at different locations of the base of the Fire Atrium [20]. Thus, only the experimental smoke layer behavior is here compared.

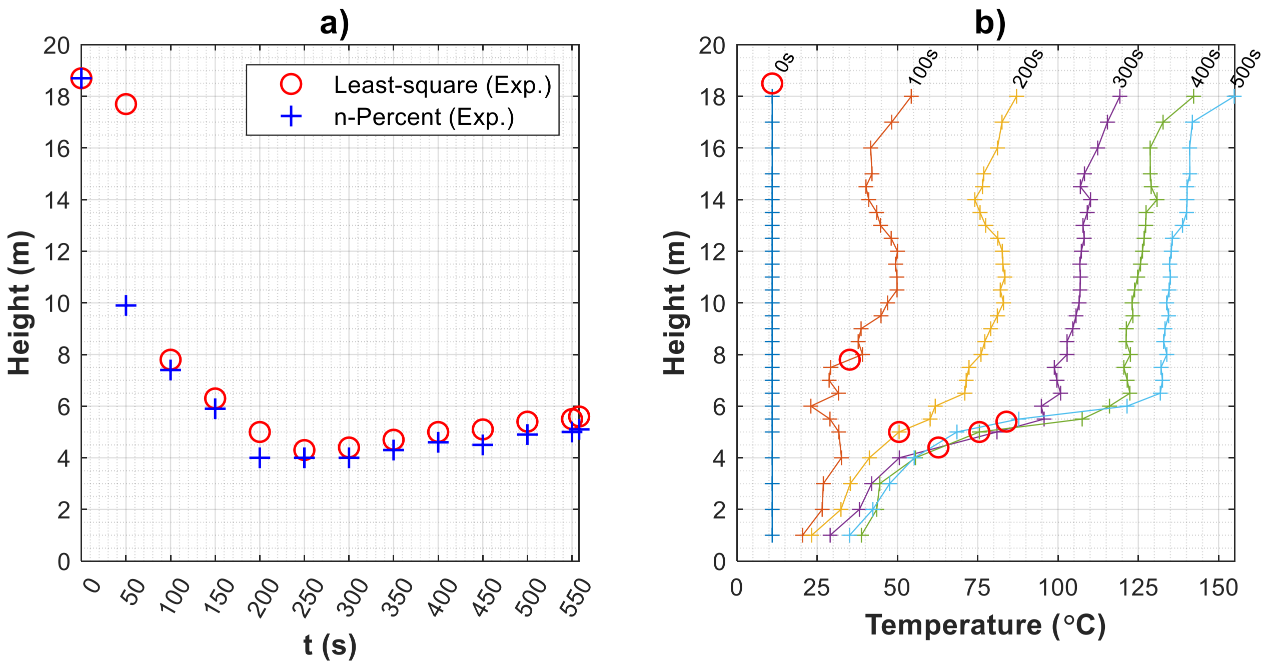

Figure 53 – Experiment #5-1. (a) Smoke layer drop. (b) Experimental smoke layer temperature profiles every 100 s. The red circles on figure (b) indicate the location of the smoke layer interface height calculated with a given profile.

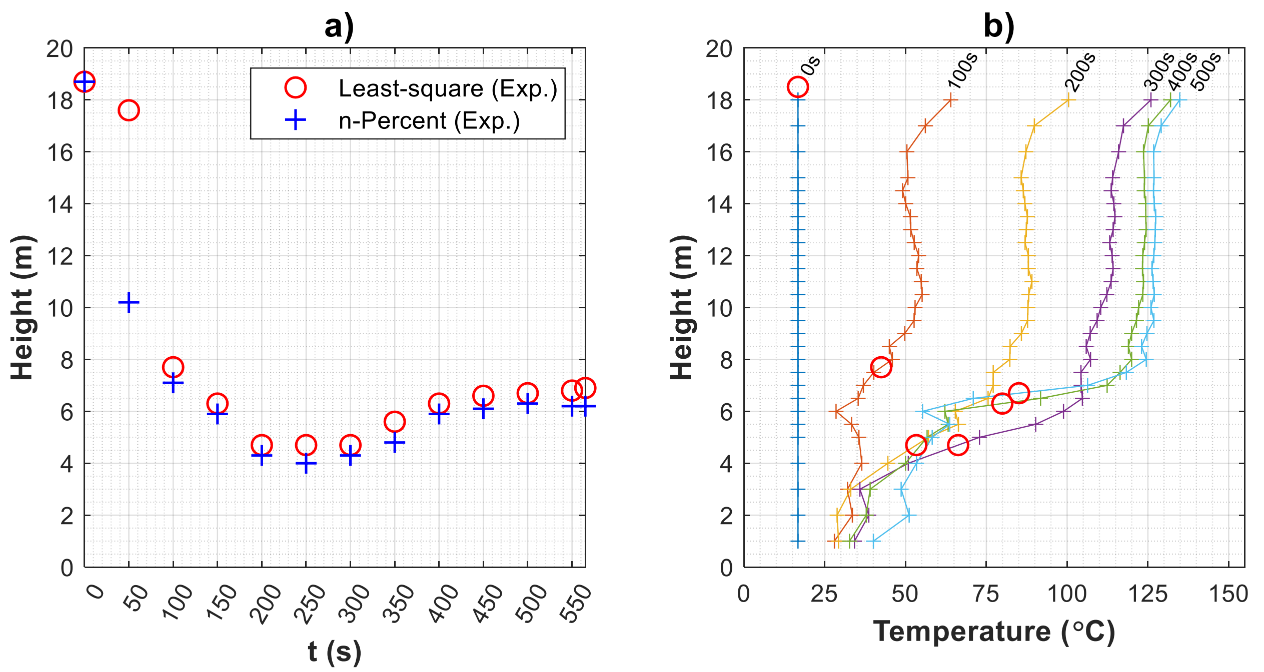

Figure 54 – Experiment #5-2. (a) Smoke layer drop. (b) Experimental smoke layer temperature profiles every 100 s. The red circles on figure (b) indicate the location of the smoke layer interface height calculated with a given profile.

In the experiment #4FX, Figure 52a, the smoke layer shows a fast descent during the first 270 s, reaching a final height of 3.9 m, evaluated with the least-square method (3.5 m, with the N-percent method). In the two additional fire experiments, the heights reached are slightly higher during the same period of time: for experiment #5_1, Figure 53a, the height is 4.3 m (4.0 m) and for experiment #5_2, Figure 53a, the height is 4.8 m (3.9 m), evaluated with the least-square and N-percent methods, respectively. Apparently, these values are similar, but during this initial period, in experiment #4FX, only the first two pool fires have completely reached the steady state, giving a total HRR of 3.4 MW, Figure 44b, compared with the values of 5.2 and 5.3 MW, for experiments #5_1 and #5_2. This relevant enhancement of the smoke production is clearly due to larger area for the entrainment of air in the case of multiple sources of fire, together with the relevant distance between them, and the enhanced turbulence generated by the more complex air flow around the individual pool fires. A higher amount of air entrainment boosts the smoke production, which constitutes the main cause of death in case of fire. Conversely, the larger dilution of smoke with fresh air significantly contributes to the reduction of the smoke layer temperature. Thus, during the initial period of 270 s, the temperature of the smoke layer is noticeable lower in the experiment #4FX, below 50 ºC, Figure 52b, than in experiment #5_1, Figure 53b, and experiment #5_2, Figure 54b, where the smoke temperature is close to 100 ºC. In addition, a less uniform temperature through the smoke layer is also observed, confirming the lower influence of the mixing process with single pool fires. The latter results demonstrate the relevance and necessity to account for more complex fire scenarios, considering multiple sources, in the design process of fire safety systems, since significantly different, more life-threatening inner conditions can be induced in these cases.

5.5 Conclusions

A novel full-scale atrium fire test of approximately 5.2 MW composed by four fires, under transient exhaust conditions and symmetric make up air configuration has been performed to assess its effect on the fire induced conditions. Subsequently, numerical simulations of the test have been conducted. Temperature results have been compared both near one of the flames (pool n.2) and in the far field, i.e. near the walls and roof. Additionally, the smoke layer interface has been calculated for both experimental study and the numerical calculations. Overall, good agreement has been found in the four fires tests between the numerical data and the experimental measurements in the near field, and also in the far field. In the near field, out of the flame region, the numerical temperature is slightly underpredicted, with average discrepancies lower than 10%. In the far field, the temperature predictions are quite accurate inside the smoke layer (10 m and 15 m), whereas larger discrepancies were observed at the smoke layer interface, i.e. 5 m high. The discrepancies at 10 m and 15 m high are lower than 10%, whereas at 5 m discrepancies up to 20% can be found, which is within the uncertainty associated with FDS. Lower smoke layer height is predicted by the simulations, caused by the larger mixing of fresh air and smoke, induced by the complex flow field at low locations.

Finally, the analysis confirms that FDS is a robust tool in determining the smoke spread and its features reasonably away from the fire region. Finally, it is worth highlighting that FDS (v6.7.1) was able to predict well the fire induced conditions in all cases when the measured HRR of the fire is an input. This confirms that the HRR plays an essential role in fire simulations and must be accurately modelled or set as input. Furthermore, spatial resolution has been found to be of special importance to properly predict the conditions near the fires, as well as local effects or interactions between fires.

The results also show the importance of considering complex fire scenarios with multiple sources due to the faster smoke production and more life-threatening induced conditions compared with those of traditional single fires.

6 Conclusions and Future Work

Modelling smoke produced by fire in enclosures poses several challenges, some of the most critical have been analyzed and discussed in this thesis. This has been done both through real-scale experiments and numerical analysis. The first challenge that has been addressed is the accuracy and usability of the empirical correlations used by the fire safety engineering community to calculate the mass of smoke produced by fire, namely the Zukoski, Heskestad, Thomas and McCaffrey correlations. The second challenge that has been addressed is the identification of the most critical numerical variables that influence the visibility through the smoke, defining the relevance of each variable on the visibility estimation. Finally, the accuracy of CFD in predicting the fluid dynamics of the smoke produced by fire has been addressed, through a verification and validation process. The following sections detail the main findings of these three areas of investigation.

6.1 Plume entrainment correlations

Plume entrainment correlations exist since the 70s and have been based upon a mix of physics and empirical correlations. These correlations have been widely investigated for fires in small enclosures, but their applicability and accuracy in large enclosures is not clear. The present work studies the suitability and applicability of these approaches to properly predict the fire induced conditions within large volumes. The results presented in this study show that the smoke layer height and its temporal evolution may be predicted with satisfactory accuracy using simple methods. This prediction improves the whole design process as the first approximation is often considered as a boundary condition for further costly numerical modeling. Use of simple plume models should be further investigated by the fire safety engineering community as they can still be considered as a valuable tool. However, the use of such models to predict the smoke production of a given fire shall be only a first approximation and not a design tool, especially using those models that have not shown a good match to the experimental data. The use of smoke plume entrainment models for the design of large-volume buildings may be questionable, since such application may extend beyond the validity range of the aforementioned models. The choice of the most appropriate model is difficult due to the large amount of approaches presented in the literature, standards and national codes. Therefore, in order to tackle this challenge and contribute to the assessment of the validity of these simplified models, a series of experiments was performed in a large-scale atrium facility. Subsequently, the experimental results have been compared to plume theory-based models focusing on the transient and steady-state layer interface height predictions[15].

The best results for the prediction of the layer height were consistently obtained with the McCaffrey model, and the best results for the evolution of the smoke layer with the Zukoski model. The popular Thomas model under-predicted the smoke generation in the atrium, yielding significantly higher smoke layer heights than measured. The reasons for such discrepancies have been studied, giving some practical recommendations for the design of smoke control in large volume buildings, such as that the use of such models to predict the smoke production of a given fire shall be only a first approximation and not a design tool, especially when using those models that have not shown a good match to the experimental data. It was further shown that this result may be improved by carefully choosing the value of HRRPUA to fit the results with experimental data. However, in practical design, the engineer is not able to choose reliable values for this parameter, thus being exposed to a significant error[15].

6.2 Visibility through smoke

Many variables can be used to describe the properties of the smoke induced by a fire, e.g. temperature, mass density of products, obscuration density, transmittance, toxic gasses concentration, etc. Among these numerous variables, when conducting Fire Safety Engineering (FSE) analysis, one of the most important parameter is the “visibility in smoke”. It is very common in FSE studies to see the visibility to be the first parameter that meets its critical value (tenability criteria). Visibility in numerical modeling is a result of modeling the transport of combustion products within the model, especially the soot aerosol.

In order to better understand the roles of the sub-variables of visibility, experimental tests have been performed in a 10 m x 10 m room, using different fuels with a broad range of soot yield (from 0.001 g/g for methanol to 0.178 g/g for toluene). The results have been then compared to numerical models processed with both ANSYS Fluent and Fire Dynamics Simulator. A numerical study has then been performed looking at 20 different cases, each one with a soot yield difference of 0.01 g/g (from 0.01 g/g to 0.20 g/g). In order to check the performance of the numerical models used, a preliminary validation analysis has been performed comparing the measured and predicted temperature obtained from different experiments (in particular, tests with Heptane, Propanol, Toluene and Methanol). The results show a relatively good agreement between modeled and experimental temperature data for Heptane and Propanol with a maximum discrepancy of about 20%. Higher discrepancies have been found for Methanol and Toluene, which can be attributed to the uncertainty of the HRR measurement in the model. The numerical analysis, both for ANSYS Fluent and FDS, shows an hyperbolic trend of the visibility when increasing the soot yield with a cut-off point around 0.10 g/g, around which a variation of the soot yield can produce a relevant (below 0.10 g/g) or a negligible (above 0.10 g/g) change in the visibility.

One of the major findings of this study is that, unless the materials (and thus the chemical reactions) in the building to be assessed by a Fire Engineering analysis are well known, values of soot yield below approximately 0.10 g/g should be used with extreme cautiousness when performing an ASET/RSET exercise.

6.3 CFD Validation

A novel full-scale atrium fire experiment with a maximum HRR of 5.2 MW, composed by four fires, under transient exhaust conditions and symmetric make-up air configuration has been performed to assess its effect on the fire induced conditions. This has been studied by means of temperature measurements in the plume and far close to walls. Results show that significantly worse inner conditions are induced than those in a single fire of equal power. This has been supported through the analysis of two fire experiments of a sole fire source with HRR of 5.2 and 5.3 MW. The smoke production is clearly boosted in the former case, with multiple fire sources, and untenable conditions are easily achieved in this type of large-volume enclosures, despite the reduction in the smoke temperature. The experimental data from the experiments is provided as supplementary material to be used as benchmarks for further studies.

Subsequently, numerical simulations of the experiment have been conducted. Temperature results have been compared, both near the flames (pool n.2) and in the far field, i.e. near the walls and roof. Additionally, the smoke layer interface has been calculated for both the experimental measurements and the numerical calculations. Overall, good agreement has been found in the four fires experiment between the numerical data and the experimental measurements in the near field, and also in the far field. In the near field, out of the flame region, the numerical temperature is slightly underpredicted, with average discrepancies lower than 10%. In the far field, the temperature predictions are quite accurate inside the smoke layer (10 m and 15 m), whereas larger discrepancies were observed at the smoke layer interface, i.e. 5 m high. The discrepancies at 10 m and 15 m high are lower than 10%, whereas at 5 m discrepancies up to 20% can be found, which is within the uncertainty associated with FDS. Lower smoke layer height is predicted by the simulations, caused by the larger mixing of fresh air and smoke, induced by the complex flow field at low locations. Furthermore, a grid analysis has shown that grid resolutions, D^*/δ, based on the global HRR of the fire might be sufficient to predict the fire induced conditions far from the fire. However, finer grids are required to accurately calculate the near flame conditions, where the grid resolution should be based on the HRR of the single fire modeled. The analysis confirms that FDS is a robust tool in determining the smoke spread and its features away from the fire region. Finally, the results show the importance of considering complex fire scenarios with multiple sources due to the faster smoke production and more life-threatening induced conditions compared with those of traditional single fires.

6.4 Future work

For pool fires inside an atrium facility, the fuel is the most important determinant of the fire's soot yield. However, it is acknowledged that in most practical situations, i.e. in accidental compartment fires inside buildings, the geometric properties of the fuel load and the ventilation characteristics of the compartment fire can be more important in the determination of the fire soot yield [4]. The research presented in this thesis has determined a critical value under which the effect of the soot yield on visibility is important and above which this effect does not vary substantially. This is important in order to establish which values of soot yield are conservative and which not; this is valuable information for design of fire safety and evaluation of fire risk. However, it is encouraged that future research is focused on the parameters that affect the actual soot yield in different practical situations. Researchers could investigate the importance of the geometric disposition of the fuel load and of the ventilation conditions, i.e. how do these factors affect the soot yield.

Another important parameter to calculate visibility is the mass extinction coefficient. It was concluded before that the soot yield is much more influential on the visibility than the mass extinction coefficient, nonetheless, future research projects could focus on investigating the mass extinction coefficient in order to better understand its relationship with the visibility through smoke. Furthermore, it is not well-known what parameters affect the mass extinction coefficient itself.

Currently, the visibility factor, k, is normally assumed to be one of two values when it is used to calculate the visibility through smoke: if the object that is being tried to be seen emits light, this value is 8, if the object does not emit light, its value is 3. Obviously, the fact that the object emits light or not has a big influence on its visibility, but there are other factors that affect it. For example, if said object is a sign, its content must be important. If it has text, the font would be a big factor; if it has an image, its size and level of detail probably have a substantial influence on its visibility. Further research is necessary to determine whether using just two values for the visibility factor is enough or if a wider range of values, depending on different factors, should be considered. The results of this research could potentially be very beneficial as it has been proven that signage visibility is very important to the success of an evacuation strategy [125].

Some sections of this thesis have compared two different CFD packages – FDS and ANSYS Fluent. Validation and verification of software packages can demonstrate that they are acceptable representations of the reality and this is necessary in order to use them in designs and evaluations. Furthermore, software is continuously being updated and modified, and these updates should be validated as well. Therefore, any research project that focuses on validating software with full-scale experiments can be useful.

7 References

[1] M.J. Hurley, SFPE Handbook of Fire Protection Engineering, n.d.

[2] J.H. Klote, J.A. Milke, P.G. Turnbull, A. Kashef, M.J. Ferreira, Handbook Of Smoke Control Engineering, ASHRAE, 2012.

[3] B. Park, Standard for Smoke Management Systems in Malls , Atria , and Large Spaces 2009 Edition, (2009).

[4] D. Drysdale, An Introduction to Fire Dynamics, 2011. doi:10.1016/0379-7112(86)90046-9.

[5] D.J. Rasbash, D.D. Drysdale, Fundamentals of smoke production, Fire Safety Journal. 5 (1982) 77–86. doi:10.1016/0379-7112(82)90008-X.

[6] I. Glassman, Soot formation in combustion processes, Symposium (International) on Combustion. 22 (1989) 295–311. doi:10.1016/S0082-0784(89)80036-0.

[7] B.J.A. Griffiths, J.F., Flame and combustion, 3rd Edition, Fire Safety Journal. 28 (1995) 179–181. doi:10.1016/s0379-7112(97)00003-9.

[8] H. Richter, J.B. Howard, Formation of polycyclic aromatic hydrocarbons and their growth to soot-a review of chemical reaction pathways, 2000. doi:10.1016/S0360-1285(00)00009-5.

[9] A. Raj, Formation, growth and oxidation of soot: A numerical study, University of Cambridge. 48 (2010) 319–332. doi:10.1016/j.carbon.2009.09.030.

[10] H.G. Wagner, Soot formation in combustion, Proceedings of the Combustion Institute. 17 (1979) 3–19.

[11] A. Fundacion MAFPRE, Estudio de víctimas de incendios en españa en 2017, 2017.

[12] N.F.P. Association, NFPA Handbook, 20th edn. NFPA, Quincy, MA, 2008.

[13] UK Home Office, Collection of Fire statistics UK - https://www.gov.uk/government/collections/fire-statistics, (n.d.). https://www.gov.uk/government/collections/fire-statistics.

[14] C. Gutiérrez-Montes, G. Rein, E. Sanmiguel-Rojas, A. Viedma, Smoke and fire dynamics in atria and large enclosures: An overview, 2009.

[15] G. Vigne, C. Gutierrez-Montes, A. Cantizano, W. Węgrzyński, G. Rein, Review and Validation of the Current Smoke Plume Entrainment Models for Large-Volume Buildings, Fire Technology. 55 (2019) 789–816. doi:10.1007/s10694-018-0801-4.

[16] W.K. Chow, Performance-based approach to determining fire safety provisions for buildings in the Asia-Oceania regions, Building and Environment. 91 (2015) 127–137. doi:10.1016/j.buildenv.2015.04.007.

[17] P. Tofiło, W. Węgrzyński, R. Porowski, Hand Calculations, Zone Models and CFD – Areas of Disagreement and Limits of Application in Practical Fire Protection Engineering, in: 11th Conference on Performance-Based Codes and Fire Safety Design Methods, SFPE, 2016.

[18] G. Rein, X. Zhang, P. Williams, B. Hume, A. Heise, A. Jowsey, B. Lane, J.L. Torero, Multi-story Fire Analysis for High-Rise Buildings, in: 11th

Interflam, London, 2007: pp. 605–616.

[19] C. Gutiérrez-Montes, E. Sanmiguel-Rojas, A.S. Kaiser, A. Viedma, Numerical model and validation experiments of atrium enclosure fire in a new fire test facility, Building and Environment. 43 (2008) 1912–1928. doi:10.1016/j.buildenv.2007.11.010.

[20] P. Ayala, A. Cantizano, G. Rein, G. Vigne, C. Gutiérrez-Montes, Fire Experiments and Simulations in a Full-scale Atrium Under Transient and Asymmetric Venting Conditions, Fire Technology. 52 (2016) 51–78. doi:10.1007/s10694-015-0487-9.

[21] P.H. Thomas, P.L. Hinkley, C.R. Theobald, D.L. Simms, Investigations into the flow of hot gasses in roof venting, Fire Research Technical Paper No. 7. (1963).

[22] E.E. Zukoski, T. Kubota, B. Cetegen, Entrainment in fire plumes, Fire Safety Journal. 3 (1981) 107–121. doi:10.1016/0379-7112(81)90037-0.

[23] G. Heskestad, Virtual origins of fire plumes, Fire Safety Journal. 5 (1983) 109–114. doi:10.1016/0379-7112(83)90003-6.

[24] B.J. McCaffrey, Purely Buoyant Diffusion Flames: Some Experimental Results, 1979.

[25] P. Ayala, A. Cantizano, C. Gutiérrez-Montes, G. Rein, Influence of atrium roof geometries on the numerical predictions of fire tests under natural ventilation conditions, Energy and Buildings. 65 (2013) 382–390. doi:10.1016/j.enbuild.2013.06.010.

[26] E. Sanmiguel-rojas, A. Viedma, G. Rein, Experimental data and numerical modelling of 1 . 3 and 2 . 3 MW fires in a 20 m cubic atrium, 44 (2009) 1827–1839. doi:10.1016/j.buildenv.2008.12.010.

[27] W.K. Chow, Determination of the Smoke Layer Interface Height for Hot Smoke Tests in Big Halls, Journal of Fire Sciences. 27 (2009) 125–142. doi:10.1177/0734904108096852.

[28] T. Beji, S. Verstockt, R. Van de Walle, B. Merci, Prediction of smoke filling in large volumes by means of data assimilation–based numerical simulations, Journal of Fire Sciences. 30 (2012) 300–317. doi:10.1177/0734904112437845.

[29] L.Y. Cooper, M. Harkleroad, J. Quintiere, W. Rinkinen, An Experimental Study of Upper Hot Layer Stratification in Full-Scale Multiroom Fire Scenarios, Journal of Heat Transfer. 104 (1982) 741. doi:10.1115/1.3245194.

[30] W. Węgrzyński, G. Krajewski, P. Suchy, Zmienność cech materiałowych a szacowany zasięg widzialności w analizach CFD, in: Sprawozdanie Roczne - NP-105, Instytut Techniki Budowlanej, 2015.

[31] C.S. Yih, Free convection due to boundary sources, in: Fluid Models in Geophysics, in: Proceedings of the First Symposium on the Use of Models in Geophysics, Washington, DC, 1956: pp. 117–133.

[32] B.R. Morton, G. Taylor, J.S. Turner, Turbulent Gravitational Convection from Maintained and Instantaneous Sources, Proceedings of the Royal Society A: Mathematical, Physical and Engineering Sciences. 234 (1956) 1–23. doi:10.1098/rspa.1956.0011.

[33] S. Yokoi, Study on the prevention of fire-spread caused by hot upward current, in: Report of the Building Research Institute No. 34, 1960.

[34] G. Heskestad, Fire Plumes, Flame Height, and Air Entrainment, in: SFPE Handbook of Fire Protection Engineering, Springer New York, New York, NY, 2016: pp. 396–428. doi:10.1007/978-1-4939-2565-0_13.

[35] E.E. Zukoski, Properties of Fire Plumes, in: G. Cox (Ed.), Combustion Fundamentals of Fire, Academic Press, London, 1995.

[36] M. Poreh, G. Garrad, Study of wall and corner fire plumes, Fire Safety Journal. 34 (2000) 81–98. doi:10.1016/S0379-7112(99)00040-5.

[37] G. Cox, On adhered spill plume entrainment, Fire Safety Journal. 45 (2010) 400–401. doi:10.1016/j.firesaf.2010.08.001.

[38] N. Tilley, B. Merci, Numerical study of smoke extraction for adhered spill plumes in atria: Impact of extraction rate and geometrical parameters, Fire Safety Journal. 55 (2013) 106–115. doi:10.1016/j.firesaf.2012.10.022.

[39] J.G. Ouintiere, W.J. Rinkinen, W.W. Jones, The Effect of Room Openings on Fire Plume Entrainment, Combustion Science and Technology. 26 (1981) 193–201. doi:10.1080/00102208108946960.

[40] H.P. Morgan, G.O. Hansell, Atrium building smoke flows, Fire Safety Journal. 13 (1988) 221–224. doi:10.1016/0379-7112(88)90018-5.

[41] P.H. Thomas, H.P. Morgan, N. Marshall, The spill plume in smoke control design, Fire Safety Journal. 30 (1998) 21–46. doi:10.1016/S0379-7112(97)00037-4.

[42] M. Law, A Note on Smoke Plumes from Fires in Multi-level Shopping Malls, Fire Safety Journal. 10 (1986) 197–202.

[43] R. Harrison, M. Spearpoint, The horizontal flow of gases below the spill edge of a balcony and an adhered thermal spill plume, International Journal of Heat and Mass Transfer. 53 (2010) 5792–5805. doi:10.1016/j.ijheatmasstransfer.2010.08.004.

[44] M. Poreh, H.P. Morgan, N.R. Marshall, R. Harrison, Entrainment by two-dimensional spill plumes, Fire Safety Journal. 30 (1998) 1–19. doi:10.1016/S0379-7112(97)00036-2.

[45] W. Węgrzyński, Paritions and the flow of smoke in large volume buildings (in press), Architecture, Civil Engineering, Environment. (2018).

[46] R. Harrison, Entrainment of Air into Thermal Spill Plumes, University of Canterbury, 2009.

[47] NFPA, NFPA 92 Standard for Smoke Control Systems 2015 Edition, (2015).

[48] CEN, CEN/TR 12101-5:2005 Smoke and heat control systems. Guidelines on functional recommendations and calculation methods for smoke and heat exhaust ventilation systems, 2005.

[49] CIBSE, TM 19 Relationships for smoke control calculations, in: 1995.

[50] NBN, Brandbeveiliging van gebouwen - Ontwerp en berekening van rook- en warmteafvoerinstallaties (RWA) - Deel 1 : Grote onverdeelde ruimten met een bouwlaag, in: NBN S 21-208-1, 1995.

[51] H.P. Morgan, B.K. Ghosh, G. Garrad, R. Pamlitschka, J.-C. De Smedt, L.R. Schoorbaert, Design methodologies for smoke and heat exhaust ventilation, BRE, Watford, UK, 1999.

[52] BS 5588-7:1997, Fire precautions in the design, construction and use of buildings. Code of practice for the incorporation of atria in buildings, 1997.

[53] BS 9999:2017, Fire safety in the design, management and use of buildings. Code of practice, 2017.

[54] Standards Australia, The use of ventilation and airconditioning in buildings Smoke control systems for large single compartments or smoke reservoirs, in: AS 1668.3-2001, 2001.

[55] G.Y. Wu, R.C. Chen, The analysis of the natural smoke filling times in an atrium, Journal of Combustion. 2010 (2010). doi:10.1155/2010/687039.

[56] M.H. Salley, R. Wachowiak, Nuclear Power Plant Fire Modeling Analysis Guidelines, in: NUREG- 1934, United States Nuclear Regulatory Commission, Washington, DC, 2007.

[57] J.G. Quintiere, C.A. Wade, Compartment Fire Modeling, in: SFPE Handbook of Fire Protection Engineering, Springer New York, New York, NY, 2016: pp. 981–995. doi:10.1007/978-1-4939-2565-0_29.

[58] I. Sanderson, T. Kilpatrick, J. Torero, A comparative analysis of the use of different zone models to predict the mass smoke flow for axisymetric and spill plumes, Fire Safety Science. (2008) 751–762. doi:10.3801/IAFSS.FSS.9-751.

[59] W.D. Walton, D.J. Carpenter, C.B. Wood, Zone Computer Fire Models for Enclosures, in: SFPE Handbook of Fire Protection Engineering, Springer New York, New York, NY, 2016: pp. 1024–1033. doi:10.1007/978-1-4939-2565-0_31.

[60] R.D. Peacock, G.P. Forney, P.A. Reneke, R.W. Portier, W.W. Jones, CFAST, the Consolidated Model of Fire Growth and Smoke Transport (Version 6) Technical Reference Guide, Gaithersburg, 2009.

[61] J.-F. Cadorin, J.-M. Franssen, A tool to design steel elements submitted to compartment fires—OZone V2. Part 1: pre- and post-flashover compartment fire model, Fire Safety Journal. 38 (2003) 395–427. doi:10.1016/S0379-7112(03)00014-6.

[62] C. a Wade, BRANZFIRE Technical Reference Guide 2004. BRANZ Study Report 92 (Revised)., (2004) 76.

[63] C. Wade, G. Baker, K. Frank, A. Robbins, R. Harrison, M. Spearpoint, C. Fleischmann, B-Risk User Guide and Technical Manual, Branz Study Report 282. (2013) 1–38.

[64] P.L. Hinkley, Rates of “production” of hot gases in roof venting experiments, Fire Safety Journal. 10 (1986) 57–65. doi:10.1016/0379-7112(86)90032-9.

[65] P.H. Thomas, Comparisoon between Plume Theories, Fire Safety Journal. 20 (1993) 289–292.

[66] G. Heskestad, Fire plume air entrainment according to two competing assumptions, Symposium (International) on Combustion. 21 (1988) 111–120. doi:10.1016/S0082-0784(88)80237-6.

[67] Björn Karlsson; James G. Quintiere, Enclosure Fire Dynamics, n.d.

[68] B. Merci, P. Vandevelde, Experimental study of natural roof ventilation in full-scale enclosure fire tests in a small compartment, Fire Safety Journal. 42 (2007) 523–535. doi:10.1016/j.firesaf.2007.02.003.

[69] J.G. Quintiere, Fundamentals of Fire Phenomena, John Wiley & Sons Ltd., 2006.

[70] B.M. Cetegen, E.F. Zukoski, T. Kubota, Entrainment and flame geometry of fire plumes, in: NBS-GCR-82-402, NIST, 1982: p. 209.

[71] B.M. Cetegen, E.E. Zukoski, T. Kubota, Entrainment in the Near and Far Field of Fire Plumes, Combustion Science and Technology. 39 (1984) 305–331. doi:10.1080/00102208408923794.

[72] W. Węgrzyński, M. Konecki, Influence of the Fire Location and the Size of a Compartment on the Heat and Smoke Flow Out of the Compartment (in press), AIP Conference Proceedings. (2017).

[73] P.H. Thomas, P.L. Hinkley, C.R. Theobald, D.L. Simms, Investigations into the flow of hot gases in roof venting, London, 1963.

[74] J.G. Quintiere, Scaling applications in fire research, Fire Safety Journal. 15 (1989) 3–29. doi:10.1016/0379-7112(89)90045-3.

[75] J.J. Keough, Venting fires through roofs: Experi- mental fires in an aircraft

hangar, in: Report UP 344, Commonwealth Experimental Building Station, 1972.

[76] B.J. McCaffrey, Momentum implications for buoyant diffusion flames, Combustion and Flame. 52 (1983) 149–167. doi:10.1016/0010-2180(83)90129-3.

[77] B.J. McCaffrey, G. Cox, Entrainment and Heat Flux of Buoyant Diffusion Flames, in: NBSIR 82-2473, Was, 1982.

[78] G. Heskestad, Luminous heights of turbulent diffusion flames, Fire Safety Journal. 5 (1983) 103–108. doi:10.1016/0379-7112(83)90002-4.

[79] G. Heskestad, Dynamics of the fire plume, Philosophical Transactions of the Royal Society A: Mathematical, Physical and Engineering Sciences. 356 (1998) 2815–2833. doi:10.1098/rsta.1998.0299.

[80] Society of Fire Protection Engineers, Guidelines for Substantiating a Fire Model for a Given Application, in: SFPE G.06, Bethesda, Maryland, 2011.

[81] E.D. Kuligowski, S.M. V Gwynne, L.M. Hulse, M.J. Kinsey, Guidance for the Model Developer on Representing Human Behavior in Egress Models, Fire Technology. 52 (2016) 775–800. doi:10.1007/s10694-015-0501-2.

[82] W. Węgrzyński, P. Sulik, The philosophy of fire safety engineering in the shaping of civil engineering development, Bulletin of the Polish Academy of Sciences Technical Sciences. 64 (2016). doi:10.1515/bpasts-2016-0081.

[83] G. Hadjisophocleous, E. Zalok, Development of design fires for performance-based fire safety designs, in: Fire Safety Science, 2008. doi:10.3801/IAFSS.FSS.9-63.

[84] G. Lougheed GD, Hadjisophocleous, Investigation of atrium smoke exhaust effectiveness, ASHRAE. (1997) 519–533.

[85] M.C. Kashef A, Benichou N, Lougheed G, A computational and experimental study of fire growth and smoke movement in large spaces, in: 10th Annual Conference of the CFD Society of Canada (CFD 2002), 2002: pp. 466–471.

[86] C.D. Quintiere JG, Steckler K, An assessment of fire induced flows in compartments, Fire Sci Technol. 4 (1984) 1–14.

[87] M. Janssens, H.A.O.C. Tran, Data Reduction of Room Tests for Zone Model Validation, 10 (2015) 528–555.

[88] M.L. Yaping He, Anthony Fernando, Determination of interface height from measured parameter profile in enclosure fire experiment, Fire Safety Journal. 31 (1998) 19–38.

[89] H.W. Emmons, The prediction of fires in buildings, Symposium (International) on Combustion. 17 (1979) 1101–1111. doi:10.1016/S0082-0784(79)80105-8.

[90] R.G.G. Thomas J. Ohlemiller, George W. Mulholland, Skandakumar H. Abeyesekere, James J. Filliben, World Trade Center Disaster Fire Tests of Single Office Workstations, NIST Investigation. (2005).

[91] G. Vigne, To what extent can we rely upon the results obtained from advanced smoke modelling, in: SFPE Copenhagen, 2015.

[92] T.G. Mayerhöfer, H. Mutschke, J. Popp, Employing theories far beyond their limits - the case of the (Boguer-)Beer-Lambert law, ChemPhysChem. (2016) n/a-n/a. doi:10.1002/cphc.201600114.

[93] M. Marchetti, V. Boucher, J. Dumoulin, M. Colomb, Retrieving visibility distance in fog combining infrared thermography, Principal Components Analysis and Partial Least-Square regression, Infrared Physics & Technology. 71 (2015) 289–297. doi:10.1016/j.infrared.2015.05.002.

[94] R. Nebuloni, Empirical relationships between extinction coefficient and visibility in fog, Applied Optics. 44 (2005) 3795–3804. doi:10.1364/AO.44.003795.

[95] F. Nadeem, T. Javornik, E. Leitgeb, V. Kvicera, G. Kandus, Continental fog attenuation empirical relationship from measured visibility data, Radioengineering. 19 (2010) 596–600.

[96] G.W. Mulholland, C. Croarkin, Specific extinction coefficient of flame generated smoke, Fire and Materials. 24 (2000) 227–230. doi:10.1002/1099-1018(200009/10)24:5<227::AID-FAM742>3.0.CO;2-9.

[97] G.W. Mulholland, Smoke Production and Properties, in: SFPE Handbook of Fire Protection Engineering, Fourth Edi, NFPA & SFPE, Quincy, MA, 2008.

[98] M. Konecki, M. Półka, Calculation of visibility in smoke generated during thermal decomposition and combustion of polyester materials, in: Modern Building Materials, Structures and Techniques, MBMST 2010, Vilnius, 2010.

[99] M. Konecki, M. Półka, Simple fire model for comparative studies of critical conditions during combustion of chosen polymer materials, Journal of Civil Engineering and Management. 15 (2009) 247–257. doi:10.3846/1392-3730.2009.15.247-257.

[100] J.F. Widmann, Evaluation of the planck mean absorption coefficients for radiation transport through smoke, Combustion Science and Technology. 175 (2003) 2299–2308. doi:10.1080/714923279.

[101] T. Jin, Visibility and Human Behavior in Fire Smoke, in: SFPE Handbook of Fire Protection Engineering, 3rd Editio, 2002: pp. 2-42-2–53.

[102] T. Jin, Visibility through Fire Smoke (I), Bulletin of the Fire Prevention Society of Japan. 19 (1970).

[103] T. Jin, Visibility through fire smoke, Journal of Fire and Flammability. 9 (1978) 135–155.

[104] T. Jin, Visibility through Fire Smoke (III), Bulletin of the Fire Prevention Society of Japan. 22 (1972).

[105] T. Jin, Visibility through Fire Smoke (II), Bulletin of the Fire Prevention Society of Japan. 21 (1971).

[106] L.Y. Cooper, A Mathematical Model for Estimating Available Safe Egress Time in Fires, Fire and Materials. 6 (1982) 135–144. doi:0.1002/fam.810060307.

[107] ANSYS, ANSYS Fluent 14.5.0 - Technical Documentation, 2014.

[108] K. McGrattan, R. McDermott, J. Floyd, S. Hostikka, G. Forney, H. Baum, Computational fluid dynamics modelling of fire, International Journal of Computational Fluid Dynamics. 26 (2012) 349–361. doi:10.1080/10618562.2012.659663.

[109] G. Vigne, J. Jönsson, J. Stern-Gottfried, The Use of CFD Modelling to Predict Smoke Movement in Tunnels, in: International Congress Smoke

Control in Buildings and Tunnels, Santander (Spain), 2007.

[110] M.O.A. López, G. Vigne, Influencia De Los Parametros Criticos De Visibilidad En Simulaciones Avanzadas De Humos – Estudio CFD Aplicado Al Murcia Fire Atrium, Universidad Pontificia Comillas, 2013.

[111] G. Vigne, W. Węgrzyński, Influence of Variability of Soot Yield Parameter in Assessing the Safe Evacuation Conditions in Advanced Modeling Analysis. Results of Physical and Numerical Modeling Comparison, in: 11th Conference on Performance-Based Codes and Fire Safety Design Methods, SFPE, 2016.

[112] W. Poh, Tenability criteria for design of smoke hazard management systems, Ecolibrium. 8 (2011).

[113] W. Poh, Tenability in Building Fires: Limits and Design, Fire Australia. (2010).

[114] W. Węgrzyński, G. Krajewski, Systemy wentylacji pożarowej garaży. Projektowanie, ocena, odbiór, 493/2015, Instytut Techniki Budowlanej, 2015.

[115] T. Yamada, Y. Akizuki, Visibility and Human Behavior in Fire Smoke, in: SFPE Handbook of Fire Protection Engineering, Springer New York, New York, NY, 2016: pp. 2181–2206. doi:10.1007/978-1-4939-2565-0_61.

[116] P. Rubini, Q. Zhang, J. Moss, Simulation of visibility in smoke laden environments, … Fire Science and Engineering. University of …. (2007) 3–5.

[117] K. McGrattan, S. Hostikka, R. McDermott, J. Floyd, C. Weinschenk, K. Overholt, Fire Dynamics Simulator technical reference guide, NIST Special Publication 1018-1. US Department of Commerce, National Institute of Standards and Technology. Gaithersburg, MD. 1 (2016) 175. doi:10.6028/NIST.SP.1018-1.

[118] K. Mcgrattan, R. Mcdermott, Fire Dynamics Simulator (Version 6) User's Guide, NIST SP 1019-5, (n.d.).

[119] Thunderhead Engineering, PyroSim User Manual, (2019) 167.

[120] U. NIC, Verification and validation of selected fire models for nuclear

power plant applications, 2006. http://kgrs.public.haifire.com/Generic Issues/Fire Modeling/NUREG-1824 - Fire Model Verification and Validations/NUREG 1824 Vol 1 Main Report 5-31-07 ML071650546.pdf.

[121] W.G. Weng, D. Kamikawa, Y. Fukuda, Y. Hasemi, K. Kagiya, Study on flame height of merged flame from multiple fire sources, Combustion Science and Technology. 176 (2004) 2105–2123. doi:10.1080/00102200490514949.

[122] Thunderhead Engineering, PyroSim Results User Manual, 2019. https://www.thunderheadeng.com/wp-content/uploads/dlm_uploads/2018/05/results_users_guide-3.pdf.

[123] W. Węgrzyński, G. Vigne, Experimental and numerical evaluation of the influence of the soot yield on the visibility in smoke in CFD analysis, Fire Safety Journal. (2017). doi:10.1016/j.firesaf.2017.03.053.

[124] L. Yi, W.K. Chow, Y.Z. Li, R. Huo, A simple two-layer zone model on mechanical exhaust in an atrium, Building and Environment. 40 (2005) 869–880. doi:10.1016/j.buildenv.2004.08.018.

[125] D. Nilsson, Exit choice in fire emergencies - Influencing choice of exit with flashing lights, 2009.

Appendix A

Table A1 – Experimental fire plume and wall A data experiment #4FX

Time (s)	**S1 $(z = 5.25\ m)$**		**S3 $(z = 7.25\ m)$**		**S5 $(z = 13.25\ m)$**		**S14 $(z = 5\ m)$**		**S16 $(z = 10\ m)$**		**S18 $(z = 15\ m)$**	
	DL	Err.	DL	Err.	DL	Err.	DL	Err.	DL	Err.	DL	Err.
0	14.5	1.9	14.5	1.9	14.5	1.9	14.5	1.9	14.5	1.9	14.5	1.9
30	16.6	1.9	15.7	1.9	15.1	1.9	15.0	1.9	15.4	1.9	15.0	1.9
60	19.2	2.1	17.4	2.0	17.2	2.0	15.9	1.9	17.0	2.0	20.2	2.1
90	19.1	2.1	18.6	2.0	19.7	2.1	16.2	1.9	18.3	2.0	23.6	2.2
120	20.7	2.1	20.5	2.1	22.3	2.2	17.1	2.0	21.6	2.2	25.9	2.3
150	124.6	6.4	47.8	3.2	34.3	2.7	19.3	2.1	25.4	2.3	29.1	2.5
180	146.7	7.3	63.3	3.9	41.6	3.0	22.2	2.2	30.5	2.5	33.1	2.6
210	166.1	8.1	68.1	4.1	41.4	3.0	26.7	2.4	36.7	2.8	37.6	2.8
240	154.6	7.6	67.9	4.1	45.2	3.1	32.1	2.6	43.6	3.1	42.7	3.0
270	194.9	9.3	84.6	4.7	54.2	3.5	38.9	2.9	49.5	3.3	48.2	3.2
300	212.4	10.0	92.1	5.0	61.4	3.8	49.1	3.3	54.9	3.5	54.7	3.5
330	162.7	7.9	90.7	5.0	64.7	3.9	58.9	3.7	60.0	3.7	64.2	3.9
360	194.6	9.2	93.7	5.1	69.6	4.1	68.7	4.1	72.0	4.2	76.3	4.4
390	181.0	8.7	87.8	4.9	73.7	4.3	80.8	4.6	86.3	4.8	85.4	4.8
420	207.2	9.8	106.5	5.6	87.2	4.8	90.3	5.0	92.3	5.1	94.8	5.2
450	271.7	12.4	119.6	6.2	97.1	5.3	103.3	5.5	104.6	5.6	104.7	5.6
480	143.6	7.2	116.0	6.0	101.9	5.4	109.1	5.7	110.4	5.8	111.1	5.8
510	110.8	5.8	108.6	5.7	103.7	5.5	108.2	5.7	109.6	5.8	110.9	5.8
540	101.6	5.4	108.1	5.7	103.6	5.5	107.3	5.7	107.3	5.7	108.2	5.7
570	95.0	5.2	107.7	5.7	103.3	5.5	107.2	5.7	106.7	5.6	106.6	5.6
600	91.4	5.0	105.8	5.6	102.9	5.5	106.7	5.6	104.9	5.6	106.6	5.6
630	88.2	4.9	104.9	5.6	100.9	5.4	105.3	5.6	102.8	5.5	103.6	5.5
660	86.6	4.8	103.4	5.5	99.6	5.4	104.1	5.5	102.3	5.5	102.9	5.5
690	70.2	4.1	100.2	5.4	97.6	5.3	87.7	4.9	99.0	5.3	99.7	5.4
720	52.9	3.4	97.0	5.2	94.4	5.1	70.6	4.2	94.6	5.2	94.4	5.1
750	42.7	3.0	90.2	5.0	90.4	5.0	57.4	3.6	86.3	4.8	90.5	5.0
780	36.4	2.8	81.1	4.6	84.1	4.7	42.1	3.0	79.5	4.5	87.0	4.8

Table A2 – Experimental smoke layer tree data (S32- S37) experiment #4FX

Time (s)	S32 $(z = 1\ m)$		S33 $(z = 2\ m)$		S34 $(z = 3\ m)$		S35 $(z = 4\ m)$		S36 $(z = 5\ m)$		S37 $(z = 5.5\ m)$	
	DL	Err.	DL	Err.	DL	Err.	DL	Err.	DL	Err.	DL	Err.
0	14.5	1.9	14.5	1.9	14.5	1.9	14.5	1.9	14.5	1.9	14.5	1.9
30	14.6	1.9	14.9	1.9	14.5	1.9	15.3	1.9	15.5	1.9	15.3	1.9
60	15.1	1.9	15.8	1.9	15.1	1.9	16.3	1.9	16.3	1.9	16.2	1.9
90	15.2	1.9	15.8	1.9	15.3	1.9	16.8	2.0	17.0	2.0	16.8	2.0
120	15.7	1.9	16.3	1.9	15.4	1.9	16.9	2.0	17.2	2.0	16.8	2.0
150	16.6	1.9	17.6	2.0	17.0	2.0	19.5	2.1	20.1	2.1	19.7	2.1
180	18.4	2.0	20.8	2.1	20.0	2.1	22.8	2.2	23.7	2.2	22.8	2.2
210	19.2	2.1	21.6	2.2	21.3	2.1	24.6	2.3	27.0	2.4	27.0	2.4
240	21.1	2.1	24.7	2.3	23.4	2.2	28.3	2.4	32.8	2.6	33.8	2.7
270	22.3	2.2	27.2	2.4	25.2	2.3	33.0	2.6	40.0	2.9	39.9	2.9
300	23.7	2.2	29.8	2.5	28.9	2.5	43.7	3.1	48.6	3.3	49.4	3.3
330	25.6	2.3	32.3	2.6	36.0	2.7	52.6	3.4	55.7	3.6	56.5	3.6
360	29.2	2.5	35.5	2.7	49.6	3.3	68.4	4.1	69.8	4.1	69.0	4.1
390	31.4	2.6	37.2	2.8	50.3	3.3	76.9	4.4	79.2	4.5	78.8	4.5
420	35.9	2.7	39.4	2.9	50.4	3.3	82.6	4.7	86.9	4.8	86.4	4.8
450	39.2	2.9	42.7	3.0	57.5	3.6	89.2	4.9	94.1	5.1	94.7	5.2
480	37.4	2.8	41.9	3.0	53.1	3.4	95.5	5.2	101.8	5.4	102.6	5.5
510	33.8	2.7	36.7	2.8	44.0	3.1	84.0	4.7	100.0	5.4	101.4	5.4
540	34.1	2.7	36.3	2.8	35.5	2.7	61.6	3.8	91.8	5.0	99.4	5.3
570	28.8	2.5	29.3	2.5	33.4	2.6	52.7	3.4	94.8	5.2	98.9	5.3
600	26.4	2.4	28.5	2.4	36.5	2.8	49.5	3.3	92.6	5.1	97.7	5.3
630	27.7	2.4	29.6	2.5	32.5	2.6	45.3	3.1	85.8	4.8	93.9	5.1
660	26.0	2.3	28.1	2.4	29.3	2.5	45.2	3.1	84.8	4.7	92.4	5.1
690	28.0	2.4	30.4	2.5	31.0	2.5	39.0	2.9	71.0	4.2	86.2	4.8
720	29.1	2.5	31.0	2.5	31.7	2.6	35.2	2.7	49.3	3.3	71.8	4.2
750	28.3	2.4	29.8	2.5	30.6	2.5	32.8	2.6	39.2	2.9	52.9	3.4
780	24.8	2.3	27.9	2.4	29.1	2.5	28.2	2.4	30.5	2.5	37.2	2.8

Table A3 – Experimental smoke layer tree data (S38- S42) experiment #4FX

Time (s)	S38 ($z = 6$ m)		S39 ($z = 6.5$ m)		S40 ($z = 7$ m)		S41 ($z = 7.5$ m)		S42 ($z = 8$ m)	
	DL	Err.	DL	Err.	DL	Err.	DL	Err.	DL	Err.
0	14.5	1.9	14.5	1.9	14.5	1.9	14.5	1.9	14.5	1.9
30	15.2	1.9	15.2	1.9	15.5	1.9	15.4	1.9	15.6	1.9
60	16.2	1.9	16.5	1.9	16.6	2.0	16.4	1.9	16.7	2.0
90	17.0	2.0	17.4	2.0	17.8	2.0	17.6	2.0	18.0	2.0
120	16.7	2.0	16.7	2.0	16.9	2.0	16.7	2.0	17.3	2.0
150	19.6	2.1	21.6	2.2	21.8	2.2	22.0	2.2	23.4	2.2
180	22.3	2.2	25.4	2.3	26.3	2.4	26.8	2.4	29.0	2.5
210	28.2	2.4	31.6	2.6	32.0	2.6	32.5	2.6	34.4	2.7
240	35.0	2.7	37.4	2.8	37.5	2.8	37.8	2.8	39.6	2.9
270	40.4	2.9	43.3	3.0	43.2	3.0	44.2	3.1	47.0	3.2
300	49.6	3.3	52.6	3.4	53.1	3.4	53.1	3.4	54.0	3.5
330	56.5	3.6	58.5	3.7	59.5	3.7	58.8	3.7	59.5	3.7
360	67.9	4.1	69.6	4.1	69.0	4.1	68.3	4.1	67.9	4.1
390	77.7	4.5	79.1	4.5	78.6	4.5	77.7	4.5	78.0	4.5
420	85.4	4.8	87.4	4.9	87.1	4.8	87.1	4.8	86.1	4.8
450	95.4	5.2	96.1	5.2	96.0	5.2	96.7	5.2	96.0	5.2
480	102.5	5.5	103.5	5.5	103.5	5.5	104.2	5.5	102.8	5.5
510	102.6	5.5	103.7	5.5	104.0	5.5	104.3	5.5	103.6	5.5
540	100.6	5.4	102.4	5.5	103.7	5.5	104.2	5.5	104.8	5.6
570	99.9	5.4	100.6	5.4	101.7	5.4	101.6	5.4	103.6	5.5
600	98.9	5.3	100.6	5.4	101.4	5.4	101.9	5.4	102.3	5.5
630	96.1	5.2	98.8	5.3	100.2	5.4	100.6	5.4	100.6	5.4
660	95.1	5.2	97.2	5.3	98.3	5.3	98.9	5.3	99.5	5.3
690	90.8	5.0	94.0	5.1	95.5	5.2	96.0	5.2	96.3	5.2
720	83.5	4.7	89.0	4.9	91.7	5.0	92.9	5.1	93.6	5.1
750	63.8	3.9	72.9	4.3	84.2	4.7	85.6	4.8	87.4	4.9
780	46.1	3.2	51.6	3.4	59.7	3.7	69.1	4.1	75.7	4.4

Table A3 – Experimental smoke layer tree data (S43 – S48) experiment #4FX

Time (s)	S43 $(z = 8.5\ m)$		S44 $(z = 9\ m)$		S45 $(z = 9.5\ m)$		S46 $(z = 10\ m)$		S47 $(z = 10.5 m)$		S48 $(z = 11\ m)$	
	DL	Err.	DL	Err.	DL	Err.	DL	Err.	DL	Err.	DL	Err.
0	14.5	1.9	14.5	1.9	14.5	1.9	14.5	1.9	14.5	1.9	14.5	1.9
30	15.1	1.9	15.1	1.9	15.7	1.9	15.0	1.9	15.5	1.9	15.1	1.9
60	16.3	1.9	16.3	1.9	17.0	2.0	16.1	1.9	16.5	1.9	15.8	1.9
90	17.4	2.0	17.7	2.0	18.5	2.0	17.5	2.0	17.9	2.0	17.6	2.0
120	17.5	2.0	18.6	2.0	20.7	2.1	20.4	2.1	21.2	2.1	21.2	2.1
150	22.4	2.2	22.9	2.2	24.7	2.3	23.6	2.2	25.2	2.3	24.8	2.3
180	28.5	2.4	29.5	2.5	31.7	2.6	31.1	2.5	31.4	2.6	30.3	2.5
210	34.7	2.7	36.2	2.8	37.7	2.8	36.7	2.8	36.9	2.8	36.2	2.8
240	38.9	2.9	40.1	2.9	41.6	3.0	40.7	2.9	41.2	3.0	40.6	2.9
270	46.1	3.2	46.7	3.2	47.7	3.2	46.6	3.2	46.9	3.2	46.4	3.2
300	52.6	3.4	52.3	3.4	52.9	3.4	51.5	3.4	51.6	3.4	51.0	3.4
330	58.8	3.7	58.9	3.7	59.8	3.7	58.5	3.7	58.5	3.7	57.5	3.6
360	66.3	4.0	66.1	4.0	67.2	4.0	66.2	4.0	66.2	4.0	65.8	4.0
390	76.5	4.4	76.4	4.4	76.3	4.4	75.9	4.4	75.1	4.3	74.1	4.3
420	85.9	4.8	85.8	4.8	85.8	4.8	85.9	4.8	86.5	4.8	85.6	4.8
450	95.4	5.2	94.8	5.2	95.6	5.2	94.9	5.2	94.1	5.1	93.9	5.1
480	103.7	5.5	103.1	5.5	104.0	5.5	103.5	5.5	102.4	5.5	101.8	5.4
510	103.6	5.5	103.5	5.5	104.0	5.5	104.3	5.5	103.9	5.5	103.3	5.5
540	104.9	5.6	105.3	5.6	106.0	5.6	104.8	5.6	104.7	5.6	103.7	5.5
570	103.2	5.5	103.1	5.5	104.8	5.6	103.1	5.5	103.8	5.5	102.7	5.5
600	102.1	5.5	102.0	5.5	103.0	5.5	102.2	5.5	102.1	5.5	101.6	5.4
630	100.3	5.4	100.7	5.4	101.5	5.4	100.1	5.4	101.2	5.4	100.7	5.4
660	98.8	5.3	98.9	5.3	100.3	5.4	99.0	5.3	99.8	5.4	99.1	5.3
690	96.3	5.2	96.4	5.2	97.4	5.3	96.5	5.2	97.1	5.3	97.0	5.2
720	93.5	5.1	93.9	5.1	94.5	5.1	94.1	5.1	94.7	5.2	94.4	5.1
750	87.5	4.9	88.6	4.9	89.2	4.9	89.2	4.9	89.6	4.9	89.8	5.0
780	78.6	4.5	80.2	4.6	80.4	4.6	81.3	4.6	81.0	4.6	81.8	4.6

Table A4 – Experimental smoke layer tree data (S49 - S53) experiment #4FX

Time (s)	**S49 $(z = 11.5m)$**		**S50 $(z = 12\ m)$**		**S51 $(z = 12.5m)$**		**S52 $(z = 13\ m)$**		**S53 $(z = 13.5m)$**	
	DL	Err.	DL	Err.	DL	Err.	DL	Err.	DL	Err.
0	14.5	1.9	14.5	1.9	14.5	1.9	14.5	1.9	14.5	1.9
30	14.7	1.9	15.2	1.9	15.5	1.9	14.6	1.9	14.6	1.9
60	15.2	1.9	15.7	1.9	16.0	1.9	15.3	1.9	15.7	1.9
90	17.2	2.0	17.9	2.0	18.3	2.0	18.0	2.0	18.5	2.0
120	20.5	2.1	21.5	2.2	21.9	2.2	21.4	2.1	21.4	2.1
150	23.2	2.2	24.7	2.3	25.4	2.3	24.6	2.3	24.9	2.3
180	29.0	2.5	29.7	2.5	30.4	2.5	29.4	2.5	29.5	2.5
210	35.0	2.7	35.5	2.7	35.2	2.7	33.8	2.7	33.9	2.7
240	39.3	2.9	40.0	2.9	39.3	2.9	38.8	2.9	39.0	2.9
270	45.6	3.1	46.1	3.2	45.1	3.1	43.8	3.1	43.3	3.0
300	49.4	3.3	49.8	3.3	49.2	3.3	48.7	3.3	48.7	3.3
330	56.4	3.6	57.1	3.6	55.9	3.6	55.9	3.6	55.9	3.6
360	66.2	4.0	66.2	4.0	67.3	4.0	67.4	4.0	67.4	4.0
390	74.2	4.3	75.0	4.3	76.7	4.4	75.8	4.4	75.6	4.4
420	85.2	4.8	85.8	4.8	85.7	4.8	85.5	4.8	85.6	4.8
450	93.0	5.1	93.3	5.1	93.4	5.1	92.5	5.1	92.7	5.1
480	102.1	5.5	101.9	5.4	102.5	5.5	103.3	5.5	103.1	5.5
510	103.1	5.5	103.4	5.5	103.6	5.5	103.6	5.5	103.8	5.5
540	102.7	5.5	103.2	5.5	103.4	5.5	102.9	5.5	102.8	5.5
570	102.6	5.5	102.9	5.5	103.8	5.5	102.9	5.5	102.6	5.5
600	101.5	5.4	101.7	5.4	102.4	5.5	102.5	5.5	102.2	5.5
630	99.5	5.3	100.0	5.4	100.4	5.4	100.2	5.4	100.2	5.4
660	98.2	5.3	99.0	5.3	99.5	5.4	99.3	5.3	98.9	5.3
690	96.2	5.2	97.0	5.2	97.6	5.3	97.3	5.3	97.1	5.3
720	94.1	5.1	94.5	5.1	94.4	5.1	94.4	5.1	94.3	5.1
750	89.6	4.9	89.9	5.0	90.4	5.0	90.5	5.0	90.5	5.0
780	83.4	4.7	83.2	4.7	84.1	4.7	85.2	4.8	85.5	4.8

Table A5 – Experimental smoke layer tree data (S54 -S59) experiment #4FX

Time (s)	**S54** $(\mathbf{z = 14\ m})$		**S55** $(\mathbf{z = 14.5m})$		**S56** $(\mathbf{z = 15\ m})$		**S57** $(\mathbf{z = 16\ m})$		**S58** $(\mathbf{z = 17\ m})$		**S59** $(\mathbf{z = 18\ m})$	
	DL	Err.	DL	Err.	DL	Err.	DL	Err.	DL	Err.	DL	Err.
0	14.5	1.9	14.5	1.9	14.5	1.9	14.5	1.9	14.5	1.9	14.5	1.9
30	14.9	1.9	14.9	1.9	15.1	1.9	15.5	1.9	16.1	1.9	15.7	1.9
60	16.6	1.9	16.4	1.9	16.6	2.0	16.3	1.9	17.9	2.0	19.5	2.1
90	19.2	2.1	19.1	2.1	19.1	2.1	19.3	2.1	21.2	2.1	22.8	2.2
120	22.0	2.2	22.0	2.2	22.1	2.2	22.5	2.2	23.9	2.2	25.6	2.3
150	25.2	2.3	25.4	2.3	26.2	2.3	26.8	2.4	28.8	2.5	28.7	2.4
180	29.7	2.5	29.6	2.5	30.5	2.5	31.4	2.6	33.5	2.6	34.3	2.7
210	34.1	2.7	34.4	2.7	35.5	2.7	37.3	2.8	39.0	2.9	38.9	2.9
240	38.6	2.9	38.8	2.9	40.3	2.9	41.4	3.0	43.5	3.1	44.8	3.1
270	42.9	3.0	43.1	3.0	44.1	3.1	44.6	3.1	46.7	3.2	48.9	3.3
300	48.8	3.3	49.0	3.3	49.9	3.3	51.8	3.4	56.4	3.6	57.3	3.6
330	55.7	3.6	55.8	3.6	56.0	3.6	57.7	3.6	61.0	3.8	63.4	3.9
360	67.8	4.1	68.0	4.1	68.3	4.1	70.4	4.2	72.7	4.3	73.5	4.3
390	76.5	4.4	76.7	4.4	77.0	4.4	78.5	4.5	81.8	4.6	82.1	4.6
420	86.1	4.8	85.9	4.8	86.9	4.8	88.2	4.9	90.9	5.0	91.6	5.0
450	93.4	5.1	93.3	5.1	94.6	5.1	94.9	5.2	99.3	5.3	102.9	5.5
480	103.4	5.5	102.2	5.5	102.7	5.5	103.6	5.5	104.1	5.5	105.2	5.6
510	104.3	5.5	103.7	5.5	104.5	5.6	104.7	5.6	106.1	5.6	105.7	5.6
540	103.4	5.5	103.4	5.5	104.6	5.6	105.2	5.6	106.8	5.6	106.7	5.6
570	102.8	5.5	102.5	5.5	103.1	5.5	104.1	5.5	105.4	5.6	104.9	5.6
600	102.3	5.5	102.2	5.5	102.7	5.5	103.4	5.5	104.0	5.5	103.4	5.5
630	100.2	5.4	100.1	5.4	100.9	5.4	102.5	5.5	102.9	5.5	101.8	5.4
660	99.0	5.3	98.9	5.3	100.0	5.4	100.2	5.4	101.1	5.4	100.6	5.4
690	97.4	5.3	97.3	5.3	97.7	5.3	98.0	5.3	97.9	5.3	96.9	5.2
720	94.7	5.2	94.7	5.2	95.3	5.2	95.7	5.2	95.2	5.2	93.5	5.1
750	90.9	5.0	90.7	5.0	91.1	5.0	91.8	5.0	91.3	5.0	89.9	5.0
780	86.3	4.8	86.4	4.8	86.6	4.8	86.9	4.8	87.0	4.8	85.6	4.8

Table A6 – Experimental smoke layer tree data (S32 – S37) experiment #5_1

Time (s)	**S32 $(\mathbf{z = 1\ m})$**		**S33 $(\mathbf{z = 2\ m})$**		**S34 $(\mathbf{z = 3\ m})$**		**S35 $(\mathbf{z = 4\ m})$**		**S36 $(\mathbf{z = 5\ m})$**		**S37 $(\mathbf{z = 5.5\ m})$**	
	DL	Err.	DL	Err.	DL	Err.	DL	Err.	DL	Err.	DL	Err.
0	11.0	1.7	11.0	1.7	11.0	1.7	11.0	1.7	11.0	1.7	11.0	1.7
30	15.5	1.9	17.8	2.0	17.3	2.0	19.3	2.1	19.4	2.1	17.1	2.0
60	18.8	2.0	22.4	2.2	22.2	2.2	25.8	2.3	26.0	2.3	22.5	2.2
90	21.3	2.1	27.1	2.4	25.6	2.3	29.2	2.5	29.3	2.5	26.4	2.4
120	22.0	2.2	29.4	2.5	30.2	2.5	34.8	2.7	33.8	2.7	31.4	2.6
150	22.9	2.2	26.5	2.4	32.1	2.6	36.6	2.8	40.1	2.9	38.5	2.8
180	20.6	2.1	28.1	2.4	33.9	2.7	39.3	2.9	45.4	3.1	53.3	3.5
210	24.2	2.3	32.0	2.6	34.4	2.7	42.5	3.0	54.2	3.5	65.0	3.9
240	26.9	2.4	36.1	2.8	38.2	2.8	49.4	3.3	64.5	3.9	77.0	4.4
270	28.1	2.4	35.7	2.7	38.4	2.8	49.1	3.3	80.1	4.6	87.2	4.8
300	29.0	2.5	38.2	2.8	42.0	3.0	50.6	3.3	81.0	4.6	95.7	5.2
330	33.9	2.7	42.1	3.0	45.8	3.1	53.5	3.5	79.3	4.5	101.5	5.4
360	37.5	2.8	45.9	3.2	44.5	3.1	55.9	3.6	80.1	4.6	105.3	5.6
390	38.0	2.8	43.2	3.0	45.5	3.1	56.5	3.6	75.3	4.4	112.1	5.9
420	34.9	2.7	40.5	2.9	42.4	3.0	54.3	3.5	75.8	4.4	107.5	5.7
450	30.5	2.5	37.7	2.8	40.7	2.9	54.1	3.5	73.6	4.3	105.5	5.6
480	31.0	2.5	39.7	2.9	45.9	3.2	52.7	3.4	70.6	4.2	95.1	5.2
510	36.9	2.8	44.1	3.1	48.2	3.2	57.1	3.6	69.4	4.1	89.2	4.9
540	38.3	2.8	45.2	3.1	48.7	3.3	59.5	3.7	69.6	4.1	84.4	4.7

Table A7 – Experimental smoke layer tree data (S38 – S42) experiment #5_1

Time (s)	**S38** $(\mathbf{z = 6\ m})$		**S39** $(\mathbf{z = 6.5\ m})$		**S40** $(\mathbf{z = 7\ m})$		**S41** $(\mathbf{z = 7.5\ m})$		**S42** $(\mathbf{z = 8\ m})$	
	DL	Err.	DL	Err.	DL	Err.	DL	Err.	DL	Err.
0	11.0	1.7	11.0	1.7	11.0	1.7	11.0	1.7	11.0	1.7
30	13.8	1.8	19.0	2.1	16.9	2.0	15.8	1.9	18.1	2.0
60	17.0	2.0	24.3	2.3	21.3	2.1	19.9	2.1	23.9	2.2
90	21.4	2.1	30.3	2.5	27.1	2.4	26.6	2.4	33.9	2.7
120	27.1	2.4	37.5	2.8	37.1	2.8	38.7	2.9	48.2	3.2
150	37.2	2.8	49.1	3.3	52.1	3.4	54.4	3.5	61.5	3.8
180	54.0	3.5	62.4	3.8	63.1	3.9	64.1	3.9	68.8	4.1
210	65.1	3.9	75.0	4.3	74.5	4.3	74.9	4.3	78.7	4.5
240	75.5	4.4	84.3	4.7	84.0	4.7	83.7	4.7	87.2	4.8
270	86.6	4.8	93.7	5.1	92.9	5.1	92.9	5.1	96.6	5.2
300	94.8	5.2	100.8	5.4	99.6	5.4	98.9	5.3	102.8	5.5
330	102.7	5.5	108.4	5.7	107.2	5.7	107.1	5.7	111.4	5.8
360	107.9	5.7	113.2	5.9	112.3	5.9	111.7	5.8	116.0	6.0
390	114.7	6.0	120.3	6.2	119.2	6.2	118.1	6.1	120.9	6.2
420	116.0	6.0	123.8	6.3	123.2	6.3	122.6	6.3	124.9	6.4
450	120.5	6.2	127.4	6.5	127.0	6.5	126.7	6.5	128.3	6.5
480	121.9	6.3	129.8	6.6	130.1	6.6	129.5	6.6	131.5	6.7
510	119.9	6.2	131.7	6.7	133.1	6.7	133.1	6.7	134.9	6.8
540	120.1	6.2	131.2	6.6	132.9	6.7	133.2	6.7	135.6	6.8

Table A8 – Experimental smoke layer tree data (S43 – S48) experiment #5_1

Time	**S43**		**S44**		**S45**		**S46**		**S47**		**S48**	
(s)	$(\mathbf{z = 8.5\ m})$		$(\mathbf{z = 9\ m})$		$(\mathbf{z = 9.5\ m})$		$(\mathbf{z = 10\ m})$		$(\mathbf{z = 10.5m})$		$(\mathbf{z = 11\ m})$	
	DL	Err.	DL	Err.	DL	Err.	DL	Err.	DL	Err.	DL	Err.
0	11.0	1.7	11.0	1.7	11.0	1.7	11.0	1.7	11.0	1.7	11.0	1.7
30	15.4	1.9	15.8	1.9	17.4	2.0	16.5	1.9	17.7	2.0	17.3	2.0
60	21.0	2.1	22.5	2.2	25.6	2.3	25.7	2.3	28.4	2.4	29.1	2.5
90	32.7	2.6	34.8	2.7	42.6	3.0	44.3	3.1	46.0	3.2	45.6	3.1
120	45.9	3.2	47.5	3.2	52.4	3.4	53.3	3.5	55.7	3.6	55.4	3.5
150	58.1	3.7	59.1	3.7	63.8	3.9	65.3	3.9	66.8	4.0	67.0	4.0
180	67.3	4.0	70.4	4.2	74.1	4.3	75.7	4.4	76.0	4.4	77.1	4.4
210	79.2	4.5	81.3	4.6	84.0	4.7	85.6	4.8	85.9	4.8	86.2	4.8
240	87.2	4.8	88.9	4.9	90.8	5.0	92.7	5.1	93.4	5.1	93.8	5.1
270	95.7	5.2	97.1	5.2	98.7	5.3	100.9	5.4	101.5	5.4	102.1	5.5
300	102.8	5.5	104.6	5.6	105.6	5.6	106.6	5.6	106.9	5.7	107.0	5.7
330	110.1	5.8	111.4	5.8	113.8	5.9	115.0	6.0	114.7	6.0	115.9	6.0
360	114.7	6.0	115.1	6.0	116.6	6.1	116.9	6.1	118.0	6.1	119.2	6.2
390	119.2	6.2	119.2	6.2	120.9	6.2	120.8	6.2	121.6	6.3	123.1	6.3
420	124.1	6.4	124.9	6.4	126.7	6.5	126.6	6.5	126.7	6.5	127.6	6.5
450	128.3	6.5	129.1	6.6	130.0	6.6	129.9	6.6	130.2	6.6	131.3	6.7
480	130.5	6.6	130.6	6.6	132.3	6.7	131.9	6.7	132.3	6.7	133.3	6.7
510	133.7	6.7	134.0	6.8	135.1	6.8	134.6	6.8	135.5	6.8	135.6	6.8
540	134.7	6.8	135.5	6.8	136.5	6.9	136.0	6.8	136.7	6.9	136.9	6.9

Table A9 – Experimental smoke layer tree data (S49 - S53) experiment #5_1

Time (s)	**S49** $(\mathbf{z = 11.5m})$		**S50** $(\mathbf{z = 12\ m})$		**S51** $(\mathbf{z = 12.5m})$		**S52** $(\mathbf{z = 13\ m})$		**S53** $(\mathbf{z = 13.5m})$	
	DL	Err.	DL	Err.	DL	Err.	DL	Err.	DL	Err.
0	11.0	1.7	11.0	1.7	11.0	1.7	11.0	1.7	11.0	1.7
30	16.3	1.9	18.0	2.0	17.4	2.0	13.9	1.8	14.5	1.9
60	28.2	2.4	29.8	2.5	29.9	2.5	25.8	2.3	26.6	2.4
90	44.5	3.1	44.6	3.1	43.1	3.0	39.6	2.9	38.5	2.8
120	54.5	3.5	55.6	3.6	55.4	3.5	50.7	3.4	51.1	3.4
150	66.3	4.0	66.6	4.0	65.5	4.0	59.0	3.7	59.7	3.7
180	76.3	4.4	76.0	4.4	75.4	4.4	73.5	4.3	74.7	4.3
210	85.2	4.8	85.0	4.8	83.3	4.7	78.0	4.5	76.2	4.4
240	93.6	5.1	94.2	5.1	93.1	5.1	90.1	5.0	90.1	5.0
270	101.2	5.4	102.1	5.5	100.9	5.4	97.6	5.3	97.5	5.3
300	106.8	5.6	107.3	5.7	108.2	5.7	107.8	5.7	109.1	5.7
330	115.5	6.0	114.9	6.0	115.3	6.0	113.6	5.9	114.6	6.0
360	120.5	6.2	121.4	6.2	120.5	6.2	120.6	6.2	123.5	6.3
390	123.5	6.3	124.6	6.4	125.1	6.4	125.2	6.4	125.0	6.4
420	128.3	6.5	129.3	6.6	129.9	6.6	131.4	6.7	131.9	6.7
450	131.2	6.6	132.2	6.7	132.5	6.7	135.3	6.8	136.2	6.9
480	133.0	6.7	133.9	6.8	135.0	6.8	137.7	6.9	139.0	7.0
510	135.2	6.8	135.9	6.8	136.6	6.9	139.2	7.0	140.5	7.0
540	136.3	6.9	137.1	6.9	137.5	6.9	140.7	7.0	142.0	7.1

Table A10 – Experimental smoke layer tree data (S54 - S59) experiment #5_1

Time	**S54**		**S55**		**S56**		**S57**		**S58**		**S59**	
(s)	$(\mathbf{z = 14\ m})$		$(\mathbf{z = 14.5m})$		$(\mathbf{z = 15\ m})$		$(\mathbf{z = 16\ m})$		$(\mathbf{z = 17\ m})$		$(\mathbf{z = 18\ m})$	
	DL	Err.	DL	Err.	DL	Err.	DL	Err.	DL	Err.	DL	Err.
0	11.0	1.7	11.0	1.7	11.0	1.7	11.0	1.7	11.0	1.7	11.0	1.7
30	14.8	1.9	15.5	1.9	16.8	2.0	15.5	1.9	16.9	2.0	24.8	2.3
60	26.1	2.3	27.8	2.4	29.0	2.5	27.9	2.4	29.5	2.5	37.3	2.8
90	36.8	2.8	36.0	2.7	37.3	2.8	36.8	2.8	42.0	3.0	53.4	3.5
120	49.5	3.3	49.2	3.3	50.1	3.3	50.4	3.3	54.4	3.5	64.5	3.9
150	59.7	3.7	62.5	3.8	62.0	3.8	63.0	3.9	62.4	3.8	71.7	4.2
180	72.5	4.2	73.1	4.3	73.4	4.3	70.8	4.2	70.9	4.2	83.9	4.7
210	75.6	4.4	81.9	4.6	81.6	4.6	83.8	4.7	85.0	4.8	88.6	4.9
240	85.6	4.8	87.4	4.9	90.4	5.0	92.3	5.1	96.9	5.2	108.8	5.7
270	94.5	5.1	100.2	5.4	99.9	5.4	101.3	5.4	102.8	5.5	114.8	6.0
300	110.1	5.8	107.0	5.7	108.2	5.7	112.4	5.9	115.4	6.0	119.3	6.2
330	116.4	6.0	119.1	6.2	116.6	6.0	120.9	6.2	119.2	6.2	132.1	6.7
360	117.9	6.1	121.3	6.2	124.5	6.4	122.4	6.3	125.3	6.4	135.3	6.8
390	130.3	6.6	127.8	6.5	128.2	6.5	128.2	6.5	132.2	6.7	141.7	7.1
420	132.4	6.7	133.6	6.7	132.0	6.7	131.6	6.7	133.7	6.8	146.2	7.3
450	136.3	6.9	137.6	6.9	137.4	6.9	137.4	6.9	137.8	6.9	149.7	7.4
480	139.1	7.0	139.1	7.0	140.0	7.0	139.9	7.0	140.8	7.0	153.8	7.6
510	140.6	7.0	140.6	7.0	141.5	7.1	141.4	7.1	142.3	7.1	155.3	7.6
540	142.1	7.1	142.1	7.1	143.0	7.1	142.9	7.1	144.4	7.2	156.8	7.7

Table A11 – Experimental smoke layer tree data (S32 – S37) experiment #5_2

Time (s)	**S32 $(\mathbf{z = 1\ m})$**		**S33 $(\mathbf{z = 2\ m})$**		**S34 $(\mathbf{z = 3\ m})$**		**S35 $(\mathbf{z = 4\ m})$**		**S36 $(\mathbf{z = 5\ m})$**		**S37 $(\mathbf{z = 5.5\ m})$**	
	DL	Err.	DL	Err.	DL	Err.	DL	Err.	DL	Err.	DL	Err.
0	16.7	2.0	16.7	2.0	16.7	2.0	16.7	2.0	16.7	2.0	16.7	2.0
30	21.3	2.1	23.9	2.2	23.1	2.2	25.1	2.3	24.7	2.3	22.8	2.2
60	24.4	2.3	28.0	2.4	27.8	2.4	32.0	2.6	30.6	2.5	27.6	2.4
90	28.1	2.4	32.4	2.6	31.3	2.6	34.4	2.7	34.3	2.7	31.9	2.6
120	29.0	2.5	34.9	2.7	33.8	2.7	39.8	2.9	38.1	2.8	37.2	2.8
150	26.8	2.4	32.2	2.6	35.5	2.7	43.1	3.0	46.1	3.2	46.3	3.2
180	25.7	2.3	30.9	2.5	34.2	2.7	44.4	3.1	52.8	3.4	58.2	3.7
210	28.6	2.4	28.9	2.5	35.9	2.7	47.9	3.2	59.1	3.7	70.1	4.1
240	29.3	2.5	36.1	2.7	41.1	3.0	52.4	3.4	65.9	4.0	81.6	4.6
270	30.4	2.5	40.8	2.9	43.8	3.1	54.5	3.5	70.2	4.1	91.6	5.0
300	34.2	2.7	38.6	2.9	35.9	2.7	50.8	3.4	72.9	4.3	90.3	5.0
330	32.0	2.6	34.8	2.7	36.0	2.7	45.4	3.1	61.7	3.8	80.8	4.6
360	29.3	2.5	33.5	2.6	40.0	2.9	50.5	3.3	57.7	3.6	67.2	4.0
390	31.2	2.5	37.7	2.8	41.1	3.0	50.1	3.3	57.6	3.6	64.2	3.9
420	31.2	2.6	34.9	2.7	34.0	2.7	48.5	3.3	56.6	3.6	60.9	3.8
450	34.9	2.7	43.2	3.0	41.0	3.0	49.2	3.3	55.9	3.6	64.2	3.9
480	39.1	2.9	50.0	3.3	46.8	3.2	52.8	3.4	59.4	3.7	64.6	3.9
510	39.2	2.9	51.0	3.4	49.5	3.3	52.0	3.4	58.8	3.7	63.5	3.9
540	38.3	2.8	53.5	3.5	50.0	3.3	51.1	3.4	60.3	3.7	63.1	3.9

Table A12 – Experimental smoke layer tree data (S38 – S42) experiment #5_2

Time (s)	**S38 (z = 6 m)**		**S39 (z = 6.5 m)**		**S40 (z = 7 m)**		**S41 (z = 7.5 m)**		**S42 (z = 8 m)**	
	DL	Err.	DL	Err.	DL	Err.	DL	Err.	DL	Err.
0	16.7	2.0	16.7	2.0	16.7	2.0	16.7	2.0	16.7	2.0
30	19.9	2.1	25.0	2.3	22.8	2.2	21.2	2.1	23.8	2.2
60	23.3	2.2	30.1	2.5	27.9	2.4	26.3	2.4	29.0	2.5
90	26.6	2.4	34.2	2.7	34.3	2.7	36.4	2.8	41.8	3.0
120	32.5	2.6	42.0	3.0	44.1	3.1	46.3	3.2	52.7	3.4
150	44.4	3.1	56.0	3.6	56.7	3.6	58.1	3.7	64.4	3.9
180	57.7	3.6	68.4	4.1	70.6	4.2	71.7	4.2	76.4	4.4
210	69.7	4.1	79.9	4.5	80.3	4.6	81.2	4.6	86.0	4.8
240	81.3	4.6	90.2	5.0	89.3	4.9	89.3	4.9	93.5	5.1
270	92.6	5.1	99.2	5.3	98.1	5.3	98.6	5.3	101.4	5.4
300	98.9	5.3	104.7	5.6	104.3	5.5	104.3	5.5	107.2	5.7
330	97.0	5.2	109.9	5.8	109.7	5.8	109.7	5.8	113.2	5.9
360	77.8	4.5	107.1	5.7	112.5	5.9	114.5	6.0	117.5	6.1
390	62.3	3.8	98.0	5.3	113.5	5.9	116.0	6.0	119.2	6.2
420	57.5	3.6	83.2	4.7	110.6	5.8	116.3	6.0	120.4	6.2
450	55.0	3.5	76.1	4.4	108.6	5.7	116.6	6.1	123.3	6.3
480	56.7	3.6	75.9	4.4	101.0	5.4	116.1	6.0	123.4	6.3
510	55.9	3.6	72.8	4.3	101.7	5.4	116.0	6.0	125.1	6.4
540	55.7	3.6	72.9	4.3	96.6	5.2	116.3	6.0	125.0	6.4

Table A13 – Experimental smoke layer tree data (S43 – S48) experiment #5_1

Time (s)	S43 $(z = 8.5\ m)$		S44 $(z = 9\ m)$		S45 $(z = 9.5\ m)$		S46 $(z = 10\ m)$		S47 $(z = 10.5 m)$		S48 $(z = 11\ m)$	
	DL	Err.	DL	Err.	DL	Err.	DL	Err.	DL	Err.	DL	Err.
0	11.0	1.7	11.0	1.7	11.0	1.7	11.0	1.7	11.0	1.7	11.0	1.7
30	15.4	1.9	15.8	1.9	17.4	2.0	16.5	1.9	17.7	2.0	17.3	2.0
60	21.0	2.1	22.5	2.2	25.6	2.3	25.7	2.3	28.4	2.4	29.1	2.5
90	32.7	2.6	34.8	2.7	42.6	3.0	44.3	3.1	46.0	3.2	45.6	3.1
120	45.9	3.2	47.5	3.2	52.4	3.4	53.3	3.5	55.7	3.6	55.4	3.5
150	58.1	3.7	59.1	3.7	63.8	3.9	65.3	3.9	66.8	4.0	67.0	4.0
180	67.3	4.0	70.4	4.2	74.1	4.3	75.7	4.4	76.0	4.4	77.1	4.4
210	79.2	4.5	81.3	4.6	84.0	4.7	85.6	4.8	85.9	4.8	86.2	4.8
240	87.2	4.8	88.9	4.9	90.8	5.0	92.7	5.1	93.4	5.1	93.8	5.1
270	95.7	5.2	97.1	5.2	98.7	5.3	100.9	5.4	101.5	5.4	102.1	5.5
300	102.8	5.5	104.6	5.6	105.6	5.6	106.6	5.6	106.9	5.7	107.0	5.7
330	110.1	5.8	111.4	5.8	113.8	5.9	115.0	6.0	114.7	6.0	115.9	6.0
360	114.7	6.0	115.1	6.0	116.6	6.1	116.9	6.1	118.0	6.1	119.2	6.2
390	119.2	6.2	119.2	6.2	120.9	6.2	120.8	6.2	121.6	6.3	123.1	6.3
420	124.1	6.4	124.9	6.4	126.7	6.5	126.6	6.5	126.7	6.5	127.6	6.5
450	128.3	6.5	129.1	6.6	130.0	6.6	129.9	6.6	130.2	6.6	131.3	6.7
480	130.5	6.6	130.6	6.6	132.3	6.7	131.9	6.7	132.3	6.7	133.3	6.7
510	133.7	6.7	134.0	6.8	135.1	6.8	134.6	6.8	135.5	6.8	135.6	6.8
540	134.7	6.8	135.5	6.8	136.5	6.9	136.0	6.8	136.7	6.9	136.9	6.9

Table A14 – Experimental smoke layer tree data (S49 - S53) experiment #5_1

Time (s)	**S49 ($z = 11.5m$)**		**S50 ($z = 12\ m$)**		**S51 ($z = 12.5m$)**		**S52 ($z = 13\ m$)**		**S53 ($z = 13.5m$)**	
	DL	Err.	DL	Err.	DL	Err.	DL	Err.	DL	Err.
0	11.0	1.7	11.0	1.7	11.0	1.7	11.0	1.7	11.0	1.7
30	16.3	1.9	18.0	2.0	17.4	2.0	13.9	1.8	14.5	1.9
60	28.2	2.4	29.8	2.5	29.9	2.5	25.8	2.3	26.6	2.4
90	44.5	3.1	44.6	3.1	43.1	3.0	39.6	2.9	38.5	2.8
120	54.5	3.5	55.6	3.6	55.4	3.5	50.7	3.4	51.1	3.4
150	66.3	4.0	66.6	4.0	65.5	4.0	59.0	3.7	59.7	3.7
180	76.3	4.4	76.0	4.4	75.4	4.4	73.5	4.3	74.7	4.3
210	85.2	4.8	85.0	4.8	83.3	4.7	78.0	4.5	76.2	4.4
240	93.6	5.1	94.2	5.1	93.1	5.1	90.1	5.0	90.1	5.0
270	101.2	5.4	102.1	5.5	100.9	5.4	97.6	5.3	97.5	5.3
300	106.8	5.6	107.3	5.7	108.2	5.7	107.8	5.7	109.1	5.7
330	115.5	6.0	114.9	6.0	115.3	6.0	113.6	5.9	114.6	6.0
360	120.5	6.2	121.4	6.2	120.5	6.2	120.6	6.2	123.5	6.3
390	123.5	6.3	124.6	6.4	125.1	6.4	125.2	6.4	125.0	6.4
420	128.3	6.5	129.3	6.6	129.9	6.6	131.4	6.7	131.9	6.7
450	131.2	6.6	132.2	6.7	132.5	6.7	135.3	6.8	136.2	6.9
480	133.0	6.7	133.9	6.8	135.0	6.8	137.7	6.9	139.0	7.0
510	135.2	6.8	135.9	6.8	136.6	6.9	139.2	7.0	140.5	7.0
540	136.3	6.9	137.1	6.9	137.5	6.9	140.7	7.0	142.0	7.1

Table A15 – Experimental smoke layer tree data (S43 – S48) experiment #5_2

Time (s)	S43 ($z = 8.5$ m)		S44 ($z = 9$ m)		S45 ($z = 9.5$ m)		S46 ($z = 10$ m)		S47 ($z = 10.5$m)		S48 ($z = 11$ m)	
	DL	Err.	DL	Err.	DL	Err.	DL	Err.	DL	Err.	DL	Err.
0	16.7	2.0	16.7	2.0	16.7	2.0	16.7	2.0	16.7	2.0	16.7	2.0
30	20.9	2.1	21.2	2.1	23.2	2.2	21.6	2.2	23.5	2.2	23.1	2.2
60	25.9	2.3	27.4	2.4	32.1	2.6	31.6	2.6	35.2	2.7	35.7	2.7
90	39.0	2.9	40.6	2.9	44.8	3.1	45.4	3.1	50.1	3.3	50.3	3.3
120	52.0	3.4	58.2	3.7	62.2	3.8	62.1	3.8	62.9	3.8	62.8	3.8
150	63.0	3.9	68.1	4.1	71.3	4.2	72.1	4.2	74.0	4.3	73.9	4.3
180	73.9	4.3	76.5	4.4	79.5	4.5	79.0	4.5	80.9	4.6	81.6	4.6
210	87.3	4.8	90.0	5.0	92.1	5.0	92.1	5.0	92.3	5.1	92.6	5.1
240	93.8	5.1	96.3	5.2	98.9	5.3	99.9	5.4	100.0	5.4	101.4	5.4
270	100.7	5.4	103.0	5.5	105.8	5.6	107.2	5.7	108.3	5.7	109.1	5.7
300	105.9	5.6	107.1	5.7	109.3	5.8	110.4	5.8	112.3	5.9	113.6	5.9
330	110.9	5.8	111.6	5.8	114.3	6.0	113.7	5.9	115.7	6.0	116.7	6.1
360	117.8	6.1	119.0	6.1	120.3	6.2	120.8	6.2	121.4	6.2	121.7	6.3
390	118.3	6.1	119.3	6.2	121.0	6.2	121.9	6.3	123.2	6.3	123.3	6.3
420	119.2	6.2	120.6	6.2	123.1	6.3	123.6	6.3	124.5	6.4	124.6	6.4
450	122.3	6.3	123.4	6.3	125.6	6.4	125.4	6.4	126.1	6.4	125.6	6.4
480	123.2	6.3	124.9	6.4	127.2	6.5	126.7	6.5	127.1	6.5	126.8	6.5
510	124.5	6.4	125.7	6.4	127.3	6.5	126.1	6.4	127.2	6.5	126.9	6.5
540	124.0	6.4	125.8	6.4	127.3	6.5	126.4	6.5	127.7	6.5	127.3	6.5

Table A16 – Experimental smoke layer tree data (S49 - S53) experiment #5_2

Time (s)	**S49 $(z = 11.5m)$**		**S50 $(z = 12\ m)$**		**S51 $(z = 12.5m)$**		**S52 $(z = 13\ m)$**		**S53 $(z = 13.5m)$**	
	DL	Err.	DL	Err.	DL	Err.	DL	Err.	DL	Err.
0	16.7	2.0	16.7	2.0	16.7	2.0	16.7	2.0	16.7	2.0
30	21.7	2.2	23.6	2.2	23.4	2.2	21.5	2.2	22.2	2.2
60	36.3	2.8	38.3	2.8	37.8	2.8	36.8	2.8	37.3	2.8
90	49.5	3.3	50.5	3.3	49.4	3.3	47.8	3.2	47.7	3.2
120	61.1	3.8	61.6	3.8	60.4	3.7	60.1	3.7	60.0	3.7
150	72.4	4.2	72.3	4.2	71.2	4.2	71.2	4.2	71.5	4.2
180	80.4	4.6	80.9	4.6	80.5	4.6	81.7	4.6	82.2	4.6
210	91.5	5.0	91.7	5.0	90.7	5.0	90.3	5.0	90.7	5.0
240	100.9	5.4	100.9	5.4	99.3	5.3	100.1	5.4	100.1	5.4
270	109.1	5.7	108.9	5.7	107.3	5.7	107.8	5.7	107.3	5.7
300	114.2	6.0	113.9	5.9	113.2	5.9	114.2	6.0	114.8	6.0
330	117.7	6.1	118.3	6.1	120.1	6.2	121.1	6.2	122.0	6.3
360	121.2	6.2	121.9	6.3	121.8	6.3	122.1	6.3	122.4	6.3
390	122.7	6.3	122.6	6.3	123.2	6.3	123.6	6.3	124.0	6.4
420	124.5	6.4	124.2	6.4	124.9	6.4	125.0	6.4	124.8	6.4
450	125.0	6.4	125.6	6.4	125.6	6.4	125.6	6.4	125.8	6.4
480	126.3	6.4	127.2	6.5	126.6	6.5	127.0	6.5	127.1	6.5
510	126.6	6.5	127.1	6.5	127.6	6.5	127.5	6.5	127.7	6.5
540	127.5	6.5	127.6	6.5	128.2	6.5	128.2	6.5	128.3	6.5

Table A17 – Experimental smoke layer tree data (S54 - S59) experiment #5_2

Time (s)	**S54 $(z = 14\ m)$**		**S55 $(z = 14.5m)$**		**S56 $(z = 15\ m)$**		**S57 $(z = 16\ m)$**		**S58 $(z = 17\ m)$**		**S59 $(z = 18\ m)$**	
	DL	Err.	DL	Err.	DL	Err.	DL	Err.	DL	Err.	DL	Err.
0	14.5	1.9	14.5	1.9	14.5	1.9	14.5	1.9	14.5	1.9	14.5	1.9
30	14.9	1.9	14.9	1.9	15.1	1.9	15.5	1.9	16.1	1.9	15.7	1.9
60	16.6	1.9	16.4	1.9	16.6	2.0	16.3	1.9	17.9	2.0	19.5	2.1
90	19.2	2.1	19.1	2.1	19.1	2.1	19.3	2.1	21.2	2.1	22.8	2.2
120	22.0	2.2	22.0	2.2	22.1	2.2	22.5	2.2	23.9	2.2	25.6	2.3
150	25.2	2.3	25.4	2.3	26.2	2.3	26.8	2.4	28.8	2.5	28.7	2.4
180	29.7	2.5	29.6	2.5	30.5	2.5	31.4	2.6	33.5	2.6	34.3	2.7
210	34.1	2.7	34.4	2.7	35.5	2.7	37.3	2.8	39.0	2.9	38.9	2.9
240	38.6	2.9	38.8	2.9	40.3	2.9	41.4	3.0	43.5	3.1	44.8	3.1
270	42.9	3.0	43.1	3.0	44.1	3.1	44.6	3.1	46.7	3.2	48.9	3.3
300	48.8	3.3	49.0	3.3	49.9	3.3	51.8	3.4	56.4	3.6	57.3	3.6
330	55.7	3.6	55.8	3.6	56.0	3.6	57.7	3.6	61.0	3.8	63.4	3.9
360	67.8	4.1	68.0	4.1	68.3	4.1	70.4	4.2	72.7	4.3	73.5	4.3
390	76.5	4.4	76.7	4.4	77.0	4.4	78.5	4.5	81.8	4.6	82.1	4.6
420	86.1	4.8	85.9	4.8	86.9	4.8	88.2	4.9	90.9	5.0	91.6	5.0
450	93.4	5.1	93.3	5.1	94.6	5.1	94.9	5.2	99.3	5.3	102.9	5.5
480	103.4	5.5	102.2	5.5	102.7	5.5	103.6	5.5	104.1	5.5	105.2	5.6
510	104.3	5.5	103.7	5.5	104.5	5.6	104.7	5.6	106.1	5.6	105.7	5.6
540	103.4	5.5	103.4	5.5	104.6	5.6	105.2	5.6	106.8	5.6	106.7	5.6
570	102.8	5.5	102.5	5.5	103.1	5.5	104.1	5.5	105.4	5.6	104.9	5.6
600	102.3	5.5	102.2	5.5	102.7	5.5	103.4	5.5	104.0	5.5	103.4	5.5
630	100.2	5.4	100.1	5.4	100.9	5.4	102.5	5.5	102.9	5.5	101.8	5.4
660	99.0	5.3	98.9	5.3	100.0	5.4	100.2	5.4	101.1	5.4	100.6	5.4
690	97.4	5.3	97.3	5.3	97.7	5.3	98.0	5.3	97.9	5.3	96.9	5.2
720	94.7	5.2	94.7	5.2	95.3	5.2	95.7	5.2	95.2	5.2	93.5	5.1
750	90.9	5.0	90.7	5.0	91.1	5.0	91.8	5.0	91.3	5.0	89.9	5.0
780	86.3	4.8	86.4	4.8	86.6	4.8	86.9	4.8	87.0	4.8	85.6	4.8